Spatial modelling of community effects

Kirill Batmanov

Modélisation spatiale des effets de communauté

Spatial modelling of community effects

THÈSE

présentée et soutenue publiquement le 26 mars 2014

pour l'obtention du

Doctorat de l'Université Lille1 - Sciences et Technologies
(spécialité informatique)

par

Kirill Batmanov

Composition du jury

Rapporteurs :	Enrico Carlon, Associate Professor	University of Leuven
	Hidde de Jong, DR INRIA Grenoble	INRIA Grenoble
Examinateurs :	Céline Kuttler, MdC, *co-directrice*	LIFL, Univ. Lille 1
	Cédric Lhoussaine, HDR, *directeur*	LIFL, Univ. Lille 1
	Joachim Niehren, HDR, *co-directeur*	INRIA Lille, LIFL
	Ovidiu Radulescu, HDR	DIMNP, Univ. Montpellier 2
	Yasushi Saka, Senior Lecturer	University of Aberdeen

UNIVERSITÉ DE LILLE 1 - SCIENCES ET TECHNOLOGIES
ÉCOLE DOCTORALE SCIENCES POUR L'INGÉNIEUR
Laboratoire d'Informatique Fondamentale de Lille - UMR 8022
U.F.R. d'I.E.E.A. - Bât. M3 - 59655 VILLENEUVE D'ASCQ CEDEX
Tél. : +33 (0)3 28 77 85 41 - Télécopie : +33 (0)3 28 77 85 37 - email : direction@lifl.fr

ABSTRACT

A developing embryo, consisting initially of identical cells, transforms itself into a spatially organized structure made of distinct tissues with clear boundaries. This process, known as pattern formation, is studied in the field of developmental biology. Cell interaction plays a key role in pattern formation, and the community effect is an example of such an interaction.

A population of cells in an embryo is said to exhibit a community effect when they form a cell community with a common identity by virtue of exchanging diffusible signalling molecules (morphogens). This effect helps the cell community to maintain a common gene expression profile over an extended period of time, and to eventually differentiate co-ordinately into a functional tissue, such as muscle.

Self-organizing processes like community effects are difficult to understand intuitively. Instead, a satisfactory description can be given in the form of a formal model. Several computational models of community effects were given in the literature. However, the concept of space was not explicitly included in these models, making it difficult to understand how community effects participate in pattern formation.

In this work, we study the behaviour of a community effect in space and investigate its roles in other pattern formation processes, using computational modelling. Main contributions of this thesis are the following:

- A model reduction method is developed for stochastic analysis, and using it we have shown how the model of the community effect in *Xenopus* is influenced by stochastic noise.
- Using the simplest possible spatial community effect model, we show that the community effect must eventually spread across the entire population of cells which respond to the morphogen. This is confirmed in a more detailed model.
- Two models demonstrating how this expansion can be controlled are presented. First, if the community effect is augmented with a negative feedback mechanism, it forms a reaction-diffusion system which self-organizes and forms a stable, localized area of activation. Second, when a simple cross-repression gene circuitry is combined with a community effect loop, a gene expression pattern with a well-demarcated boundary appears in response to a transient morphogen gradient. The pattern remains stable even after the gradient disappears, which shows that the gene network has the memory of morphogen dynamics.

RÉSUMÉ

Un embryon, initialement composé de cellules identiques, se transforme progressivement en une structure spatialement organisée de tissus distincts aux frontières clairement démarquées. Ce processus de formation de motifs est étudié dans le domaine de la biologie du développement. Les interactions cellulaires jouent un rôle clé dans la formation de motifs, et l'effet de communauté est un exemple d'une telle interaction.

Une population de cellules dans un embryon présente un effet de communauté quand elle forme une communauté de cellules ayant une identité commune obtenue grâce à l'échange de molécules de signalisation qui diffusent dans le milieu (i.e. des morphogènes). Cet effet permet aux cellules de la communauté de maintenir un profil d'expression génétique commun pendant une période prolongée, et pour se différencier finalement de manière coordonnée dans un tissu fonctionnel, comme le muscle.

Les processus auto-organisés tels que l'effet de communauté sont difficiles à comprendre intuitivement. Une description satisfaisante peut être obtenue sous la forme d'un modèle formel. Quelques modèles computationnels des effets de la communauté ont été donnés dans la littérature. Cependant, la notion d'espace n'ayant pas été explicitement incluse dans ces modèles, il est difficile de comprendre comment l'effet de communauté participe à la formation de motifs.

Dans ce travail, nous étudions le comportement de l'effet de communauté dans l'espace et étudions ses rôles dans d'autres processus de formation de motif, en utilisant la modélisation computationnelle. Les contributions principales de cette thèse sont les suivantes:

- Une méthode de réduction de modèle est développée pour l'analyse stochastique. Par cette méthode nous avons pu démontrer que le modèle de l'effet de communauté dans *Xenopus* est influencé par un bruit stochastique.

- En utilisant un modèle spatial simple d'effet de communauté, nous montrons que celui-ci doit finalement se propager dans l'ensemble de la population de cellules qui réagissent au morphogène. Cela est confirmé par un modèle plus détaillé.

- Deux modèles montrant comment cette expansion peut être contrôlée sont présentés. Tout d'abord, si l'effet de communauté est augmenté d'un mécanisme de rétroaction négative, il forme un système de réaction-diffusion qui s'auto-organise et forme une zone d'activation stable et localisée. En second lieu, quand un circuit simple de repression génétique est associé au circuit produisant l'effet de communauté, un motif d'expression de gène avec une

frontière bien démarquée apparaît en réponse à un gradient de morphogène transitoire. Le motif reste stable y compris après disparition du gradient, ce qui indique que le réseau de gènes garde en mémoire la dynamique du morphogène.

CONTENTS

ACKNOWLEDGEMENT

I would like to thank my supervisors, Céline Kuttler and Cédric Lhoussaine, for their good advice, patience and help. I am extremely grateful for their support, both on an academic and a personal level.

I would also like to thank Yasushi Saka, whose work on community effects in *Xenopus* was the starting point for this thesis. Much of the work presented here was done in collaboration with him.

I would like to thank François Lemaire, whose advice and patience made it possible to complete the part of work related to moment closure.

I am grateful to Joachim Niehren, my co-supervisor, for his excellent advice on writing the papers and doing presentations. I would like to thank Cristian Versari for many discussions about the symmetric reduction. I would also like to thank Michel Petitot for many meetings in which he shared his broad expertise in various applied mathematics subjects, and the French lessons.

I appreciate a lot of help, kindness and friendship of my colleagues from the BioComputing team in LIFL.

Last, but by no means least, I would like to thank my wife Ying Fan for her support, help and great patience at all times. My mother and aunt have given me their unequivocal support throughout, for which I am extremely grateful as well.

1 INTRODUCTION

1.1 COMMUNITY EFFECTS

During animal *development* from a fertilized egg (a single cell) into a multicellular organism, embryos undergo complex series of transformations. By activating specific sets of genes, identical cells differentiate and are partitioned into distinct tissues with clear boundaries. Differentiating tissues are simultaneously patterned and moved to their final destinations. This biological process, in which an organism develops its shape, is called *morphogenesis* – a term coined in the late 19th century, having as origin the Greek words *morphe* (shape) and *genesis* (origin, creation, generation). During the self-organized, finely regulated process of morphogenesis, cells constantly create and exchange information by means of *diffusible factors*. These signalling molecules diffuse from a central source to other cells in the growing organism, forming a concentration gradient along an axis. Alan Turing introduced the term *morphogen* for diffusible factors in development, in his seminal paper *The chemical basis of morphogenesis* [Turing, 1952]. A morphogen is rigorously defined as a diffusing chemical whose concentration varies across the embryo and which is involved in pattern formation. Cells respond differently to different concentrations of the morphogen, and effectively its concentration provides positional information [Wolpert et al., 1998].

A *community effect* is a developmental phenomenon allowing to establish a *cell community with a common identity*. Upon reception of an inducing signal, a cell population starts co-ordinately expressing a specific set of genes. Whenever the population size exceeds a certain critical threshold, the cells maintain their common gene expression profile over an extended period of time. Upon terminal differentiation, the cell community has become a functional tissue, such as muscle.

A community effect was first identified in the African clawed toad *Xenopus laevis*, where it assists differentiation of muscle precursor cells [Gurdon, 1988, Gurdon et al., 1993]. In the experiments, Gurdon took mesoderm cells from 9 hours old *Xenopus* embryos, separated them, and then inserted them into a structure that he called *sandwich*, which is two layers of 7 hours old ectoderm tissue. The mesoderm cells are implanted between the two layers. The cells were left there for 20 hours, and then tested for presence of *Xenopus* MyoD protein, which is only expressed in the nuclei of muscle cells. The presence of XMyoD means that the cell has differentiated into muscle. Figure 1 shows the diagram of these experiments.

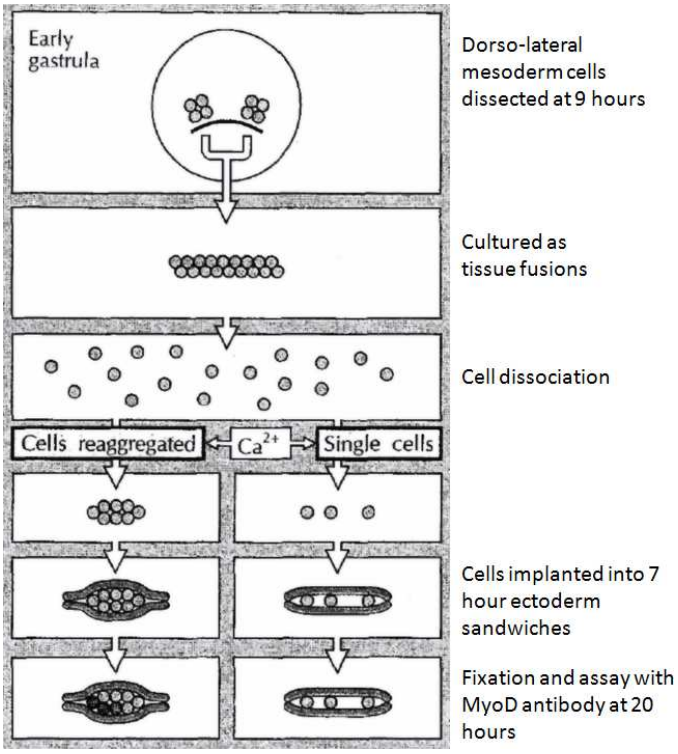

Figure 1: Diagram of sandwich experiments from [Gurdon et al., 1993].

Gurdon found that in order to differentiate into muscle, there must be a large number, about 100 to 200, of mesoderm cells clustered together. If this condition was not met, the XMyoD was not detected. This suggested that cell to cell interaction is required to begin differentiation: the cells could sense how many of their kind are around, hence the name "community effect". The large number of cells needed, called *the critical number*, means that the interaction is likely to be long-range, therefore an involvement of a morphogen was hypothesized.

Community effects have subsequently been observed in other organisms. Examples include the sea urchin oral ectoderm specification [Bolouri and Davidson, 2010], differentiation of mesoderm cells into muscle cells in mice [Cossu et al., 1995], differentiation of dorsal epidermal anlage cells into epidermal cells in drosophila [Stüttem and Campos-Ortega, 1991]. Community effect has been conjectured to be a widespread phenomenon in development [Davidson, 2006].

The topic of this thesis is modelling of community effects. In particular, we consider in detail spatial aspects of community effects for the first time.

1.2 WHY DO WE NEED MODELLING

In recent years, quantitative modelling has become an important activity in biology. Theoreticians have modelled biological processes in a purely mathematical way for a long time, for example [Turing, 1952].

However, these models were usually highly abstract and difficult to connect to the real data collected in the labs, and thus largely ignored by the wider community of "real biologists" [Barnes and Chu, 2010].

The main reason for this was that a mathematical modelling activity usually seeks a simple formula which explains the relationship between variables of the system in study. Such analytical solutions are attractive, because they provide an easily understandable insight into the behaviour of the system. Unfortunately, for many real-world modelling problems, which often feature many interactions and non-linear dependencies between components, it is very hard or impossible to find such exact solutions. This forced theoreticians to use models which were simplified and abstract (e.g. pattern formation models of Turing [1952], Gierer and Meinhardt [1972]).

Advances in computer science (for example, development of efficient numerical analysis methods [Hildebrand, 1987]), as well as increasing availability of computing power, have led to widespread application of computational, numerical techniques to analyse models. Computational approaches can be often used to treat systems where attempts for analytical solutions, even approximate, are currently hopeless. Using computational modelling to study biological systems is the topic of the field of *Computational Biology* [Kitano, 2002]. The use of numerical techniques has a price, however: results obtained in this way usually take the form of numbers which depend on parameters of the model. This dependency is often not obvious, which makes the results harder to interpret compared to analytical approaches. Typically one has to scan the parameter space in order to discover dependencies between variables and draw general conclusions about the system's behaviour.

In this thesis, we will model community effects using computational modelling as the main tool, with an occasional excursion into analytical treatment.

1.3 RESEARCH QUESTIONS AND CONTRIBUTIONS

1.3.1 *Stochastic phenomena in community effects*

During development, a multicellular organism must generate many different types of cells. Because the cells are genetically identical, differentiation must rely on tuning expression levels of certain genes. Gene expression is inherently noisy [Raj and van Oudenaarden, 2009], as is cell signalling and generally all chemical processes which determine the regulatory state of a cell. This noise ultimately comes from the Brownian motion of molecules and takes the form of randomly fluctuating counts of proteins involved in gene regulation.

This noise has been found to have a functional role in many processes during development [Eldar and Elowitz, 2010, Balázsi et al., 2011]. However, the embryo must build the organism in a highly reproducible and

robust way, despite the omnipresent noise. Mechanisms of noise reduction in embryo patterning is the subject of many studies [Arias and Hayward, 2006, Horikawa et al., 2006].

Previous models of the community effect were mainly analysed in the deterministic regime, ignoring the stochastic noise. Saka et al. [2011] performed a stochastic analysis of their model of the community effect in *Xenopus*. This analysis, which was the starting point of the present thesis, indicated the presence of stochastic effects, but this was not explored further. Therefore a more detailed analysis of the stochastic behaviour is desirable. The questions here are: whether the community effect in this model is robust with respect to stochastic noise, which should be the case for a basic patterning mechanism in the embryo; and how the stochastic effects affect the critical number.

The analysis performed in Chapter 3 shows that this model of the community effect is still present if the stochastic noise is accounted for. However, stochastic effects increase the critical number by about 20%. The model was analysed using a method called *moment closure*. In general, the computational complexity of this analysis grows quadratically with the size of the model, and it becomes prohibitively high for the community effect model with about 100 cells. The main contribution of this part of the work is a new model reduction technique, first proposed in Batmanov et al. [2012a], which exploits model's symmetries. In a highly symmetric model such as the space-less community effect, this method makes the complexity of the analysis independent of number of cells.

1.3.2 *Spatial modelling of community effects*

The *space* in which community effects occur was disregarded in previous models. However, different communities within the embryo are spatially organized, with clearly demarcated boundaries. These important phenomena could not be explained without explicit treatment of space in the models. Therefore, to study properties of community effects in space, in Chapter 4 we adopt a spatial model in which cells are arranged along a one-dimensional row. One dimensional space was chosen for computational efficiency; it corresponds to spherically symmetric geometry in three dimensions. Diffusible factors for intercellular communication can migrate from one cell to the two directly neighbouring cells in this one dimensional grid. Although considering only one dimension might appear simplistic, compared to the three dimensions along which an embryo develops, we can obtain useful insights from it.

First we studied the *minimal model* of a community effect, which is schematically illustrated in Figure 2a. This model, and the others from this section, were first presented in [Batmanov et al., 2012b]. It distils essential properties of previous community effect models. In this model, there is a unique chemical species $\mathfrak{u}$, which is exchanged between

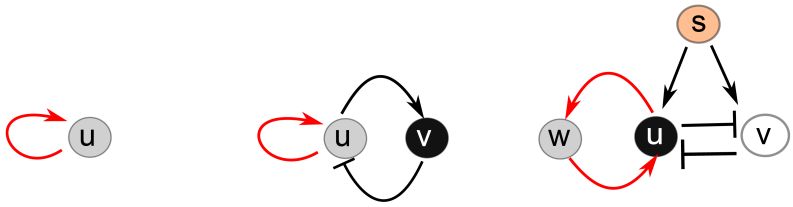

(a) minimal model (b) Turing pattern model (c) dynamic morphogen gradient model

Figure 2: Illustrations of three models analysed in Chapter 4. The feedback loop responsible for community effects is highlighted in red.

cells (thus being a morphogen) and promotes its own production. The inducing signal for initial activation of $\mathfrak{u}$, which will be self-sustained by the positive feedback loop, is represented by injecting some $\mathfrak{u}$ at the start of simulations into some cells.

We will show through stochastic simulations that, in this configuration, a community effect spreads across the system. The central question that arises is '*How can we limit the community effect in space?*'. Intuitively, the system needs some negative feedback control mechanism, which will limit the area of activation. To address this issue, we propose two approaches.

THE TURING PATTERN MODEL adds a second diffusible factor $\mathfrak{v}$ with an inhibitory effect to the minimal model's self-sustaining species $\mathfrak{u}$. This second species is highlighted in black in Figure 2b. In order to close the loop of mutual dependencies, $\mathfrak{u}$ activates not only itself, but also $\mathfrak{v}$. Intuitively, the effect of this seemingly small change in one dimensional space is not clear. Using stochastic simulations, we obtain the insight that *in this system, the spread of the community effects in space is restricted.* How can this be explained?

Alan Turing's paper, *The Chemical Basis of Morphogenesis* [Turing, 1952], deals with the above network from the perspective of pattern formation. Turing called it the reaction-diffusion system. When two diffusible factors interact in the manner shown in Figure 2b, the reaction-diffusion system may generate the so-called *Turing patterns*. The intuitive explanation is that the inhibitor morphogen $\mathfrak{v}$, which diffuses faster than the activator $\mathfrak{u}$, reaches distant areas of the population first, and prevents their activation later. The result is an area of activation centred on the place of initial induction, with a stable size and position.

It has been shown that this system can generate many diverse patterns observed in development [Meinhardt, 1982], for instance, colour stripes on fish skin [Kondo and Miura, 2010, Sanderson et al., 2006], colourings of sea shells [Meinhardt, 1995], establishment of the left-right asymmetry in vertebrates [Hamada et al., 2002] and plant growth

[Jonsson et al., 2005]. The community effect, however, has not been considered in the context of the reaction-diffusion system.

This model offers a plausible explanation of the community effect in *sea urchin*, described by Bolouri and Davidson [2010], with u being the Nodal protein and v its antagonist Lefty. Further evidence to support this model is given by Duboc et al. [2008].

THE DYNAMIC MORPHOGEN GRADIENT MODEL sketched in Figure 2c introduces a diffusible factor s, which activates two mutually inhibitory species v and u. The latter participates in a self-activating feedback loop with w, another diffusible species. Figure 2c highlights the u-w community effect loop in red. Without the community effect loop and diffusion of the morphogen s in continuous space, this gene regulatory network (GRN) was previously considered in [Saka and Smith, 2007].

Mutual repression between two species is widespread, and results in exclusive activation of either one species or the other [Cherry and Adler, 2000]. It is often referred to as a genetic *toggle switch*, and controls various aspects of cell fate decision, e.g., the genetic switch of the bacteriophage lambda [Ackers et al., 1982, Ptashne, 2004], the gap gene network [Jaeger et al., 2004a,b, Papatsenko and Levine, 2011], and neural tube patterning [Ribes and Briscoe, 2009].

In our model, the morphogen s spreads along one dimensional space from a localized source, and creates a *morphogen gradient*. It is postulated that embryonic cells learn their position by sensing the local morphogen level in a gradient for pattern formation [Wolpert, 1969]. This system is analogous to embryonic induction, where one tissue instructs and patterns the neighbouring tissue by diffusible factors.

Analysing the dynamic morphogen gradient model, we demonstrate that it efficiently limits community effects in continuous space. We also show that a *transient* morphogen gradient is sufficient for pattern formation in this system. This self-organizing property was previously unknown. Our analysis using stochastic simulations of the system indicates that community effects confer *robustness* to this patterning process. Interestingly, we found that even when the morphogen distribution eventually becomes uniform, the system can maintain the pattern. Thus our model confers *memory* to the system.

This model is based on a community effect GRN found in *Xenopus*, as described in [Saka et al., 2011, Saka and Smith, 2007].

1.4 STRUCTURE OF THE THESIS

Chapter 2 gives an overview of modelling and analysis methods relevant to the topic of the thesis. All techniques which are used in this work, and their theoretical foundations, are explained.

Chapter 3 presents an extended stochastic analysis of a community effect model without considering space. A major point there is the proposed model reduction method which exploits symmetries in the model to simplify the analysis.

Chapter 4 presents new spatial models of community effects. Various properties of these models related to pattern formation in embryos are studied.

Chapter 5 discusses findings of the work and connects them to related works from the literature.

Conclusions in Chapter 6 provide the overview of the results and outline directions for the future work.

1.5 PUBLICATIONS

This thesis is based on two publications:

- [Batmanov et al., 2012a] presents the symmetry-based model reduction method for moment closures, with an application to the *Xenopus* community effect model without space.
- In [Batmanov et al., 2012b], the spatial models of community effects were presented for the first time.

In addition, during the PhD study, the author participated in the ICEBERG ANR project, in particular developing a microscopy image processing tool. A paper about that is in preparation.

2

COMPUTATIONAL MODELLING OF BIOLOGICAL SYSTEMS

Computational biology in general is a diverse field. There are many modelling techniques which are suitable for different problems [de Jong, 2002]. In developmental biology, three modelling scales are important: molecular, cellular and tissue [Setty, 2012]. In the following we will review modelling techniques which are necessary to demonstrate how community effects at tissue level arises from a gene regulatory network at the molecular level.

The main purpose of this review is to show how modelling methods which will be used later are derived from first principles. In the author's opinion, it is important to understand that these methods, however abstract they may seem, are firmly grounded in basic physical laws, with clear assumptions which allow simplified treatments. Understanding these assumptions helps choosing the right modelling approaches in particular cases.

After defining a useful informal graphical way to easily describe models at high level in Section 2.1, we define a formal language of chemical reactions in Section 2.2. Some basic definitions are given, and a short overview of early empirical approaches to modelling the dynamics of chemical reactions.

Section 2.3 lays the theoretical foundation for all other modelling methods in this chapter by introducing the Smoluchowski model and the Doi model. In these models, individual molecules are the basic entities, and their positions and diffusion speeds are taken into account.

Section 2.4 considers an important class of models which all share the assumption of fast diffusion. This assumption simplifies the state representation of the model, as we only have to track population counts of different molecular species.

Section 2.5 borrows some assumptions behind models in Section 2.4, except the assumption of fast diffusion. The goal is to model systems with slow diffusion efficiently, and thus make spatial modelling feasible.

2.1 GENE REGULATORY NETWORKS

A *gene regulatory network (GRN)* is a collection of genes which interact with each other. An expressed (activated) gene produces its protein, which may activate or inhibit expression of other genes or itself. An schematic representation of a GRN may be given using a directed graph, such as Figure 3, for example.

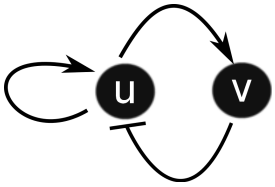

Figure 3: A gene regulatory network.

A node in the graph represents a gene. The GRN on Figure 3 has two genes, u and v. Directed edges on the graph represent gene interactions by means of protein production and subsequent regulation of expression of another gene by that protein. A regular arrowhead on the edge from u to v means that the interaction is activation of v by the protein produced by u. We will simply say that u activates v. Another regular arrow from u to itself denotes self-activation of u. A T-shaped arrowhead on the edge from v to u represents inhibition of u's expression by v. Interactions may involve intermediate agents, such as signalling pathways, which are usually omitted from the graph.

Graphical GRNs are useful to introduce and present models of genetic interactions. Similar notations are widely used as a knowledge representation language in biological literature [Alon, 2007, Davidson, 2010]. However, they are too abstract to faithfully represent the models of biological mechanisms used in this thesis. In the following, a more detailed modelling language will be reviewed, the language of chemical reactions.

2.2 BIOCHEMICAL REACTION SYSTEMS

For studying the community effect, the scale of interest is gene regulation and cell to cell communication. At this level, systems are often modelled using chemical reactions [Bower and Bolouri, 2001], and this will be the starting point for all the models that follow.

A chemical reaction

$$A + 2B \xrightarrow{k} 3C + 4D \tag{1}$$

states that a molecule of type A can react with two molecules of type B to produce three molecules C and four D. Molecules on the left side of the arrow are called *reactants*, while molecules on the right are called *products*. The numbers before molecule names are called *stoichiometric coefficients*. A reaction may have any number of reactants and products. k is the *reaction rate constant*, which is a parameter specifying the speed of this reaction. Reaction speeds are specified by functions, called *rate laws*, which may depend on molecule counts and other parameters. An unambiguous specification of this function must be written above the arrow. Specification of the rate law as a reaction rate constant in this case assumes the mass action law, which will be explained shortly.

In general a reaction among n chemical species (we will write the species as a sequence $(X_1, \ldots, X_n)$ for notational convenience), can be specified by a triplet $(l, \boldsymbol{\alpha}, \boldsymbol{\beta})$. $\boldsymbol{\alpha} = (\alpha_1, \ldots, \alpha_n)$ are stoichiometric coefficients on the left hand side, corresponding to reactants. $\boldsymbol{\beta} = (\beta_1, \ldots, \beta_n)$ are the stoichiometric coefficients on the right hand side. l is an expression specifying the law used to compute the reaction speed, which should return a real number. If a chemical species does not participate in a certain reaction, its stoichiometric coefficient is 0.

For example, the reaction (1), if we order the species as (A, B, C, D), has $l = k[A][B]^2$, $\boldsymbol{\alpha} = (1, 2, 0, 0)$, $\boldsymbol{\beta} = (0, 0, 3, 4)$. $[A]$ and $[B]$ are the concentrations of A and B.

In order to analyse systems of chemical reactions, we need some way to compute the reaction speeds, i.e. to define the aforementioned law. In the following subsections, we will review empirical approaches to that task. Later, starting from Section 2.3, we will follow a more principled approach.

2.2.1 *Empirical rate laws*

Traditionally, chemical systems were analysed under assumption of constant compartment volume, high molecule counts and fast diffusion. In these conditions we can define *reaction rate* v [McNaught and Wilkinson, 1997], e.g. for the reaction above:

$$v = -\frac{d[A]}{dt} = -\frac{1}{2}\frac{d[B]}{dt} = \frac{1}{3}\frac{d[C]}{dt} = \frac{1}{4}\frac{d[D]}{dt}$$

where $[A](t)$ is the *concentration* of species A in the compartment, treated as a non-negative real number. The unit of v is concentration per second, e.g. $\mathrm{mol} \cdot l^{-1} \cdot s^{-1}$. The equalities follow from the mass conservation law: for each molecule A that disappears three C molecules appear, hence $\frac{d[C]}{dt} = -3\frac{d[A]}{dt}$, and so on. Note that this definition is only valid in a closed system where only a single reaction occurs.

Historically, the first approach to identify the laws governing reaction speeds was purely empirical: a reaction was isolated to reasonably fulfil the above conditions, and then concentrations of participating species were measured over a period of time. It was found that the reaction rate usually depends on concentrations of reactants, and also products in case of reversible reactions [Connors, 1990]. For an *elementary reaction*, i.e. a reaction which occurs in a single step and which has no intermediate products created during the reaction, the *law of mass action* is usually observed:

$$v = k \prod_{i=1}^{n} [X_i]^{\alpha_i}$$

For instance, if the reaction (1) is an elementary one, its rate would be [1]

$$v = k[A][B]^2$$

More generally, an arbitrary irreversible reaction is said to follow the law of mass action if its rate follows the form

$$v = k\prod_{i=1}^{n}[X_i]^{y_i}$$

where $[X_i]$ are the concentrations of n reactants involved in the reaction, and y_i is the *order of reaction w.r.t.* X_i. For elementary reactions $y_i = \alpha_i$. The overall *order of reaction* is $\sum_{i=1}^{n} y_i$.

Sometimes it is useful to consider a chain of elementary reactions as a single, non-elementary reaction. One example of this is an *enzymatic reaction*, which is a fundamental reaction type in biochemical systems [Chen et al., 2010]. The vast majority of reactions taking place in living organisms are of this type [Erdi and Toth, 1992]. The canonical model for an enzymatic reaction is the following system:

$$E + S \underset{k_b}{\overset{k_f}{\rightleftharpoons}} C$$

$$C \xrightarrow{k_{cat}} E + P$$

It is a succession of a reversible binding step, where a substrate molecule S binds to an *enzyme* (or catalyst) E, and a largely irreversible catalytic step where the enzyme turns the substrate into the product P.

To provide a simple treatment of this important system, the following assumptions are adopted:

1. All three reactions follow the law of mass action.
2. The enzyme does not participate significantly in other reactions, therefore the conservation laws $[E](t) + [C](t) = E_0$, $[S](t) + [C](t) + [P](t) = S_0$ hold.
3. The rate of the reversible reaction is much higher than the rate of the catalytic step.

The last point allows to split the system into a fast and a slow one. For the fast subsystem, defined by the reversible reaction, the concentration of S is considered constant, since it changes slowly. For the slow subsystem, the concentration of C is considered to be at its equilibrium limit at all times (it is said to exhibit quasi-steady-state behaviour). Under these conditions, the rate of change of S in the slow subsystem is

$$v = \frac{V_{max}[S]}{[S] + K_M}$$

1 Not to be confused with the stochastic propensity function, which will have a coefficient of 1/2, see Section 2.4

where $K_M = \frac{k_{cat}+k_b}{k_f}$ is the *Michaelis constant*, and $V_{max} = k_{cat}E_0$ is called the maximum rate. This v can be thought of as the rate of the non-elementary reaction $S \to P$, which is an approximation of the enzymatic reaction system. This reaction is said to follow Michaelis-Menten kinetic law.

2.2.2 *Approximating assumptions*

Two treatments of chemical kinetics above are made for specific systems and under many assumptions. To analyse an arbitrary system, a more general theory is needed. We would like to *derive* analysis methods for chemical systems from basic physical laws, using well-understood assumptions to simplify calculations.

The main question of interest in biochemical systems is how the co-operation between reactions gives rise to observed behaviours (rather than, for example, details of mechanics of individual reactions) [Voit, 2000]. Therefore, the appropriate initial assumption about the system is that we can ignore the internal states of the molecules. Namely we ignore orientations, angular velocities and other states which are practically unobservable in the biological context. In addition, often entire chains of reactions will be abstracted into a single reaction, ignoring the intermediate steps [Di Ventura et al., 2006]. Michaelis-Menten kinetics above is one example of this. Another one is the transcription of a gene, which is a complex set of events that creates mRNA from DNA. It is typically represented as a single reaction.

Two important additional assumptions can be considered. One states that we can ignore the positions of the molecules in space. Effectively this assumes that within the compartment of interest the diffusion of all molecules is so fast in comparison to the speed of the reactions that it can be taken to be instantaneous. The mixture of chemicals under these assumption is spatially homogeneous, which simplifies the analysis [Gillespie, 1976].

Another assumption that can be made is that the number of molecules participating in the reactions is so large that the fluctuations of the concentrations, which arise from the inherently random nature of the reactions, are negligibly small. This can be formulated alternatively as assumption of infinite volume of the compartment [Kurtz, 1972]. Together with the well-mixed assumption this allows further (dramatic) simplification of the analysis.

These approximating assumptions are not always reasonable for biochemical systems. In the following we will review the hierarchy of analyses developed for chemical reactions depending on which assumptions can be made.

First, consider the case when no additional approximating assumptions are made. Then the behaviour of the system will depend on the positions of molecules in space, therefore the state of the system will include coordinates of every molecule.

This is the most detailed level of modelling which is usually considered for biochemical systems. Correctness of various abstractions is measured using this microscopic level as the standard.

2.3.1 *Smoluchowski's diffusion-limited reactions theory*

One mathematical treatment of microscopic modelling was given by Smoluchowski in his theory of kinetics of coagulating particles [Smoluchowski, 1917, Keizer, 1982, Fange et al., 2010]. In this framework, the molecules are treated as points that diffuse in continuous space and time.

In case of uni-molecular reactions, i.e. reactions which have only a single reactant and its stoichiometric coefficient is one, the theory is simple. Since we ignore internal states of molecules, for each small period of time each molecule will have an equal probability to undergo the reaction. Therefore the reactant undergoes an *exponential decay*, and the rate of this reaction can be computed as

$$v = \lambda[A]$$

where $[A]$ is the concentration of the reactant and λ is the *decay constant*. Note that this corresponds to the mass action law for this reaction with $k = \lambda$.

Reactions which involve more than two reactant molecules simultaneously, i.e. for which $\sum_{i=1}^{n} \alpha_i > 2$, are assumed to be non-elementary, since the probability of more than two molecules colliding simultaneously is zero. In order to treat them, one has to decompose them to elementary reactions first.

The most interesting case then is the bimolecular reaction, when two molecules react with each other. In Smoluchowski's model, a reaction happens instantaneously when the distance between two reactant molecules reaches a certain *reaction radius* R, which is the only parameter of the reaction. The reasoning behind this is that bimolecular reaction rates are assumed to be *diffusion-limited*: the probability of a reaction occurring when the reactants meet in space is so high that the rate is determined only by diffusion speed. In a sense this is the inverse of the well-mixed assumption mentioned earlier.

This framework leads to a kinetic theory of such reactions, i.e. a description of this process from macroscopic perspective. As such, it treats the system as a whole, and does not address for example, phe-

nomena arising from inhomogeneous initial distributions of chemicals. Later we will review more detailed treatments.

Consider a reaction $A + B \to A$, with reaction radius R. First, assume that there is one A molecule and a large amount of B. If we look at distribution of B relative to the A molecule, we will find a gradient, because B is depleted in the vicinity of A. This gradient can be calculated as follows [Rice, 1985]. Let the time-dependent density distribution of B around A be

$$\rho(r,t) = [B](r,t)/[B_0] \tag{2}$$

where $[B_0]$ is the initial concentration of B, $[B](r,t)$ is the transient concentration of B relative to A (here only the spherically symmetric case is considered), r is the distance to A. The initial distribution is

$$\rho(r,0) = \begin{cases} 1, r > R \\ 0, r \leqslant R \end{cases} \tag{3}$$

which means that at time $t = 0$ the concentration of B is equal to $[B_0]$ everywhere except in the sphere of radius R around the A molecule.

Diffusion is considered in $\mathbb{R}^3$, therefore the boundary conditions are

$$\begin{aligned} \rho(r \to \infty, t) &= 1, t \geqslant 0 \\ \rho(R,t) &= 0, t \geqslant 0 \end{aligned} \tag{4}$$

The first condition states that the concentration of B tends to its initial value far from A. The second condition states that on the spherical boundary of radius R around the A molecule B is always depleted.

Since A acts as a sink, there will be diffusion of B towards A, which will form a gradient of B. To compute the speed of this diffusion, Fick's first law is used. This law was first empirically discovered by Adolf Fick in 1855, and later derived from the Brownian motion theory, see for example [Berg, 1993]. It relates the diffusive *flux*, i.e. measure of amount of substance which crosses a unit area per unit time, to the concentration of the diffusing species. In the basic formulation, it states:

$$J = D_B \nabla [B]$$

where J is flux of B, i.e. the number of particles per unit time crossing unit area, and D_B is called the *diffusion coefficient* of B (also diffusivity, or Fick's diffusion coefficient). ∇ is the gradient operator in space coordinates.

In our case, this simplifies to:

$$J = D \frac{\partial [B]}{\partial r}$$

where D is the mutual diffusion coefficient, $D = D_A + D_B$, the sum of diffusion coefficients of A and B. The total number I of B molecules crossing a sphere of radius x with centre at 0 per unit time is then

$$I(x) = 4\pi x^2 J(x) = 4\pi x^2 D \left.\frac{\partial[B]}{\partial r}\right|_{r=x}$$

Consider the quantity $I(x) - I(x + dx)$, which is the speed of flow (*current*) of B towards A crossing the sphere of radius x, minus the current crossing the sphere of radius $x + dx$. This is the net loss of B within a spherical shell of thickness dx per unit time. The volume of this shell is $4\pi x^2 dx$. Dividing the net loss of B in the shell by this volume gives the rate of loss of concentration of B,

$$\frac{\partial[B]}{\partial t} = D\left(\frac{\partial^2[B]}{\partial r^2} + \frac{2}{r}\frac{\partial[B]}{\partial r}\right)$$

or, using (2)

$$\frac{\partial \rho}{\partial t} = D\left(\frac{\partial^2 \rho}{\partial r^2} + \frac{2}{r}\frac{\partial \rho}{\partial r}\right)$$

Generalizing the spherically symmetric case to arbitrary three dimensional space, it can be shown that the *Laplacian operator*

$$\Delta = \nabla^2 = \frac{\partial^2}{\partial x^2} + \frac{\partial^2}{\partial y^2} + \frac{\partial^2}{\partial z^2}$$

should be used to express the diffusion:

$$\frac{\partial \rho}{\partial t} = D\Delta\rho$$

This is the well known heat equation, which can be solved analytically using the initial condition (3) and the boundary conditions (4):

$$\rho(r, t) = 1 - \frac{R}{r}\operatorname{erfc}\left(\frac{R - r}{(4Dt)^{1/2}}\right)$$

where $\operatorname{erfc}(x) = \frac{2}{\sqrt{\pi}}\int_x^\infty e^{-t^2} dt$ is the error function complement. The steady state distribution of ρ is then

$$\rho(r, \infty) = 1 - \frac{R}{r}$$

Now we can compute $I(R)$, which is actually the rate of reaction of B with the A reactant:

$$I(R) = 4\pi RD(1 + R(4\pi Dt)^{-1/2})[B_0]$$

Now consider the case of many A molecules sufficiently far from each other such that the reactions of B with them do not affect each other.

Then the rate of reaction per unit volume of all B reactants with all A reactants will be $I \cdot [A]$:

$$-\frac{d[A]}{dt} = \frac{d[B]}{dt} = 4\pi RD(1 + R(4\pi Dt)^{-1/2})[B_0][A]$$

It follows that the reaction rate coefficient as it is usually defined using law of mass action is

$$k(t) = 4\pi RD(1 + R(4\pi Dt)^{-1/2})$$

Note that the rate coefficient depends on time. In the long time limit, the steady state rate constant is

$$k(\infty) = 4\pi RD$$

This result is typically extrapolated, without justification, to any bimolecular reactions with any number of molecules [Waite, 1957]. Although this derivation is intuitive and rests upon many assumptions, it is possible to derive the same formulae more rigorously using pair distribution functions [Kotomin and Kuzovkov, 1996, Doi, 1976, Waite, 1957]. The result is convenient, because it allows using the law of mass action for macroscopic models with rates derived from microscopic parameters (diffusion coefficients and the reaction radius); i.e. the macroscopic model is derived from microscopic one. Note that this derivation does not use the well-mixed assumption, therefore the reaction rate depends on diffusion speed.

A reversible reaction in this model cannot be described as two independent reactions. In reaction $A + B \rightleftharpoons C$, a pair of A and B which has been just produced has a much greater chance of collapsing back to C than a random pair of A and B [Berlin et al., 1980, Agmon, 1984]. This means that only a portion of $C \to A + B$ reactions will be effective. It can be shown [Andrews and Bray, 2004] that the equilibrium forward reaction rate constant will be:

$$k(\infty) = \frac{4\pi R_b D}{1 - R_b/R_u} \tag{5}$$

where R_b and R_u are forward (binding) and backward (unbinding) reaction radii.

2.3.2 *Doi model*

A straightforward generalization of Smoluchowski's theory is to consider reactions which are not completely diffusion-limited: reaction rates will depend not only on diffusion speeds, but also on intrinsic probabilities of reactive interactions. Following [Isaacson, 2012], we will refer to this model as Doi model. It was introduced in [Teramoto and Shigesada, 1967] and [Doi, 1976].

In this model, a bimolecular reaction occurs with fixed probability k_0 per unit time when two reactants are separated by a distance less than R. k_0 is called *intrinsic reaction rate*. The kinetic theory can be derived in a way similar to the diffusion-limited case, only replacing sink boundary condition in (4) with flux boundary condition

$$4\pi R^2 D \left.\frac{\partial \rho(r,t)}{\partial t}\right|_{r=R} = k_0 \rho(R,t)$$

It specifies that absorption of B molecules at the distance R from an A does not happen instantaneously, but with a finite speed determined by k_0. From this new boundary condition a new expression for reaction rate constant of an irreversible reaction can be derived [Rice, 1985]:

$$k(\infty) = \frac{4\pi R D k_0}{4\pi R D + k_0} \tag{6}$$

2.3.3 *Smoluchowski equation*

The kinetic theories reviewed above may be useful to analyse spatially homogeneous systems at thermodynamic limit, but in case of biological systems it is often desirable to model stochastic effects and inhomogeneous spatial distributions of molecules.

The general equation for temporal evolution of Doi model of reaction $A + B \to C$ in d-dimensional space can be formulated as follows [Isaacson, 2012]. Let $\mathbf{q}_l^a \in \mathbb{R}^d$ denote the position of lth molecule of A when the total number of A is a. The state vector of A is then $\mathbf{q}^a = (\mathbf{q}_1^a, \ldots, \mathbf{q}_a^a) \in \mathbb{R}^{da}$. Let $f^{(a,b,c)}(\mathbf{q}^a, \mathbf{q}^b, \mathbf{q}^c, t)$ be the probability density of a molecules of A, b molecules of B and c molecules of C to be located in positions $\mathbf{q}^a$, $\mathbf{q}^b$ and $\mathbf{q}^c$ at time t. Let D_A, D_B and D_C be the diffusion constants of A, B and C. The evolution of $f^{(a,b,c)}$ is given by

$$\frac{\partial f^{(a,b,c)}}{\partial t}(\mathbf{q}^a, \mathbf{q}^b, \mathbf{q}^c, t) = (L + R) f^{(a,b,c)}(\mathbf{q}^a, \mathbf{q}^b, \mathbf{q}^c, t) \tag{7}$$

This is called *Smoluchowski equation* (without the convection term), a variant of *Fokker-Planck equation* [Kadanoff, 2000]. L is the diffusion operator which specifies how positions of molecules evolve by diffusion, R is the reaction operator which specifies how the system is changed by reactions.

The definition of L simply states Fick's second law of diffusion for every molecule. This law predicts how concentration of a diffusing species changes over time and space:

$$\frac{\partial [A]}{\partial t} = D_A \Delta [A] \tag{8}$$

It can be derived from Fick's first law and mass conservation in the absence of chemical reactions. This is also equal to the heat equation.

In case of the Smoluchowski equation, it is applied not to concentrations, but to probability densities of individual molecules:

$$Lf^{(a,b,c)} = \left(D_A \sum_{l=1}^{a} \Delta_l^a + D_B \sum_{m=1}^{b} \Delta_m^b + D_C \sum_{n=1}^{c} \Delta_n^c \right) f^{(a,b,c)}$$

where Δ_l^a is the Laplacian operator in coordinate $\mathbf{q}_l^a$.

The definition of R is more involved. Let

$$\mathbf{q}^a \backslash \mathbf{q}_l^a = (\mathbf{q}_1^a, \ldots, \mathbf{q}_{l-1}^a, \mathbf{q}_{l+1}^a, \ldots, \mathbf{q}_a^a)$$
$$\mathbf{q}^a \cup \mathbf{q} = (\mathbf{q}_1^a, \ldots, \mathbf{q}_a^a, \mathbf{q})$$

Denote $\mathbb{1}_{[0,R]}(r)$ the indicator function on the interval $[0, R]$, and $B_l^c = \{\mathbf{q} \in \mathbb{R}^d \,|\, |\mathbf{q} - \mathbf{q}_l^c| \leqslant R/2\}$ the set of points a reactant could be at to produce a C molecule at point $\mathbf{q}_l^c$. C is created in the middle point between A and B. Then the reaction operator R can be defined as

$$(Rf^{(a,b,c)})(\mathbf{q}^a, \mathbf{q}^b, \mathbf{q}^c, t) =$$
$$k_0 \Bigg(\sum_{n=1}^{c} \int_{B_n^c} f^{(a+1,b+1,c-1)}(\mathbf{q}^a \cup \mathbf{q}, \mathbf{q}^b \cup (2\mathbf{q}_n^c - \mathbf{q}), \mathbf{q}^c \backslash \mathbf{q}_n^c, t)\, d\mathbf{q} -$$
$$\sum_{l=1}^{a} \sum_{m=1}^{b} \mathbb{1}_{[0,R]}(|\mathbf{q}_l^a - \mathbf{q}_m^b|) f^{(a,b,c)}(\mathbf{q}^a, \mathbf{q}^b, \mathbf{q}^c, t) \Bigg)$$

The sum with an integral on the second line gives the total contribution of all states which could, as a result of $A + B \to C$ reaction, bring the system into the state $(\mathbf{q}^a, \mathbf{q}^b, \mathbf{q}^c)$. This contribution to the change of probability density is non-negative. The third line gives the negative contribution of possibility to leave the state $(\mathbf{q}^a, \mathbf{q}^b, \mathbf{q}^c)$ as a result of a reaction.

(7) is a system of partial integral differential equations (PIDEs). It spans all possible values of (a, b, c), and, although for this reaction it is finite (provided that the initial probability distribution spans a finite set of (a, b, c)), it may be infinite in general.

2.3.4 *Stochastic simulations*

Smoluchowski equation, like (7), has continuous space and time variables, and therefore is very difficult to solve even numerically. When the number of molecular configurations is infinite the solution is usually impossible except in very simple cases, which may be analytically solvable. The method of choice for analysis of this model is *stochastic simulation*.

This simulation can be thought of as a (potentially approximate) Monte-Carlo sample of one value of a random variable whose PDF is f defined above. Since f is a function of time, it is sampled at a set of time points, starting from some known initial condition at $t = 0$, usually a

point mass probability density representing a deterministic initial state. Then this state is updated according to the Smoluchowski equation or some approximation of it to represent a probable situation after a short period of time Δt.

There are several methods to compute the update for the simulation. In [van Zon and ten Wolde, 2005] an event-driven approach is proposed, named Green's function reaction dynamics (GFRD). The simulation algorithm can be summarized as follows:

1. Initialize positions for every molecule, set $t := 0$.
2. For every bimolecular reaction, and for every pair of its reactants, calculate the probability distribution of *time* of the reaction occurring between them, ignoring all other molecules and reactions. This distribution can be computed by numerically integrating (7) for the case $a = 1, b = 1, c = 0$. For every uni-molecular reaction, the corresponding distribution is the exponential distribution with λ being the reaction rate.
3. Draw a sample from each distribution computed on the previous step, this will be the next reaction time for the corresponding reaction. Apply the reaction to the molecule, or the pair of molecules, with the lowest next reaction time τ.
4. Adjust positions of all molecules, drawing shifts from normal distributions $N(0, 2\sqrt{D\tau})$.
5. Update the time $t := t + \tau$.
6. Go to step 2.

The computation of a bimolecular reaction's time is possible by a numerical solution of the spatio-temporal integral, thanks to the assumption that no other reaction happens. The solution involves computation of a Green's function for the $L + R$ operator, hence the name of the method.

This approach is suitable for systems with relatively long time intervals between reactions, which is the case with slow diffusion and few molecules. It is exactly this kind of situation where the approximations used by other treatments fail, when stochastic and diffusion-related effects dominate the dynamics.

As an example, the authors apply their method to analyse stochastic fluctuations of gene expression, and show that spatial effects play a major role. They call the effect *spatial fluctuations*, as opposed to stochastic fluctuations of the well-mixed model which are usually considered in the literature when studying noise in gene expression [Singh et al., 2012, Munsky et al., 2009].

If the frequency of reaction events in the system is high, the event-driven approach will be inefficient, because each step is computationally

expensive. In this case, a discrete time approach is more desirable. In [Andrews and Bray, 2004] a constant time step is used. Molecules are first moved to new positions according to Fick's diffusion model, and then those pairs which are closer than their reaction radius react. This procedure ignores potential reactions that could have happened during the update period, therefore the smaller is Δt, the more precise the simulation will be. In order to treat the reversible reaction problem described above, the monomolecular dissociation places the products slightly further than the binding radius. The effective reversible reaction rate then approaches (5) when $\Delta t \to 0$.

Using a discrete time update results in limited spatial resolution of the simulation. This means that effective reaction rate in this model depends on Δt. In order to have the simulation match the experimental data, we have to correctly specify the reaction parameters, in this case binding and unbinding radii and diffusion coefficients. While the latter is possible to know from experiments, the radii have to be fit to the observed reaction rates. In this model, this fitting has to be done with respect to specific Δt. In [Andrews and Bray, 2004] a numerical approximation is used to match R_b and R_u to the supplied effective reaction rates, and limit cases of small and large Δt are treated analytically.

To analyse a chemical system using stochastic simulations, one repeatedly performs a number of simulations, and then extracts quantities of interest from the simulated samples. Typically the results are statistics of certain variables in the samples, e.g. the mean or variance of counts of a certain molecule type at a certain time, mean time until a certain event, mean frequency of a certain reaction, a correlation coefficient of two variables etc.

An example of such analysis is given in Figure 4. It is a simple demonstration of how spatial distribution of slowly diffusing molecules affects reaction rates. The reaction being modelled is $A + B \to C$, with 200 A, 200 B and no C molecules initially. The space is a cube with side 10^{-5} meters and periodic boundary conditions. Other parameters are: diffusion coefficient of all molecules $D = 10^{-13}\mathrm{m}^2/\mathrm{s}$; reaction radius $R = 2.5 \cdot 10^{-8}\mathrm{m}$; intrinsic reaction rate $k_0 = 5 \cdot 10^{-19}\mathrm{m}^3/\mathrm{s}$.

Three different initial conditions were used. The first one is the uniform distribution of A and B molecules over the spatial domain, illustrated in Figure 4a: this corresponds to the usually considered case of thermodynamic equilibrium. In the second condition A and B molecules are put in two different halves of the cube, Figure 4b. Such a situation may occur, for example, if two adjacent tissues interact using two morphogens. In the third condition, A and B molecules are put near each other, Figure 4c. This artificially reflects the situation when both A and B are produced in a single reaction.

100 simulations of each condition with different random seeds were performed using GFRD algorithm. The results are summarized in Figure 4d in the form of a plot showing mean count of C molecules over

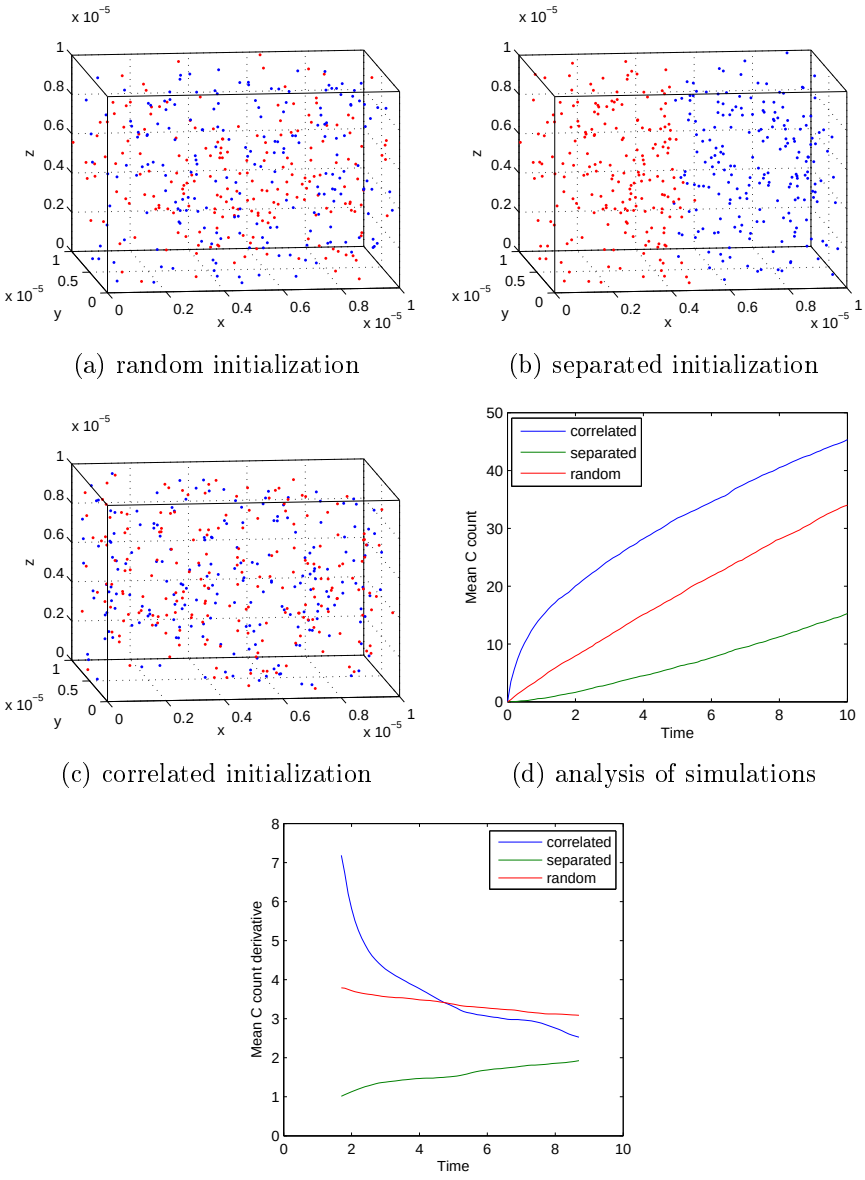

(a) random initialization

(b) separated initialization

(c) correlated initialization

(d) analysis of simulations

(e) estimated reaction rates

Figure 4: Simulations of an irreversible reaction. (a, b, c) show different initial conditions used, with A molecules in red and B in blue. (d) shows mean value of C count over time in 100 simulation runs. (e) shows numerically estimated derivatives of (d), indicating reaction rates. The simulations were done using eGFRD package, which implements GFRD algorithm.

time. The mean is taken over 100 simulations of each type. It is evident that the dynamics of the reaction is very different in each condition at the beginning of simulations, especially on the plot of the derivative of mean C count, Figure 4e. This quantity is proportional to the corresponding reaction rate. Later the dynamics become similar due to the system shifting towards thermodynamic equilibrium. The case of correlated initial condition illustrates the problem of modelling reversible reactions mentioned earlier. If a single reaction produces multiple molecules, their positions will be correlated. If these molecules can then react with each other, the dynamics of this reaction will be significantly different from what would be expected in the thermodynamic equilibrium case.

2.4 MODELLING OF WELL-MIXED COMPARTMENTS

Now consider the case when diffusion is fast compared to reaction rates. In this condition, diffusion does not play a significant role in the dynamics of the system. Instead, the dynamics are determined only by number of molecules and the probability of reactions occurring when the molecules are close enough, a concept from Doi model reviewed earlier.

Gillespie [1992] adopts a model similar to Doi model, but in the thermal equilibrium case. The exact assumptions that he uses are:

1. The probability that the centre of any randomly selected molecule of the system will be found to lie inside any container subregion of volume $\Delta\Omega$ is equal to $\Delta\Omega/\Omega$, where Ω is the total volume of the system. I will call it *well-mixed* assumption.

2. The velocity of every molecule follows a Maxwell-Boltzmann distribution. This asserts that the system is in thermal equilibrium.

From these assumptions he derives that for each reaction j, there exists a constant c_j such that $c_j dt$ is the probability that a randomly selected combination of reactants of reaction j at time t will react during the infinitesimal time interval $[t, t+dt)$. This statement means that chemical reaction systems evolve as a *continuous time Markov chain*. c_j is called *probability rate constant*. Note that probability rate constant is analogous to reaction rate constant defined for the mass action law. The precise relation between them will be derived later (18).

We can define the *propensity function* for reaction j:

$$a_j(\nu) = c_j \binom{\nu}{\alpha_j} \tag{9}$$

where $\nu(t) = (\nu_1, \ldots, \nu_n)$ is the state vector for n chemical species participating in these reactions, $\nu_i(t)$ is the count of molecules of type i at time t. The term $\binom{\nu}{\alpha_j} = \prod_{i=1}^{n} \binom{\nu_i}{\alpha_{ji}}$ gives the number of possible

combinations of reactants in state ν. Therefore $a_j(\nu)dt$ is the probability, given that the system is in state ν at time t, that one reaction j will occur in the interval $[t, t+dt)$. This allows describing transition probabilities in the Markov chain easily.

Writing the Kolmogorov forward equation for this Markov chain, we obtain the *chemical master equation (CME)*:

$$\frac{d\pi_\nu}{dt} = \sum_{j=1}^{m} a_j(\nu + \alpha_j - \beta_j)\pi_{\nu+\alpha_j-\beta_j} - a_j(\nu)\pi_\nu \tag{10}$$

where m is the number of chemical reactions, $\pi_\nu = \pi_\nu(t)$ is the probability of the system being in state ν at time t. The CME is a potentially infinite system of linear coupled ODEs.

Intuitively, (10) is similar to the Smoluchowski equation, e.g. (7), with spatial variables dropped, diffusion operator L discarded and the integral in the reaction operator R solved using the assumptions. However, the rigorous derivation is complicated.

CME has been known and used to analyse chemical systems long before this derivation was done [McQuarrie, 1967, Gillespie, 1977]. Well-mixed chemical systems were postulated to behave like a jump Markov process with states defined by counts of chemical species, and state transitions following the law of mass action. Then a Kolmogorov forward equation was written for this process, which is identical to (10). The derivation done by Gillespie has shown that this model has a valid microscopic basis.

CME is much easier to analyse than (7), and a number of exact solutions for various systems is known, mainly for means of molecule counts and for chemical equilibrium limits [McQuarrie, 1967, Jahnke and Huisinga, 2007, Gadgil et al., 2005]. If the number of possible states of the system is low enough, it may be possible to solve the CME numerically.

Here is the CME for $A + B \xrightarrow{\lambda} C$ system, which is supposed to start with two A and two B molecules in the beginning, i.e. the initial state is $\nu(0) = (2, 2, 0)$:

$$\begin{aligned}
\frac{d\pi_{(2,2,0)}}{dt} &= -4\lambda\pi_{(2,2,0)} \\
\frac{d\pi_{(1,1,1)}}{dt} &= 4\lambda\pi_{(2,2,0)} - \lambda\pi_{(1,1,1)} \\
\frac{d\pi_{(0,0,2)}}{dt} &= \lambda\pi_{(1,1,1)}
\end{aligned}$$

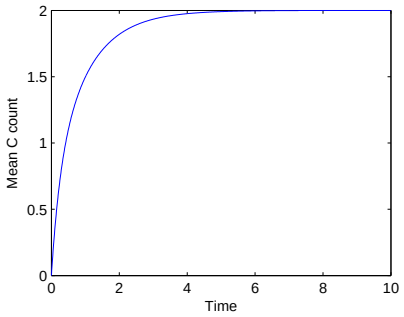

Figure 5: The exact solution of the $A + B \xrightarrow{1} C$ system with 2 initial A and B molecules.

In this case the system has only three states reachable with non-zero probability, therefore its CME is finite, and is in fact quite simple. Its analytical solution is:

$$\begin{aligned}
\pi_{(2,2,0)} &= e^{-4\lambda t} \\
\pi_{(1,1,1)} &= -\frac{4}{3}e^{-4\lambda t} + \frac{4}{3}e^{-\lambda t} \\
\pi_{(0,0,2)} &= \frac{1}{3}e^{-4\lambda t} - \frac{4}{3}e^{-\lambda t} + 1
\end{aligned} \tag{11}$$

From this we can compute, for example, mean C count, which is $2\pi_{(0,0,2)} + \pi_{(1,1,1)}$. It is plotted in Figure 5 for $\lambda = 1$.

2.4.1 *Approximate solutions of the CME*

In the most general case, when the system contains species whose count is unbounded, and there is a second order reaction, the exact analytical solution of the CME is not known. One has to resort to an approximate solution.

One class of these approximations aims to reduce the state space of the system to a manageable size, while preserving the essential dynamics. An algorithm called *finite state projection* [Munsky and Khammash, 2006] provides a way to solve the CME approximately considering a finite subset of states, and at the same time to calculate the approximation error. The idea is to ignore the states with negligible probability. The error may be reduced by considering more states, which can be done on-line. The resulting problem is a finite system of linear ODEs, for which many efficient solution methods exist. There are a number of optimizations and variations of this algorithm [Peles et al., 2006, Munsky and Khammash, 2007, Munsky et al., 2007, Henzinger et al., 2009]. Mainly they try to tune the selection of the set of states dynamically to achieve best precision/computation speed trade-off.

While the finite state projection algorithm makes the problem directly solvable, in practice the number of significant states can still be huge, especially when the number of chemical species is large. The state

space grows exponentially with the number of species, and the algorithm suffers from the curse of dimensionality. A complementary approach is to aggregate the states which are close to each other and do not have to be distinguished [Hegland et al., 2007]. Typically states are judged to be close if species' counts in them are sufficiently similar so that the difference does not affect quantities of interest significantly. After applying a finite state projection, a change of variables in the ODE system is performed, such that the new variables are probabilities of aggregated states. When the new system, which is still linear, is solved, an inverse transformation is applied to obtain the approximate probabilities of the original states. Error bounds can also be computed for this approximation [Hegland, 2008].

A different approach to approximate the CME solution is to transform it to a system of stochastic differential equations (SDEs). An SDE is a differential equation in which one or more terms is a stochastic process, making the SDE's solution a stochastic process itself. The result of transformation of CME into an SDE is called the *chemical Langevin equation* [Gillespie, 2000]. Because it is an important step towards understanding deterministic approximations, I will outline the derivation.

Let's introduce *random variables* $X_i(t) = \nu_i(t)$ which track the counts of ith chemical species in the system. Suppose the state of the system at time t is $\boldsymbol{\nu}_t$. Then for any $\tau > 0$

$$X_i(t+\tau) = \nu_{ti} + \sum_{j=1}^{m} K_j(\boldsymbol{\nu}_t, \tau)(\beta_{ji} - \alpha_{ji}), \quad i = 1, \ldots, n \tag{12}$$

where m is the total number of reactions and $K_j(\boldsymbol{\nu}_t, \tau)$ is a random variable governing the dynamics of reaction j starting from state $\boldsymbol{\nu}_t$. ν_{ti} is the ith component of the initial state vector $\boldsymbol{\nu}_t$. $K_j(\boldsymbol{\nu}_t, \tau)$ represents the number of times reaction j is going to occur during the interval τ, *considering also all other reactions*. Therefore in general, all K_j will depend on each other. So far this is just a reformulation of the CME: finding K_j is equivalent to solving the CME. Now we will find a simple approximation for K_j. Consider two assumptions for τ:

1. *Leap condition*: τ is so small that the change of the propensity functions in the time interval $[t, t+\tau]$ is negligible: $a_j(\mathbf{X}(t')) \approx a_j(\boldsymbol{\nu}_t), t' \in [t, t+\tau]$. This means that the reaction events in that time interval will be independent of each other, and $K_j(\boldsymbol{\nu}_t, \tau)$ will be simply the number of times reaction j occurs in duration τ if the propensity function is constant $a_j(\boldsymbol{\nu}_t)$, as if no other reactions have occurred. Then each $K_j(\boldsymbol{\nu}_t, \tau)$ is an independent Poisson random variable $\mathcal{P}_j(a_j(\boldsymbol{\nu}_t)\tau)$.

2. In addition to the leap condition, τ is so large that the expected number of occurrences of each reaction j in $[t, t+\tau]$ is much greater than 1:

$$E[\mathcal{P}_j(a_j(\boldsymbol{\nu}_t)\tau)] = a_j(\boldsymbol{\nu}_t)\tau \gg 1 \tag{13}$$

This allows approximating the Poisson random variables by normal random variables with the same mean and variance.

The assumptions limit τ from both sides, and for some systems such a τ does not exist. Propensity functions depend on non-negative powers of molecule counts, and the counts usually change by at most two in each reaction. Therefore if the number of reaction occurring during the interval is much smaller than the smallest count of molecular species, the leap condition will be fulfilled. This can always be satisfied if molecule counts are much larger than 1. Large molecule counts generally make it easier to satisfy (13) as well, because the propensity functions will have high values.

Using these conditions, we can rewrite (12) into

$$Z_i(t+\tau) = \nu_{ti} + \sum_{j=1}^{m} \mathcal{N}_j(a_j(\boldsymbol{\nu}_t)\tau, a_j(\boldsymbol{\nu}_t)\tau)(\beta_{ji} - \alpha_{ji}) =$$

$$\nu_{ti} + \sum_{j=1}^{m} (\beta_{ji} - \alpha_{ji}) a_j(\boldsymbol{\nu}_t)\tau + \sum_{j=1}^{m} (\beta_{ji} - \alpha_{ji})[a_j(\boldsymbol{\nu}_t)\tau]^{1/2} \mathcal{N}_j(0,1),$$

$$i = 1, \ldots, n$$

where $\mathcal{N}_j$ are m independent normally distributed random variables, and Z_i are the new, continuous state random variables representing the approximated counts of molecules in real domain.

Note that in this step we have converted discrete Poisson random variables for molecule counts into continuous real-valued normal variables.

If we treat τ as a *macroscopic infinitesimal* dt, i.e. a quantity much smaller than the time scale of interest, we can write a standard-form Langevin equation for a multivariate continuous Markov process:

$$\begin{aligned} Z_i(t+dt) = Z_i(t) + \sum_{j=1}^{m} (\beta_{ji} - \alpha_{ji}) a_j(\boldsymbol{Z}(t))dt + \\ \sum_{j=1}^{m} (\beta_{ji} - \alpha_{ji}) a_j^{1/2}(\boldsymbol{Z}(t)) \mathcal{N}_j(t)(dt)^{1/2} \end{aligned} \tag{14}$$

where $\mathcal{N}_j(t)$ are normal random variables with zero mean and unit variances, and $\mathcal{N}_j(t)$ is independent of $\mathcal{N}_{j'}(t')$ if $j \neq j'$ and $t \neq t'$. This equation approximates the jump Markov process described by the CME as a continuous Markov process.

This SDE can be analysed numerically, using stochastic simulations in a way similar to microscopic simulations mentioned before. However, here the state is a real vector of only n dimensions, representing average counts of each molecular species. In the microscopic simulations the state is an $\sum_{i=1}^{n} 3\nu_i$-dimensional real vector representing the positions of all molecules in 3D space. To simulate a system with such a large state space is much harder computationally. Efficient procedures for simulating SDEs exist [Higham, 2001].

2.4.2 *Moment closure*

A different approach to solving CME is to rewrite it in terms of *moments* of random variables $X_i(t)$. Then we can simplify the resulting system using some additional assumptions, obtaining a *moment closure (MC)*. This approach has a long history: it has been used to analyse stochastic systems in the fields of ecology [Whittle, 1957], demographics [Goodman, 1953], epidemiology [Grenfell et al., 1995] and statistical physics [Levermore, 1996]. Traditionally they were derived manually. Recently, methods for automatic MC derivation were proposed [Gillespie, 2009a, Hespanha and Singh, 2005, Vidal et al., 2010] for biochemical reaction systems.

Because we will use this method to analyse the community effect system, I will outline a derivation of the formula. It is based on usage of probability-generating functions from [Vidal et al., 2010].

A kth order *raw moment* of an integer-valued random variable X is $\mu^k = E[X^k] = \sum_x x \cdot \text{Prob}(X^k = x) = \sum_x x^k \text{Prob}(X = x)$. Given $\mathbf{k} \in \mathbb{N}^n$ we can define a *mixed moment* of a vector of n random variables $\mathbf{X}$ as $\mu^{(\mathbf{k})} = E[\mathbf{X}^{\mathbf{k}}] = E[\prod_{i=1}^{n} X_i^{k_i}]$. The order of a mixed moment is $\sum_{i=i}^{n} k_i$. Note that all the moments do not necessarily exist for all distributions.

We can also define joint *factorial moment* of the same variables:

$$\mu^{(\underline{\mathbf{k}})} = E[\mathbf{X}^{(\underline{\mathbf{k}})}] = E[X^{(\underline{k_1})} \cdots X^{(\underline{k_n})}] = \sum_{x_1} \cdots \sum_{x_n} \left[\prod_{i=1}^{n} x_i^{(\underline{k_i})} \right] \text{Prob}(\mathbf{X} = \mathbf{x}) \tag{15}$$

where $x^{\underline{y}} = x(x-1)(x-2)\cdots(x-y+1)$ is the *falling factorial*, or falling power. The raw and factorial moments are related, and can be computed from each other. In particular, $\mu^{\underline{1}} = \mu^1$, $\mu^{\underline{2}} = \mu^2 - \mu^1$. A general formula can be derived for the conversion between them using Stirling's numbers, but we will not need to convert higher-order moments.

A *probability-generating function* of a vector of integer-valued random variables $\mathbf{X}$ is

$$\phi(z) = E[z^{\mathbf{X}}]$$

$\mathbf{z}$ is a vector of *formal variables* which is introduced with this function, of the same dimension as $\mathbf{X}$. In general these formal variables are not meant to represent numbers, although we will sometimes substitute numbers for them.

One property of probability-generating functions that we will use is that by taking formal derivatives of it we can obtain factorial moments of the associated random variables:

$$\left. \frac{\partial^{\mathbf{k}} \phi}{\partial z^{\mathbf{k}}} \right|_{z=1} = \left. \frac{\partial^{k_1}}{\partial z_1^{k_1}} \cdots \frac{\partial^{k_n} \phi}{\partial z_n^{k_n}} \right|_{z=1} = \mu^{(\underline{\mathbf{k}})}$$

Consider the probability-generating function $\phi(z,t)$ for the random variable vector $\mathbf{X}(t)$ that tracks the counts of molecules of each type in a chemical system. It is possible to rewrite the CME (10) into the following PDE, which is the general evolution equation for the probability-generating function [Erdi and Toth, 1992]:

$$\frac{\partial \phi}{\partial t} = H\phi \tag{16}$$

H is a *Hamiltonian operator*

$$H = \sum_{j=1}^{m} \frac{c_j}{\alpha_j!}(z^{\beta_j} - z^{\alpha_j})\left(\frac{\partial}{\partial z}\right)^{\alpha_j}$$

where $\boldsymbol{\alpha}_j! = \prod_{i=1}^{n} \alpha_{ji}!$. It is called so by analogy to quantum physics, (16) being the analogue of the Schroedinger equation. H is a differential operator, i.e. a higher order function which takes another function as an argument and transforms it, differentiation being one of the transformations which can be applied. In this notation, multiplication by $(\frac{\partial}{\partial z_i})^k$ means taking kth derivative by z_i. Multiplication by other terms denotes the ordinary multiplication.

By taking formal derivatives of (16) and evaluating at $\boldsymbol{z} = \boldsymbol{1}$, we can produce evolution equations for arbitrary joint factorial moments of $\mathbf{X}(t)$:

$$\frac{\partial^k}{\partial z^k}\frac{\partial \phi}{\partial t}\bigg|_{z=1} = \frac{\partial}{\partial t}\frac{\partial^k \phi}{\partial z^k}\bigg|_{z=1} = \frac{d\mu^{(\underline{k})}}{dt} = \frac{\partial^k}{\partial z^k} H\phi\bigg|_{z=1}$$

All derivatives of ϕ in the last expression will be replaced by corresponding factorial moments.

In this way, we can obtain evolution equations for any moments of $\mathbf{X}(t)$. For example, the mean of molecular species i is

$$\mu^{(k)}(t) = \mu^{(\underline{k})}(t),$$
$$k_j = \delta_{ij} = \begin{cases} 1, i = j \\ 0, i \neq j \end{cases}$$

In general, an evolution equation for a moment of order N will depend on moments of orders up to $N + M - 1$, where M is the maximum order of a reaction in the system. Therefore, for first order systems, this procedure allows to obtain closed, finite and linear ODE systems for time evolution of any finite moment, which can be readily solved.

In the more interesting case of second order systems, the equation for any moment of order N will depend on moments of order $N + 1$, they in turn will depend on moments of order $N + 2$ and so on. The system of equations forms an infinite cascade, which is impossible to solve numerically, just as the CME itself. In order to solve it approximately, we

have to truncate the cascade. This is done by assuming a functional relationship between moments of order N and lower order moments for a certain N. The truncation is called *moment closure*.

One example of such a relationship is the assumption of zero covariances between counts of molecular species: $\mathrm{Cov}(X_i, X_j) = 0$. This allows expressing second order moments in terms of first order ones: $E[X_i X_j] = E[X_i]E[X_j]$. In this way a set of equations for the time evolution of first order moments, i.e. the mean molecule counts, may be derived. These equations will be equal to reaction rate equations, which will be more rigorously derived later. Note that this assumption implies zero variances for the variables as well, which makes this analysis disregard the stochastic effects. In addition it poses a technical difficulty which prevents rigorous analysis of this method: the zero-variance discrete random variable can only assume a single value, in this case a non-negative integer, therefore the ODEs for time evolution of their means do not make sense. This is because this treatment misses a crucial step, which allows replacing integer-valued molecule counts with real numbers. This was done for the chemical Langevin equation above; later we will see how this brings a rigorous derivation of the deterministic approximation.

For now, a more useful approximation is to assume that the third order mixed central moments for all variables are zero. This assumption would be true, for example, if the variables are jointly normally distributed [Isserlis, 1918]. This is impossible since the molecule counts can only take non-negative integer values, and the normal distribution allows any real value; nonetheless this assumption works quite well in practice. The relationship between the moments is given by the following:

$$\begin{aligned} 0 = E[(X_i - E[X_i])(X_j - E[X_j])(X_k - E[X_k])] = E[X_i X_j X_k] - \\ E[X_i X_j]E[X_k] - E[X_i X_k]E[X_j] - E[X_j X_k]E[X_i] + 2E[X_i]E[X_j]E[X_k] \end{aligned} \tag{17}$$

Using this relation, any third order moment can be replaced by a non-linear expression depending on first and second-order moments of the same variables. A closed system of joint time evolution of first and second order moments can thus be derived. We will call this transformation *normal closure*.

Moment closure is typically done with help of a computer algebra system to generate the equations [Vidal et al., 2010, Gillespie, 2009a, Singh and Hespanha, 2006a]. Then an ODE solver is used to simulate the resulting non-linear system.

As an example, let's consider again the system $A + B \xrightarrow{\lambda} C$. The Hamiltonian for this system is

$$H = \lambda \cdot (z_a z_b - z_c) \frac{\partial}{\partial z_a} \frac{\partial}{\partial z_b}$$

Since this is a second order systems, the moment equations form an infinite cascade. The first two levels of this cascade, involving moments of up to third order, are

$$\begin{aligned}
\frac{dE[A]}{dt} &= -\lambda E[AB] \\
\frac{dE[B]}{dt} &= -\lambda E[AB] \\
\frac{dE[C]}{dt} &= \lambda E[AB] \\
\frac{dE[AB]}{dt} &= \lambda(E[AB] - E[A^2B] - E[AB^2]) \\
\frac{dE[A^2]}{dt} &= \lambda(E[AB] - 2E[A^2B]) \\
\frac{dE[B^2]}{dt} &= \lambda(E[AB] - 2E[AB^2])
\end{aligned}$$

The equations for the third order moments $E[A^2B]$ and $E[AB^2]$ will involve fourth order moments and so on, so the ODE system is infinite and unsolvable.

Using the normal approximation (17), we can write

$$\begin{aligned}
E[A^2B] &= E[A^2]E[B] + 2E[AB]E[A] - 2E[A]^2E[B] \\
E[AB^2] &= E[A]E[B^2] + 2E[AB]E[A] - 2E[A]E[B]^2
\end{aligned}$$

This allows obtaining the normal closure for the system:

$$\begin{aligned}
\frac{dE[A]}{dt} &= -\lambda E[AB] \\
\frac{dE[B]}{dt} &= -\lambda E[AB] \\
\frac{dE[C]}{dt} &= \lambda E[AB] \\
\frac{dE[AB]}{dt} &= \lambda(2(E[A]E[B] - E[AB])(E[A] + E[B]) - E[A^2]E[B] - E[A]E[B^2] + E[AB]) \\
\frac{dE[A^2]}{dt} &= \lambda(-4E[A]E[AB] + 4E[A]^2E[B] - 2E[A^2]E[B] + E[AB]) \\
\frac{dE[B^2]}{dt} &= \lambda(-4E[B]E[AB] + 4E[A]E[B]^2 - 2E[A]E[B^2] + E[AB])
\end{aligned}$$

Simulating it from a deterministic initial condition with 200 A and 200 B molecules using an ODE solver gives the result shown on Figure 6. The only parameter of the model is the probability rate constant λ. It is computed as $\lambda = k/\Omega$, where k is the reaction rate constant and Ω is the system volume. This relation will be derived later (18). k is computed according to (6), and all other quantities are set to the same values as for the GFRD microscopic simulation example above. Theoretically the result of this normal closure approximates that example. Note, however, that (6) is derived for partially diffusion-controlled reactions,

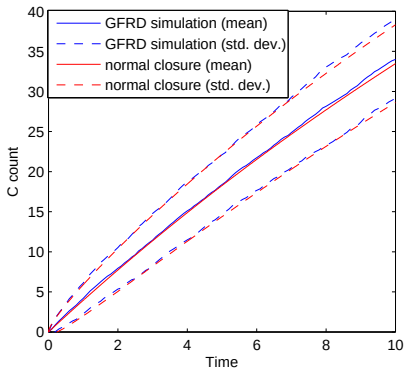

Figure 6: Normal closure and GFRD simulation results

while CME assumes well-mixed compartment at all times. Therefore this approximation will get worse with lower diffusion speed.

In Figure 6, the computed mean and standard deviation of C count is compared to those derived from GFRD simulations starting with a uniform initial condition (Figure 4a). In this case, the normal closure gives a good approximation of the Doi model simulation, and it is several orders of magnitude faster. The downside is that it is impossible to simulate the systems where the spatial distribution of molecules plays a significant role (e.g. situations on Figure 4b and Figure 4c).

2.4.3 *Gillespie algorithm*

Yet another way to obtain information from CME is through stochastic simulations. Each simulation computes a Monte-Carlo sample of a continuous time distribution described by the CME.

Simulations are preformed using a variant of *Gillespie algorithm* [Gillespie, 1977]. The basic version, called Direct Method, is as follows:

1. Initialize molecule counts $\mathbf{v} := \mathbf{v}_0$, set $t := 0$.
2. Calculate propensities a_j for all reactions using (9).
3. Choose reaction μ which happens next from the distribution $\mathrm{Prob}(\text{Reaction} = \mu) = a_\mu / \sum_{j=1}^{m} a_j$.
4. Choose the time τ of the next reaction from the exponential distribution with parameter $\lambda = \sum_{j=1}^{m} a_j$.
5. Update molecule counts $\mathbf{v} := \mathbf{v} - \boldsymbol{\alpha}_\mu + \boldsymbol{\beta}_\mu$ and time $t := t + \tau$.
6. Go to step 2.

One cycle of this algorithm, which computes a single reaction event, takes $O(m)$ time, where m is the number of reactions in the system.

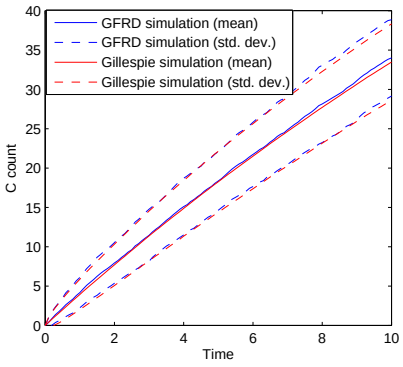

Figure 7: Gillespie algorithm and GFRD simulation results

There are optimized variants of this algorithm. *Next reaction* method [Gibson and Bruck, 2000] is $O(\log m)$. It is even possible to have $O(1)$ complexity under some conditions [Slepoy et al., 2008].

Stochastic simulations are a popular method of analysis of the CME. Theoretically it is possible to achieve arbitrary precision of the solution, using enough simulation runs. The computational complexity of simulations is proportional to the number of events we need to simulate, which in turn depends on the molecule counts in the system. Therefore this method may be problematic if the molecule counts are very high.

If *all* molecular species in the system being studied have high numbers, then arguably a chemical Langevin equation approach described earlier, or even deterministic modelling, may work well. However, it will not work if the system is heterogeneous in this respect, with some molecules being abundant and others being scarce. Also, for some species the molecule counts may vary greatly within a short time period. To address this issue, recently *hybrid* approaches have been developed [Pahle, 2009]. They work by first separating all reactions into slow and fast subsets, and then applying different simulation methods to them.

Gillespie algorithm is often called *exact* simulation algorithm, because it draws samples exactly according to probabilities described by the CME. There are also more efficient approximate simulation algorithms, notably the τ-leaping method [Gillespie, 2001]. It works well if the leap condition is satisfied, which makes it an intermediate approximation between exact simulations and the chemical Langevin equation.

Using the same $A + B \xrightarrow{\lambda} C$ example as before, Figure 7 compares result of 10000 Gillespie simulations performed in COPASI to 100 GFRD simulations with uniform initial spatial distribution of A and B. Probability rate constant λ is the same as in the moment closure example. The match between simulations is again very good. The advantage of Gillespie algorithm over moment closures is that we can control the approximation error easily: confidence bounds on every statistic can be computed, and it is straightforward to calculate the number of simulations needed to reach the desired confidence. In moment closure the

error is much harder to estimate and control. Typically it has to be compared to Gillespie simulations in order to assess its quality. To reduce the error in moment closure, one may choose a more appropriate closure type, or a higher order of the closure.

On the other hand, moment closure, being an ODE system, allows easier manipulation and formal analysis. For tasks like parameter estimation, it is vastly more efficient than a naive application of Gillespie algorithm, since the latter will require many simulations for every set of parameter values which are being tested. Another possible application is model reduction, which will be described later in Chapter 3.

2.4.4 *Deterministic modelling*

The final approximation of dynamics of chemical reaction systems is the deterministic model, called *reaction rate equation (RRE)*. It is the most widely used model, because of its simplicity and efficiency.

The derivation of RRE rests upon a further approximating assumption called *thermodynamic limit*. It is defined as the limit where the system volume Ω tends to infinity, while concentrations of the chemical species are preserved. In other words, we consider Ω as a large value, such that Ω^{-1} can be taken to be zero.

In the thermodynamic limit, all counts of chemical species are infinitely large, but the concentrations are finite. Intuitively, this allows neglecting stochastic fluctuations of molecular counts, which makes this treatment based on the thermodynamic limit deterministic. In the following, we will outline the formal derivation of the RRE, which boils down to removing the stochastic term from the chemical Langevin equation, turning it into an ODE system. This will also allow deriving exactly the relationship between reaction rates and probability rate constants.

We start from the leap condition. It is proven in [Gillespie, 2009b] that close to thermodynamic limit, the second condition of the chemical Langevin equation will also hold, therefore (14) holds.

Next, we observe that for zero-, uni- and bimolecular elementary reactions the quantity a_j/Ω, where a_j is the reaction's propensity function, is asymptotically constant when going to thermodynamic limit (although it may not be constant in time). Let's see why this is the case.

For source-like, zeroth-order reactions to behave sensibly in the thermodynamic limit, their a_j must have the form $a_j = a_{j0}\Omega$, where a_{j0} is constant w.r.t. the thermodynamic limit. If this is not so, the number of molecules introduced in the system per unit time and per unit volume would tend to zero or to infinity.

For unimolecular reactions with reactant i, $a_j = c_j\nu_i = c_j[X_i]\Omega$, where $[X_i]$ is the concentration of the reactant, which is constant in the thermodynamic limit. Therefore a_j/Ω is also a constant.

In a bimolecular reaction with reactants i and k, $a_j = c_j \nu_i \nu_k$ if $i \neq k$ and $a_j = c_j \frac{1}{2} \nu_i (\nu_i - 1)$ otherwise. Here $c_j dt = \mathrm{Prob}_c \mathrm{Prob}_r$, where Prob_c is the probability that two randomly chosen reactant molecules will collide in an infinitesimal interval dt, and Prob_r is the probability that the reaction will happen given a collision. The latter does not depend on the molecular populations and Ω. Gillespie [2009b] showed that, assuming the system is well-mixed and in thermal equilibrium, $\mathrm{Prob}_c = (k'/\Omega)dt$, where k' does not depend on molecular populations and Ω. Combining all, we get $a_j = (k'/\Omega)\mathrm{Prob}_r \nu_i \nu_k = k' \mathrm{Prob}_r [X_i][X_k]\Omega$ in case of different reactants, and $a_j = (k'/\Omega)\mathrm{Prob}_r \frac{1}{2} \nu_i (\nu_i - 1) = \frac{1}{2} k' \mathrm{Prob}_r ([X_i]^2 \Omega - [X_i])$ for a reaction of i with itself. In both cases, a_j/Ω is asymptotically constant in thermodynamic limit.

Now if we divide (14) by Ω and go to thermodynamic limit, the coefficient of the random variable goes to zero, and we obtain the ODE:

$$[X_i](t + dt) = [X_i](t) + \sum_{j=1}^{m} (\beta_{ji} - \alpha_{ji}) a_j([\mathbf{X}](t))/\Omega dt$$

or equivalently,

$$\frac{d[X_i]}{dt} = \sum_{j=1}^{m} (\beta_{ji} - \alpha_{ji}) a_j([\mathbf{X}](t))/\Omega$$

Using the thermodynamic limit, we can simplify the right hand side as follows. In case of source-like reactions, $a_j([\mathbf{X}](t))/\Omega = a_{j0}$, for unimolecular reactions $a_j([\mathbf{X}](t))/\Omega = c_j [X_i]$. For bimolecular reactions with different reactants, $a_j([\mathbf{X}](t))/\Omega = c_j \Omega [X_i][X_k]$, and for self-reaction $a_j([\mathbf{X}](t))/\Omega = \frac{1}{2} c_j \Omega [X_i]^2$. Therefore we can write the convenient form of the RRE:

$$\frac{d[X_i]}{dt} = \sum_{j=1}^{m} k_j (\beta_{ji} - \alpha_{ji}) [\mathbf{X}]^{\alpha_j}$$

where k_j is the reaction rate constant of the mass action law. The relation between the deterministic reaction rate constant and stochastic probability rate constant c_j is now clear:

$$k_j = \begin{cases} c_j/\Omega, \text{for source-like reactions with zero reactants} \\ c_j, \text{for unimolecular reactions} \\ c_j \Omega, \text{for bimolecular reactions with different reactants} \\ \frac{1}{2} c_j \Omega, \text{for reactions between the same molecular species} \end{cases} \tag{18}$$

The rates must be converted accordingly when switching between different analysis methods. Note that it is necessary to know the system volume Ω in order to perform the conversion.

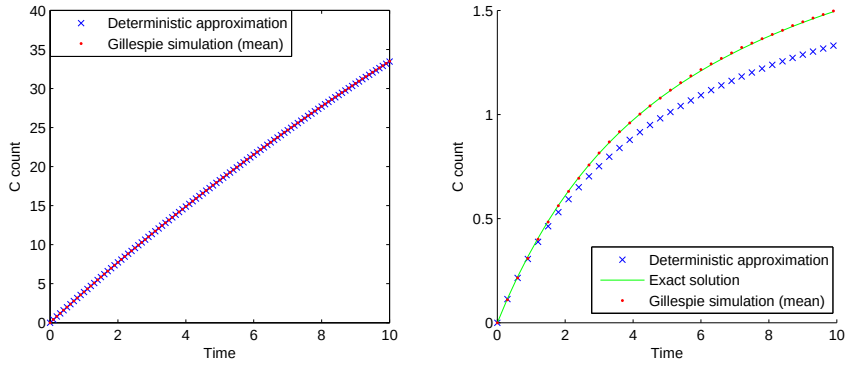

(a) initial A and B: 200 (b) initial A and B: 2

Figure 8: Deterministic approximation compared to Gillespie simulations and an exact solution.

The first formal derivation of RRE from the microscopic model was given in [Kurtz, 1972]. It did not use the chemical Langevin equation, however the argument was more mathematically involved.

Applying deterministic approximation to the $A + B \xrightarrow{\lambda} C$ system yields the following RRE:

$$\frac{d[A]}{dt} = \frac{d[B]}{dt} = -k[A][B]$$
$$\frac{d[C]}{dt} = k[A][B]$$

Its solution is plotted on Figure 8, together with the mean of 10000 Gillespie simulations, meant to indicate the exact solution of the CME. k is set according to (18), with the same λ as in the examples before. Concentration $[C]$ was converted back to molecular counts. On Figure 8a, the initial condition is the same as before, and the agreement between stochastic simulations and the deterministic approximation is good. On Figure 8b, molecule counts are low and the system volume is 1000 times smaller. Under this condition, the thermodynamic limit assumption of RRE is no longer justified, and we observe a considerable approximation error. The exact solution of the CME (11) is plotted for reference.

2.5 SPATIAL MODELLING

When the diffusion is too slow for the well-mixed assumption to be justified, we have to model the spatial distribution of the molecules. Microscopic models directly based on Smoluchowski equation, like GFRD, are computationally very expensive, so approximations are typically used instead. This is a very large subject, so I will briefly review only the approaches used in this thesis.

2.5.1 *Reaction-diffusion systems*

A natural extension of the RRE approach is to consider concentrations as functions of time and space and add diffusion terms to the equations. The ODEs will be transformed into PDEs [Edelstein-Keshet, 2005]. For mass action law this PDE is:

$$\frac{\partial[X_i]}{\partial t} = \sum_{j=1}^{m} k_j(\beta_{ji} - \alpha_{ji})[\mathbf{X}]^{\alpha_j} + D_i \Delta[X_i]$$

where concentration $[X_i] = [X_i](x, t)$ is the function of space $x \in \mathbb{R}^d$ and time, $\Delta[X_i]$ is the Laplacian operator and D_i is the diffusion coefficient of i molecules. This equation can be derived by combining the mass conservation law with Fick's second law of diffusion (8) and the RRE model of reactions [Edelstein-Keshet, 2005]. In order to solve this equation, the boundary and initial conditions must be specified.

Such equations are typically solved using a variant of the finite volume method [Eymard et al., 2000], which first subdivides the space into a number of small sub-volumes, or cells. Then the PDE is transformed into an ODE for each sub-volume, with the time as the variable. All the ODEs are coupled by terms describing fluxes of concentrations across cell boundaries. In reaction-diffusion systems these fluxes will be only due to diffusion. Within each cell, concentrations are represented by their volume averages, thus the local ODEs for the cells are just identical RREs. Sometimes such a discretization is constructed manually [Turing, 1952].

Reaction-diffusion systems are often used to model pattern formation in living organisms [Turing, 1952, Meinhardt and Gierer, 1974, Kondo and Asai, 1995, Miura and Maini, 2004, Sheth et al., 2012]. They are appealing since they provide very simple explanations for complex pattern formation phenomena, typically requiring interaction of only a few substances.

2.5.2 *Reaction-diffusion master equation*

Sometimes the deterministic treatment with the PDEs is not satisfactory, because it rests on the assumption of thermodynamic limit. This may become especially problematic with numerical solutions by space discretization, since with a fine mesh molecule counts in the sub-volumes may be low enough for stochastic effects to become significant. This calls for an intermediate method between microscopic simulations and the CME, which accounts for both spatial inhomogeneity and stochasticity, but does not require tracking of individual molecules. *Reaction-diffusion master equation (RDME)* is such a method. It was introduced in [Kuramoto, 1974] and [Gardiner et al., 1976].

The idea is similar to the finite volume method for solving reaction-diffusion systems. The space is divided in sub-volumes ΔV_r. For each

sub-volume the CME is written, with the additional diffusion reactions. The diffusion reactions are first order reactions describing jumps of molecules into a neighbour sub-volume. Probability rate constants of these new reactions depend on the volumes and the surfaces of the contacts between neighbours. In case of a homogeneous subdivision [Baras and Mansour, 1996]:

$$D_i = \frac{l^2}{2d}\lambda_i$$

where λ_i is the probability rate constant of the diffusion reaction of species i, D_i is its Fick's diffusion coefficient, d is the dimension of the space and $l = \Delta V^{1/d}$ is the characteristic length of the cell.

The result is again a large CME. It can be solved by any method described above. In addition there is a specialized variant of the Gillespie algorithm, called Next Subvolume method [Elf and Ehrenberg, 2004].

Special care must be taken when choosing the sub-volume size for discretization in this method. Obviously the cells should not be too large, or the model will fail to represent spatial inhomogeneity adequately. But there is also a lower bound on the cell size. If the volumes approach zero, bimolecular reactions in this model will have zero probability, because reactants will almost never meet in the same volume [Hellander et al., 2012]. Computing the minimum volume size for which the results agree with the microscopic model is difficult, because it depends on the system geometry and reactions. A correction called Convergent RDME has been proposed [Isaacson, 2012], but it requires that molecules in the different volumes react with each other, making simulations more computationally expensive.

There is no formal derivation of the general RDME from other models, so it should be regarded as a heuristic extension of CME. However, the derivation was done for some simple special cases [Isaacson, 2009], and extensive numerical testing showed good agreement with microscopic models [Baras and Mansour, 1996, Bernstein, 2005].

RDME is used to study a range of phenomena, for example intracellular signalling [Elf et al., 2003], spatiotemporal oscillations in cells [Fange and Elf, 2006], and gene expression [Isaacson et al., 2011].

Figure 9 shows the RDME method applied to the $A + B \xrightarrow{\lambda} C$ system. First, the cube is split into smaller tetrahedrons using Gmsh finite element mesh generator, see Figure 9a. Then the resulting mesh together with the chemical reaction system is processed by the STEPS simulator [Hepburn et al., 2012], which generates appropriate diffusion reactions between neighbour subvolumes. A 1000 simulation runs is then performed. On Figure 9b, A and B are distributed uniformly across the space at $t = 0$. In this case the agreement with GFRD simulations is good, but this is not an interesting case since even deterministic approximation can handle it (Figure 8a and Figure 7).

RDME is also capable of treating inhomogeneous cases, like the spatially separated initialisation example of Figure 4b. However, the pre-

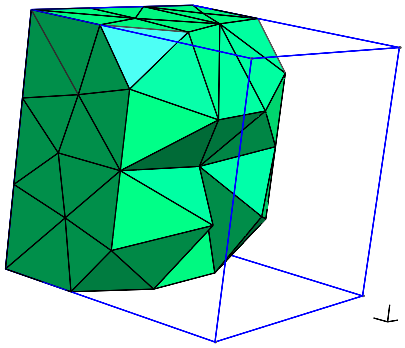

(a) cross section of the cube showing subvolumes computed by Gmsh

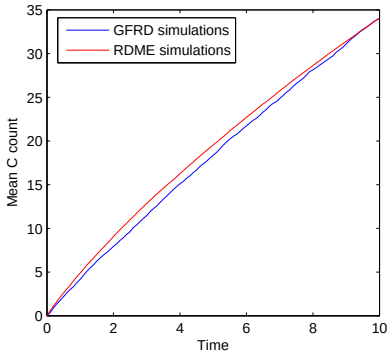

(b) uniform initial distribution of A and B

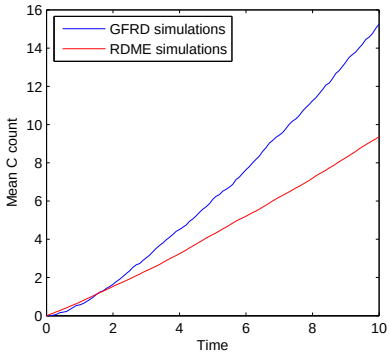

(c) spatially separated initial distribution of A and B

Figure 9: Comparison of RDME and GFRD simulations. Subvolumes for RDME were generated by Gmsh, and simulations were performed using STEPS.

cision of RDME in this case is not as good, as shown on Figure 9c. Making the mesh finer does not improve the agreement between simulations. There is no guarantee that theoretically-derived parameters of the system will work well for RDME, because it was not derived formally from the basic models. The simulation is still useful, but the parameters have to be adjusted if numerically precise results are desired.

2.6 MODELLING LANGUAGES AND TOOLS

All modelling methods described in this chapter have been implemented in various tools. Some of them are listed in Table 1.

Because all the methods are approximations based on assumptions whose validity is difficult to establish, it is often useful to compare the results of different methods with varying degrees of approximation. However, many of the tools use their own languages to specify the models, making it difficult to analyse the same system with different methods.

SBML [Hucka et al., 2003] is an XML-based modelling language aiming to be a standard to describe biochemical models. It is extensible and widely supported, however it currently has no rule-based facilities which are necessary to describe some systems. For example, if the system has some repetitive structure, there is no method to describe it in a compact way. It is also inconvenient (although possible, as in MesoRD) to describe geometries.

The tools developed during this work use SBML for specification of chemical reaction systems.

Name of the tool	**Modelling language used**	**Analysis methods implemented**
Smoldyn [Andrews et al., 2010]	Custom rule-based language to describe reactions and geometry	Simulator of a discrete-time approximation of Smoluchowski model
MCell [Stiles and Jr, 1998]	Custom language (MDL) to describe reactions, events and geometry	Simulator of a discrete-time approximation of Doi model
E-Cell [Takahashi et al., 2003]	Custom imperative language (also possible to use C++) and modelling environment	GFRD for Doi model
COPASI [Hoops et al., 2006]	SBML	Gillespie and τ-leaping simulator, RRE
Biocham [Chabrier-Rivier et al., 2004]	Custom rule-based language, SBML extension	Gillespie and τ-leaping simulator, RRE and a boolean approximation with a temporal logic-based analysis
KaSim [Danos and Laneve, 2004]	Rule-based language Kappa	Gillespie simulator, RRE, a model reduction method
React(C) [John et al., 2011]	Rule-based language React(C)	Gillespie simulator
MomentClosure [Gillespie, 2009a]	SBML	Generates ODEs of moment closure
MesoRD [Hattne et al., 2005]	SBML with extensions to describe geometry	RDME with automatic cubic mesh generation, reaction-diffusion PDE solver using the same mesh
STEPS [Hepburn et al., 2012]	SBML for reactions, several mesh formats for geometry, Python to connect them into a model	RDME, reaction-diffusion PDE solver on the custom mesh, Gillespie simulator and RRE
URDME [Drawert et al., 2012]	Custom Matlab-based system to specify the model, Comsol 3D modelling software to specify its geometry	RDME with custom mesh, finite state projection on the sub-volumes

Table 1: Modelling tools

3

STOCHASTIC ANALYSIS OF A SPACE-LESS COMMUNITY EFFECT MODEL

In this chapter, we will first review three existing models of community effects from Bolouri and Davidson [2010] and Saka et al. [2011], and their main analysis results.

In sections 3.2 - 3.3.3, a more in-depth analysis of the detailed model from Saka et al. [2011] is given, with an emphasize on stochastic effects in particular. The method of choice for the stochastic analysis is moment closure, the detailed description of which was given in subsection 2.4.2. It works by rewriting the CME of the chemical system into a finite set of ODEs, with original system's parameters in it. This is an advantage if we want to scan a range of parameters of the system, which is often the case in quantitative analysis.

A disadvantage of the moment closure method is that the number of generated ODEs quickly grows with the system size, making it potentially difficult to scale to larger systems. *Reduction techniques* are needed to keep the analysis tractable. In Section 3.3, we exploit *symmetries in cell signalling* to perform model reduction.

To understand the notion of symmetry in chemical reaction networks, consider a pool of identical cells communicating over a short distance through the exchange of molecules, which are released by one cell, then diffuse and make contact with another cell. The reaction set

$$r_i : \qquad A_i + B_i \rightleftharpoons C, \qquad \text{for } i \in \{1 \dots n\} \tag{19}$$

describes such a system with n cells. Its symmetry is illustrated in Figure 10. A reaction between a pair of A and B, within the i^{th} cell, results in a C, which is expelled to the extracellular medium. Note that the extracellular C lacks a positional index, unlike the other molecules. C can migrate back from the extracellular medium to *any* of the n cells. The symmetry of this minimal system clearly appears, with C as the centre, around which the n equal cells gather, and through which they communicate. Our model reduction strategy uses a notion of symmetry based on *invariance under certain changes of the chemical reaction*

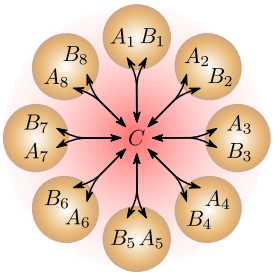

Figure 10: Symmetry in cell-to-cell communication: n cells with equal intracellular reaction network, involving molecules A and B, interact through the exchange of the extracellular molecule C.

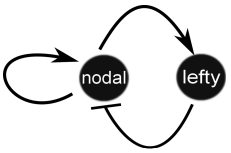

$$
\begin{aligned}
L + A &\underset{kr_1}{\overset{kf_1}{\rightleftharpoons}} LA \\
L &\xrightarrow{kd_L} \\
LA &\xrightarrow{kd_L} A \\
L + N &\underset{kr_2}{\overset{kf_2}{\rightleftharpoons}} LN \\
N &\xrightarrow{kd_N} \\
LN &\xrightarrow{kd_L} N \\
LN &\xrightarrow{kd_N} L \\
N + A &\underset{kr_3}{\overset{kf_3}{\rightleftharpoons}} NA \\
NA &\xrightarrow{kd_N} A
\end{aligned}
\qquad
\begin{aligned}
&\xrightarrow{\text{InitialActivator}} N_{mRNA} \\
NA &\xrightarrow{kt_N} N_{mRNA} + NA \\
N_{mRNA} &\xrightarrow{ks_N} N + N_{mRNA} \\
N_{mRNA} &\xrightarrow{kd_{N_{mRNA}}} \\
NA &\xrightarrow{kt_L} L_{mRNA} + NA \\
L_{mRNA} &\xrightarrow{ks_L} L + L_{mRNA} \\
L_{mRNA} &\xrightarrow{kd_{L_{mRNA}}}
\end{aligned}
$$

(a) GRN (b) Chemical reactions

Figure 11: Model of the community effect in sea urchin.

network. Intuitively, we observe that the global dynamics of the system remains invariant as we swap cell indices, because all cells are equal.

3.1 PREVIOUS MODELS OF COMMUNITY EFFECTS

3.1.1 *Bolouri and Davidson's model*

First computational model of a community effect was made for the community effect in *sea urchin* [Bolouri and Davidson, 2010]. The model considers a single cell, and has no notion of space. Its GRN is given in Figure 11a. It is the same as the abstract GRN in Figure 2b, which will be studied later in Chapter 4. It consists of two interacting genes, *nodal* and *lefty*. Both proteins they produce are morphogens, i.e. they can diffuse out of the cell and affect other cells in the embryo. *nodal* activates itself forming a positive feedback loop, which is hypothesized to underlie the community effect circuit. The role of *lefty*, which inhibits *nodal*, is to keep *nodal*'s expression from accelerating continuously. This would explain the observed evidence that *nodal*'s expression stabilizes at the level of only a few percent of its theoretical maximum which it could reach if not inhibited.

The original model is given in [Bolouri and Davidson, 2010] as a system of ODEs. An approximation of it in the chemical reaction language is given in Figure 11b. N, L, and A denote free (unbound) Nodal, Lefty, and Alk4. Alk4 is a receptor which resides on the surface of cells and reacts to presence of Nodal in the extracellular environment. LA, LN,

and NA are the pairwise complexes of the three proteins. L_{mRNA} and N_{mRNA} are mRNA produced by *lefty* and *nodal* genes.

The reactions on the left hand side of Figure 11b describe the formation of the complexes, their dissociation and degradation. The reactions on the right describe gene expression of *lefty* and *nodal*. Note that Alk_4 does not degrade, so its overall quantity, including the complexes, is constant. It was set to 100000.

The gene expression follows a two step model, and the genes are not explicitly represented. In the first step mRNA is created either from initial activator, of from Nodal-Alk_4 complexes. This models: a) the chain of chemical reactions initiated by an Alk_4 receptor in the presence of Nodal, which ultimately leads to gene transcription, i.e. the propagation of the signal of Nodal's presence through a signalling pathway; b) the gene transcription itself. The second step is the translation, which produces the protein from its mRNA.

In this model Lefty acts as inhibitor of Nodal's ability to activate genes by binding competitively to the Alk_4 receptor, as well as binding to Nodal directly, this behaviour has been demonstrated previously [Chen and Shen, 2004]. Lefty has been shown to be an essential modulator of Nodal activity in sea urchin embryos [Duboc et al., 2008]. Nodal can activate expression of itself as well as Lefty.

The model was analysed deterministically using the following ODE system:

$$
\begin{aligned}
\frac{d[LA]}{dt} &= kf_1[L][A] - kr_1[LA] \\
\frac{d[LN]}{dt} &= kf_2[L][N] - kr_2[LN] \\
\frac{d[NA]}{dt} &= kf_3[N][A] - kr_3[NA] \\
[A] &= [A_{total}] - [LA] - [NA] \\
[N] &= [N_{total}] - [LN] - [NA] \\
[L] &= [L_{total}] - [LN] - [LA] \\
\frac{d[N_{mRNA}]}{dt} &= [\text{InitialActivator}] + kt_N[NA] - kd_{N_{mRNA}}[N_{mRNA}] \\
\frac{d[N_{total}]}{dt} &= ks_N[N_{mRNA}] - kd_N[N_{total}] \\
\frac{d[L_{mRNA}]}{dt} &= kt_L[NA] - kd_{L_{mRNA}}[L_{mRNA}] \\
\frac{d[L_{total}]}{dt} &= ks_L[L_{mRNA}] - kd_L[L_{total}]
\end{aligned}
\tag{20}
$$

The authors argue that the linear transcription model is appropriate, since the gene expression in the sea urchin embryo occurs on short time scales [Bolouri and Davidson, 2003].

The model's parameters were fit to observed data or set to plausible numbers where the data was not available. The model reproduces

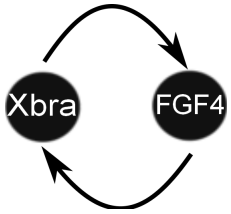

Figure 12: GRN of the community effect in *Xenopus*.

certain aspects of the community effect at the single cell level, for example formation of steady state level of Nodal under the influence of Lefty negative feedback. However, being a model of a single cell, it is unable to reproduce cellular interactions leading to the formation of the threshold of population size, and the appearance of the community effect zone.

The authors also used a much simpler model resembling a two dimensional cellular automaton to show that the community effect may lead to uniform gene expression across the domain where it is active.

3.1.2 *Saka et al.'s model*

In [Saka et al., 2011], two models of the community effect in *Xenopus* are presented. It includes multiple cells and cell to cell communication, and allows deeper understanding of the phenomenon.

Both models have the same underlying GRN illustrated in Figure 12. Two genes are involved, *Xbra* and *FGF4*. FGF_4 proteins can diffuse out of cells and activate *Xbra* in other cells, which in turn activates *FGF4*, closing the positive feedback loop.

The first model is a highly abstract formalization of that GRN, and the second one is more detailed. In the formal models, the proteins are not called by their names, emphasizing that the analysis is generally applicable to any system which has the same GRN.

The simplified model

The reactions of the simplified model are given in Figure 13a. x_i and y_i represent two proteins in cell i, z represents the morphogen in the extracellular environment; V_s is the total system volume, V_c is the volume of a cell, and N is the number of cells. The first three reactions follow Michaelis-Menten kinetics with the two parameters given above their arrows. The model was analysed using the RRE given in Figure 13b.

In this model, synthesis of x_i is activated by the morphogen z, y_i is activated by x_i, and z is the y_i transported out of the cell i. The transcription and translation are not explicitly modelled, instead the ODEs specify Michaelis-Menten kinetics for gene expression. Expression of $V_c/(V_s - N \cdot V_c)$ is the factor of concentration adjustment. It accounts for volume difference between intracellular and extracellular space.

$$
\begin{aligned}
z &\xrightarrow{k_1,1} x_i + z \\
x_i &\xrightarrow{k_2,1} y_i + x_i \\
y_i &\xrightarrow{\frac{V_c k_3}{V_s - N\cdot V_c},1} z + y_i \\
x_i &\xrightarrow{\delta_1} \\
y_i &\xrightarrow{\delta_2} \\
z &\xrightarrow{\delta_3} \\
i &= 1 \dots N
\end{aligned}
\qquad\qquad
\begin{aligned}
\frac{dx_i}{dt} &= \frac{k_1 z}{z+1} - \delta_1 x_i \\
\frac{dy_i}{dt} &= \frac{k_2 x_i}{x_i+1} - \delta_2 y_i \\
\frac{dz}{dt} &= \sum_{j=1}^{N} \left(\frac{V_c}{V_s - N\cdot V_c} \frac{k_3 y_j}{y_j+1} \right) - \delta_3 z, \\
i &= 1 \dots N
\end{aligned}
$$

(a) Reactions (b) ODEs

Figure 13: The simplified model.

The morphogen exported from cells forms an extracellular pool, from where it can enter any other cell with equal rate. Therefore there is no notion of space in this model, since any cell affects any other cell equally.

For the initial condition $x_i = 0, y_i = 0, z > 0$, it is easy to see that $x_i(t) = x_j(t), y_i(t) = y_j(t)$ for $i, j = 1 \dots N$ and all t. Using this we can reduce the model, introducing new variables $x = x_i, y = y_i$:

$$
\begin{aligned}
\frac{dx}{dt} &= \frac{k_1 z}{z+1} - \delta_1 x \\
\frac{dy}{dt} &= \frac{k_2 x}{x_i+1} - \delta_2 y \\
\frac{dz}{dt} &= \frac{\mu y}{y+1} - \delta_3 z
\end{aligned}
\tag{21}
$$

where

$$
\mu = \frac{N\cdot V_c k_3}{V_s - N\cdot V_c}
$$

The reduced model consists of just three ODEs parametrized by the number of cells N. It can be solved for the steady state analytically, and a higher than zero steady state is only possible for

$$
N > N_c = \frac{V_s}{V_c(\xi+1)}
$$

where

$$
\xi = \frac{k_1 k_2 k_3}{\delta_1 \delta_2 \delta_3}
$$

This means that if the number of cells is greater than N_c, which is called the *critical number*, the activity in the system will sustain itself indefinitely, while if $N \leqslant N_c$, the activity will cease, see Figure 14.

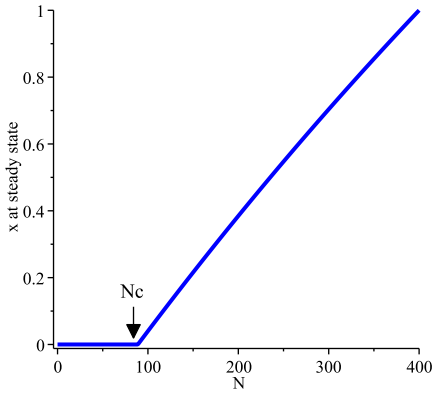

Figure 14: In the simplified model, cell population size determines sustained activity

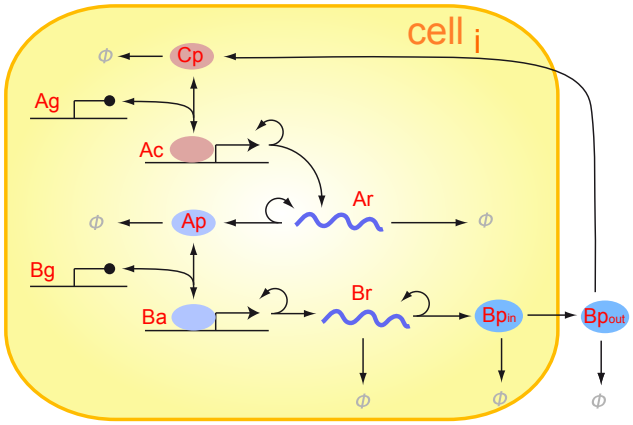

Figure 15: Scheme of the detailed model

This is one of the main features of the community effect. Note that the outcome doesn't depend on the initial conditions, provided that any of x, y or z is greater than zero.

If we define the *cell density* $\eta = N \cdot V_c/V_s$, we can infer the *critical cell density*

$$\eta_c = \frac{1}{\xi + 1}$$

If $\eta > \eta_c$, the system will show sustained activity. Therefore we can say that in this model the community effect is cell density-dependent.

The detailed model

The detailed model has the same underlying structure as the simplified model, but translation and transcription of the genes are treated explicitly, rather than using abstract Michaelis-Menten kinetics. The model is represented schematically in Figure 15. The reactions, which all follow mass action kinetic law, are given in Figure 16.

The model consists of a linear cascade of two genes, A and B. Ag and Bg are inactive forms of the genes, while Ac and Ba are their activated

$$
\begin{aligned}
Cp_i + Ag_i &\underset{\alpha_2}{\overset{\alpha_1}{\rightleftharpoons}} Ac_i & Cp_i &\xrightarrow{\delta_c}\\
Ac_i &\xrightarrow{\beta} Ar_i + Ac_i & Ap_i &\xrightarrow{\delta_a}\\
Ar_i &\xrightarrow{\gamma} Ap_i + Ar_i & Ar_i &\xrightarrow{\delta_m}\\
Ap_i + Bg_i &\underset{\alpha_2}{\overset{\alpha_1}{\rightleftharpoons}} Ba_i & Bp_{in_i} &\xrightarrow{\delta_b}\\
Ba_i &\xrightarrow{\beta} Br_i + Ba_i & Br_i &\xrightarrow{\delta_m}\\
Br_i &\xrightarrow{\gamma} Bp_{in_i} + Br_i & Bp_{out} &\xrightarrow{\delta_d}\\
Bp_{in_i} &\xrightarrow{\kappa} Bp_{out} & i &= 1 \dots N\\
Bp_{out} &\xrightarrow{\varepsilon} Cp_i
\end{aligned}
$$

Figure 16: Reactions of the detailed model

$$
\begin{aligned}
\frac{d[Ac]}{dt} &= \alpha_1[Cp][Ag] - \alpha_2[Ac]\\
\frac{d[Ar]}{dt} &= \beta[Ac] - \delta_m[Ar]\\
\frac{d[Ap]}{dt} &= \gamma[Ar] - \alpha_1[Ap][Bg] + \alpha_2[Ba] - \delta_a[Ap]\\
\frac{d[Ba]}{dt} &= \alpha_1[Ap][Bg] - \alpha_2[Ba]\\
\frac{d[Br]}{dt} &= \beta[Ba] - \delta_m[Br]\\
\frac{d[Bp_{in}]}{dt} &= \gamma[Br] - (\kappa + \delta_b)[Bp_{in}]\\
\frac{d[Bp_{out}]}{dt} &= N \cdot \kappa[Bp_{in}] - (N \cdot \varepsilon + \delta_d)[Bp_{out}]\\
\frac{d[Cp]}{dt} &= \varepsilon[Bp_{out}] - \alpha_1[Cp][Ag] + \alpha_2[Ac] - \delta_c[Cp]\\
[Ag] + [Ac] &= [Bg] + [Ba] = 1
\end{aligned}
$$

Figure 17: ODEs of the reduced detailed model.

forms. Gene B produces the protein Bp. Bp_{in} is the Bp inside a cell, and Bp_{out} is the same protein in the extracellular environment. Bp_{in} diffuses out of the cell with rate κ, producing Bp_{out}. When Bp_{out} binds to one of the cells, it produces the activator Cp. This conversion of Bp_{out} into Cp is an abstract representation a complicated call signalling process, with a single rate ε. Cp activates the gene A, whose product Ap activates the gene B, closing the positive feedback loop. As before, the chemical species are indexed by the number of cell they reside in, so Ap_i is the A's protein in cell i.

The model was first analysed deterministically. The RRE is given in Figure 17, already reduced in the same way as (21). After this reduction, we drop cell indices from names of species, since concentrations of corresponding molecules is the same in all cells: $[Ap_i] = [Ap], i = 1 \dots N$ etc. The last equation specifies the conservation law of the genes, similar to the conservation of Alk_4 was specified in (20). Total concentration of 1 here is arbitrary.

The parameters were set to biologically plausible values taken from various sources. ε was chosen such that the community effect can be observed.

Using the same steady state analysis as for the simplified model, we get

$$N_c = \frac{\delta_d}{\varepsilon(\rho - 1)}$$

where

$$\rho = \frac{\alpha_1^2 \beta^2 \gamma^2 \kappa}{\alpha_2^2 \delta_a \delta_c \delta_m^2 (\kappa + \delta_b)} \tag{22}$$

The conclusion is that the behaviour of this model is similar to the simplified model. It demonstrates the threshold population size found experimentally, which doesn't depend on initial conditions as long as they are non-zero. This leads to the important conclusion that the community effect is a self-organizing system: in the absence of external control it reaches the same state independently of the amount of initial induction.

Being more detailed, this model allows investigating the influence of gene copy number on the community effect. Also from (22) we can see which parameters influence the critical number: the parameters which promote the gene expression make N_c lower, while the opposite parameters, like degradation rates, increase it.

One drawback of the deterministic treatment of the detailed model is that the gene count is continuous. Instead of assuming only two states, active and inactive, the genes assume a concentration value between 0 and 1. As was discussed previously, the model with such low molecule count doesn't fulfil the assumptions behind RRE modelling. Because of this, and also to investigate the effect of the noise on N_c, stochastic simulations of the same model were performed.

The outcome of the Gillespie simulations was approximately in agreement with the deterministic treatment. When N is close to N_c the system may enter the sustained activation, or the activity may stop with some probability. Only when N is somewhat higher than N_c the activation becomes reliable.

3.2 STOCHASTIC ANALYSIS OF THE SPACE-LESS MODEL OF THE COMMUNITY EFFECT

To study the stochastic aspect of the community effect in the detailed model from the previous section, namely the threshold on the number cells, we need to redefine the notion of sustained activation. In the stochastic case we consider the *probability* of sustained activation, since the outcomes are now random.

Also it is easy to see that the system in Figure 16 has an absorbing state, where $Ag_i = Bg_i = 1$ and none of the other species are present. Once the system falls into this inactive state, no further reactions can happen. The absorbing state is reachable from any other state, because all molecules can degrade with non-zero probabilities. In addition, none of the species can accumulate indefinitely with non-zero probability, again because of the degradation. All together this means that in the long time limit, the system is doomed to fall into the absorbing state, making it the only true steady state.

This observation is not very helpful, however, because once the system has reached a high level of activation and accumulated large amounts of molecules in cells, the probability of collapsing to the absorbing state becomes extremely small, and this will not happen for a very long time. We are more interested in the notion of *quasi steady state* (or "transient steady state"), which we will define simply as the system's state after a fixed, sufficiently long period of time. We consider the system to be at a quasi steady state at time $T = 10^5$ seconds after the initial induction.

We can now define the critical number N_c in the stochastic setting as the smallest number of cells in the system for which the probability of collapsing to the inactive state at time T is less than 0.5. The objective of the following is to compute this N_c.

3.2.1 *Stochastic simulations*

First we performed Gillespie simulations of the detailed model in Figure 16. Three examples of these simulations are shown in Figure 18. It is evident that as the number of cells N grows, so does the probability of the system to enter the active quasi steady state: the community effect works. If we consider the average behaviour of the system across many simulations, we can see that the deterministic approximation diverges significantly from the exact solution. In particular, for $N = 100$ (Figure 18a) almost all stochastic simulations end in the inactive state at

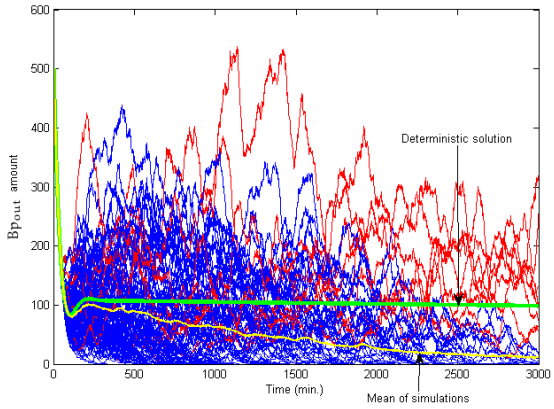

(a) N = 100

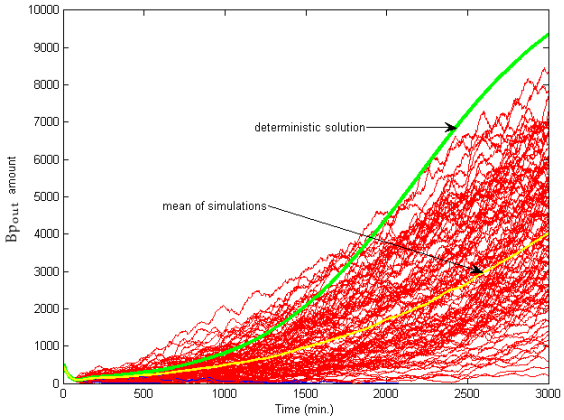

(b) N = 160

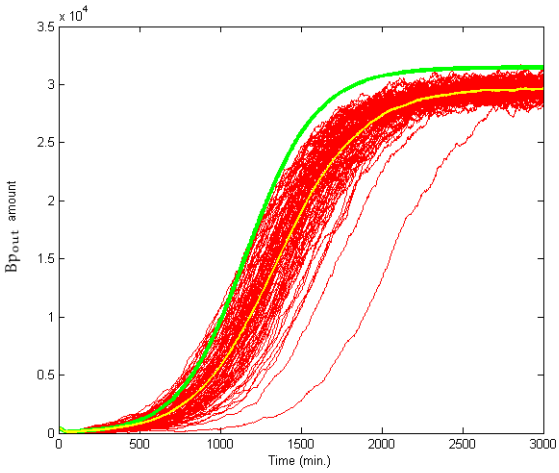

(c) N = 300

Figure 18: Gillespie simulations of the detailed model for different cell counts. Bp_{out} is plotted as a function of time. Green: deterministic solution; yellow: mean of simulations; red: individual simulations which end in the active state at $t = T$; blue: simulations which end in the inactive state.

$t = T$, and the mean of Bp_{out}, which we consider as the main indicator of system's activity, is converging to zero. The deterministic approximation, on the other hand, predicts a non-zero steady state for all $N > 97$. The divergence of the mean of Bp_{out} in stochastic and deterministic simulations is also significant for higher cell counts (Figure 18b), but becomes relatively smaller as the cell count grows (Figure 18c).

We performed a parameter scan of the number of cells in the stochastic simulations for $N = 0 \ldots 210$, which is summarized in Figure 19. Figure 19a demonstrates the all-or-nothing behaviour of the system, with the probability of the system to be partially active is essentially zero in all cases. We used $Ap_i > 0$ as the indicator of an active cell, following [Saka et al., 2011]. The same data is presented differently in Figure 19b. The statistically estimated critical number N_c is about 117 according to the simulations, which is 20% higher than 97 predicted by the deterministic approximation, making the divergence significant.

While stochastic simulations provide a simple way to study the stochastic behaviour of chemical reaction systems, they do not provide the same flexibility of analysis as the deterministic approximation because of the associated computational cost. The simulations above took over ten days to compute on a desktop computer. It is very inconvenient to perform parameter scans like those in [Saka et al., 2011] using exact simulations.

To overcome this problem, we will apply moment closure method to the detailed community effect model.

3.3 APPLICATION OF MOMENT CLOSURES

We have implemented a software tool which can compute a moment closure of a given system. The tool is written in Maple[1] symbolic computation package, which allows easy manipulation of equations. The actual algorithm closely follows the outline in subsection 2.4.2, first described by Vidal et al. [2010].

Moment closure of order m for a system with n species generates $O(n^m)$ ODEs, because moments for all combinations of n species may be included. For the second order closure of the community effect model, which has 9 species per cell, the moment closure procedure generates $40.5N^2 + 22.5N + N$ moment equations[2] up to order two for N cells. For 120 cells, which is near this system's true N_c, it would generate 585902 equations. This by far exceeds processing capabilities of the software we used. The naive application of moment closure to systems of this size is impractical. Attempts were made to simplify models based on various properties, e.g. conservation laws and bounds on numbers of species [Vidal et al., 2010]. In the following, a model reduction method based on *symmetries in the reaction set* is presented, which can reduce

1 http://www.maplesoft.com/

2 This is always an integer.

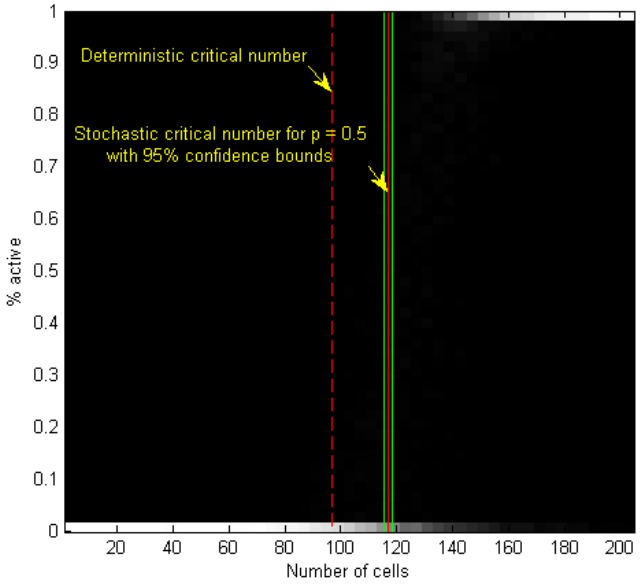

(a) 2D histogram of different percentages of active cells at the end of simulations for various N. Brightness of a square denotes the count of simulations with given number of cells which ended with the corresponding percent of active cells. This graph is analogous to Figure 5A in [Saka et al., 2011]

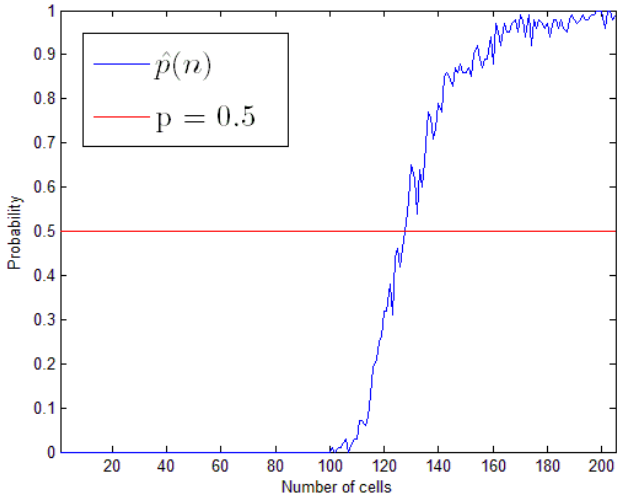

(b) Estimated probability of entering the active quasi steady state as a function of number of cells

Figure 19: Results of scan of $N = 0 \ldots 210$ by stochastic simulations.

the model dramatically in some cases, including the community effect model. It first appeared in [Batmanov et al., 2012a].

3.3.1 *Reduction by example*

We demonstrate the idea by a simple example. Consider the set of $p = 2n+1$ chemical species $A_1, \ldots, A_n, B_1, \ldots, B_n, C$ associated with state random variables $\mathbf{x}(t) = (A_1(t), \ldots, A_n(t), B_1(t), \ldots, B_n(t), C(t))$ and the following set of reactions

$$\mathcal{R} = \{A_i + B_i \underset{\kappa_2}{\overset{\kappa_1}{\rightleftharpoons}} C \mid i \in \{1, \ldots, n\}\}$$

This system is shown graphically in Figure 10. We assume that for any fixed time t, $\mathcal{R}$ and an initial state $\mathbf{x}(0) = \boldsymbol{\nu}_0 \in \mathbb{N}^p$ defines a probability distribution over $\mathbf{x}(t)$ with probability mass function $\pi_{\boldsymbol{\nu}}(t)$. For instance, considering combinatorial mass action kinetics, $\pi_{\boldsymbol{\nu}}(t)$ will be the solution of the CME (10).

We want to identify moment equalities from simple *symmetries* in the reaction system. Since a moment is fully defined by *marginal distributions* of variables composing it, we actually identify equal marginal distributions from symmetries. The marginal distribution of the variables A_1 and B_1 is the probability distribution of this set of variables, ignoring the others. By symmetry of the reaction set, we mean that the reaction set remains *invariant under permutation of the chemical species*. An obvious permutation of this kind for $\mathcal{R}$ is swapping A_1 with A_2 and B_1 with B_2. In that case, $\mathcal{R}$ remains unchanged. Suppose we further assume that the initial state is invariant with respect to the same permutation. That is, initial numbers of A_1 and A_2 are the same, as well as those of B_1 and B_2. Because we consider probability distributions that are completely defined by the reactions $\mathcal{R}$ and the initial state, the stochastic dynamics of the variable set $\{A_1, B_1\}$ cannot be distinguished from that of $\{A_2, B_2\}$. As proved below, this means that their marginal distributions are equal

$$\mathsf{Prob}(A_1(t) = a, B_1(t) = b) = \mathsf{Prob}(A_2(t) = a, B_2(t) = b), \quad \forall t \in \mathbb{R}_{\geqslant 0}, a, b \in \mathbb{N}$$

Permuting of C with itself, we get

$$\begin{aligned} &\mathsf{Prob}(A_1(t) = a, B_1(t) = b, C(t) = c) = \\ &\mathsf{Prob}(A_2(t) = a, B_2(t) = b, C(t) = c), \\ &\forall t \in \mathbb{R}_{\geqslant 0}, a, b, c \in \mathbb{N} \end{aligned} \tag{23}$$

Importantly, this entails the moment equalities $\mathsf{E}[A_1^i B_1^j C^k] = \mathsf{E}[A_2^i B_2^j C^k]$ for any $i, j, k \geqslant 0$. As another example of symmetry, assuming $n \geqslant 4$ one can swap A_1 with A_3, A_2 with A_4, B_1 with B_3, B_2 with B_4, C

with itself. Again, also assuming invariance of the initial state by this permutation, we have

$$\begin{aligned}&\mathrm{Prob}(A_1(t)=a_1, A_2(t)=a_2, B_1(t)=b_1, B_2(t)=b_2, C(t)=c) = \\ &\mathrm{Prob}(A_3(t)=a_1, A_4(t)=a_2, B_3(t)=b_1, B_4(t)=b_2, C(t)=c), \\ &\forall t \in \mathbb{R}_{\geqslant 0}, a_1, a_2, b_1, b_2, c \in \mathbb{N}\end{aligned} \tag{24}$$

It is straightforward to use equalities of the form (23)-(24) to reduce a set of moment equations of the system. For example, the system considered above generates, among others, the following moment equations for second order moments:

$$\begin{aligned}\frac{dE[A_iC]}{dt} = \kappa_1\Big(\sum_{j=1}^{n} E[A_iA_jB_j]\Big) - \kappa_1(E[A_iB_i]+E[A_iB_iC]) - \\ \kappa_2(E[C]-E[C^2]+n\cdot E[A_iC]) \qquad i=1\dots n\end{aligned} \tag{25}$$

Using relations as (23), we can infer the following moment equalities: $E[A_iC] = E[A_1C]$, $E[A_iB_i] = E[A_1B_1]$, $E[A_iB_iC] = E[A_1B_1C]$, $E[A_i^2B_i] = E[A_1^2B_1]$, and using equalities as (24) we have $E[A_iA_jB_j] = E[A_1A_2B_2], i=1\dots n, j=1\dots n, i\neq j$. Therefore we can equivalently rewrite all n equations in (25) into one:

$$\begin{aligned}\frac{dE[A_1C]}{dt} &= \kappa_1((n-1)E[A_1A_2B_2]+E[A_1^2B_1]) - \\ &\quad \kappa_1(E[A_1B_1]+E[A_1B_1C]) - \\ &\quad \kappa_2(E[C]-E[C^2]+n\cdot E[A_1C])\end{aligned} \tag{26}$$

We can't exchange moments for A_i and B_i because they may have different initial conditions in general. Using this approach, the system of moment equations up to order two is reduced from $2n^2+5n+2$ to 11 ODEs for any $n \geqslant 2$. The rest of the equations are redundant and can be safely excluded. The transformation is exact, and we can recover the dynamics of the original system from the reduced one. In order to compute the moment dynamics, it is necessary to perform a closure of the reduced system as described in subsection 2.4.2.

3.3.2 *Formal reduction*

We now formally define the previous notions. We however won't make use of marginal distributions, since equivalence of the full joint probability distribution entails equivalence of its marginal distributions.

We consider permutations σ over the set of species indices $\{1,\dots,n\}$. Permutations of vectors and reaction sets are defined as

$$\begin{aligned}\mathbf{a}_\sigma &= (a_{\sigma(1)},\dots,a_{\sigma(n)}) \\ \mathcal{R}_\sigma &= \{(\kappa, \boldsymbol{\alpha}_\sigma, \boldsymbol{\beta}_\sigma) \mid (\kappa, \boldsymbol{\alpha}, \boldsymbol{\beta}) \in \mathcal{R}\}\end{aligned}$$

We say that a vector $\mathbf{a}$, resp. a reaction set $\mathcal{R}$, is σ-*invariant*, iff $\mathbf{a} = \mathbf{a}_\sigma$, resp. $\mathcal{R} = \mathcal{R}_\sigma$. We denote $\mathcal{P}$ the function that, for a given set $\mathcal{R}$ of reactions, initial state $\boldsymbol{\nu}_0$ and time t, gives a probability distribution over the counts of the species with probability mass function $\pi_{\boldsymbol{\nu}}(t)$. Somehow $\mathcal{P}$ gives the solution of the stochastic dynamics of the system. For example, $\mathcal{P}$ could be the solution of the system's CME, or an approximation of it, like a moment closure. We make the following assumption about $\mathcal{P}$.

Assumption 1. *Let* $\pi_{\boldsymbol{\nu}}(t) = \mathcal{P}(\mathcal{R}, \boldsymbol{\nu}_0, t)$ *and* $\pi'_{\boldsymbol{\nu}}(t) = \mathcal{P}(\mathcal{R}_\sigma, \boldsymbol{\nu}_{0\sigma}, t)$, *for some reaction set* $\mathcal{R}$, *initial state* $\boldsymbol{\nu}_0$, *time* t, *and permutation* σ *of the species indices. For any* $\boldsymbol{\nu} \in \mathbb{N}^n$, *we have* $\pi_{\boldsymbol{\nu}}(t) = \pi'_{\boldsymbol{\nu}}(t)$.

This assumption relates permutations at the level of reactions to permutation at the level of its stochastic semantics. It just states that the stochastic dynamics of a species A provided by $\mathcal{P}$ does not depend on its position in the state vector. Saying it differently, we assume that the stochastic behaviour is insensitive to species renaming, provided that this renaming doesn't create name conflicts. This is a reasonable assumption that is, for instance, satisfied by the master equation.

Theorem 3.3.1. *Let* $\mathcal{R}$ *be a set of* k *reactions of* n *species,* $\boldsymbol{\nu}_0 \in \mathbb{N}^n$ *be an initial state, and* σ *be a permutation over* $\{1, \ldots, n\}$. *Let* $\pi_{\boldsymbol{\nu}}(t) = \mathcal{P}(\mathcal{R}, \boldsymbol{\nu}_0, t)$, *if* $\mathcal{R}$ *and* $\boldsymbol{\nu}_0$ *are* σ-*invariant, then, for any* $\boldsymbol{\nu} \in \mathbb{N}^n$, $\pi_{\boldsymbol{\nu}}(t) = \pi_{\boldsymbol{\nu}_\sigma}(t)$.

Proof. This theorem is a straightforward consequence of the above assumption. Indeed, let $\pi_{\boldsymbol{\nu}}(t) = \mathcal{P}(\mathcal{R}, \boldsymbol{\nu}_0, t)$ and $\pi'_{\boldsymbol{\nu}}(t) = \mathcal{P}(\mathcal{R}_\sigma, \boldsymbol{\nu}_{0\sigma}, t)$, since $\mathcal{R} = \mathcal{R}_\sigma$ and $\boldsymbol{\nu}_0 = \boldsymbol{\nu}_{0\sigma}$, we have $\pi_{\boldsymbol{\nu}}(t) = \pi'_{\boldsymbol{\nu}}(t)$. By the Assumption 1 it follows that $\pi_{\boldsymbol{\nu}}(t) = \pi'_{\boldsymbol{\nu}_\sigma}(t) = \pi_{\boldsymbol{\nu}_\sigma}(t)$. □

Corollary 3.3.2. *Let* $\mathcal{R}$ *be a set of* k *reactions of* n *species,* $\boldsymbol{\nu}_0 \in \mathbb{N}^n$ *be an initial state and* σ *a permutation of the species indices. If* $\mathcal{R}$ *and* $\boldsymbol{\nu}_0$ *are* σ-*invariant, then* $\mu^{(\mathbf{m})} = \mu^{(\mathbf{m}_\sigma)}$.

Proof. At any time t we have

$$\begin{aligned}
\mu^{(\mathbf{m})}(t) &= \mathbb{E}[\mathbf{x}^{\mathbf{m}}(t)] \\
&= \textstyle\sum_{\boldsymbol{\nu}} \boldsymbol{\nu}^{\mathbf{m}} \pi_{\boldsymbol{\nu}}(t) \\
&= \textstyle\sum_{\boldsymbol{\nu}} \boldsymbol{\nu}_\sigma^{\mathbf{m}_\sigma} \pi_{\boldsymbol{\nu}}(t) \text{ by commutativity of multiplication} \\
&= \textstyle\sum_{\boldsymbol{\nu}} \boldsymbol{\nu}_\sigma^{\mathbf{m}_\sigma} \pi_{\boldsymbol{\nu}_\sigma}(t) \text{ by Theorem 3.3.1} \\
&= \mathbb{E}[\mathbf{x}^{\mathbf{m}_\sigma}(t)] = \mu^{(\mathbf{m}_\sigma)}(t)
\end{aligned}$$

□

We denote by $\Sigma(\mathcal{R}, \boldsymbol{\nu}_0)$ the set of permutations σ such that $\mathcal{R}$ and $\boldsymbol{\nu}_0$ are σ-invariant. By Corollary 3.3.2, this set defines equivalence classes $[\mu^{(\mathbf{m})}]_\Sigma$ of moments, i.e. the set of moments $\mu^{(\mathbf{m}')}$ such that

$\mu^{(\mathbf{m}')} = \mu^{(\mathbf{m}_\sigma)}$ for some $\sigma \in \Sigma = \Sigma(\mathcal{R}, \boldsymbol{\nu}_0)$. As usual, we also write $[\mu^{(\mathbf{m})}]_\Sigma$ for the representative moment of this set that is, for instance, the smallest of those moments for the lexicographical order on $\mathbb{N}^n$. We denote $\boldsymbol{\mu}_k$ a vector of all M moments up to order k. Let

$$\mathcal{M}(\mathcal{R}, k) = \{\dot{\mu}^{(\mathbf{m})} = L \cdot \boldsymbol{\mu}_h \mid \mathit{order}(\mathbf{m}) \leqslant k, L \in \mathbb{R}^M\}$$

be a set of moment equations obtained by some moment generation method, with moments up to order k (recall that moment equations are always linear). h is the maximum order of the moments in the equations, it can be greater than k for systems of moment equations with an unclosed cascade of dependencies.

The *reduced set of moment equations* is defined by

$$\mathcal{M}_{red}(\mathcal{R}, \boldsymbol{\nu}_0, k) = \{\rho(\dot{\mu}^{(\mathbf{m})}) = L \cdot \rho(\boldsymbol{\mu}_h) \mid (\dot{\mu}^{(\mathbf{m})} = L \cdot \boldsymbol{\mu}_h) \in \mathcal{M}(\mathcal{R}, k)\}$$

where ρ is the substitution of moments for their representative

$$\rho = \{\mu^{(\mathbf{m})} \text{ is substituted by } [\mu^{(\mathbf{m})}]_\Sigma \mid \mathit{order}(\mathbf{m}) \leqslant k \text{ and } \Sigma = \Sigma(\mathcal{R}, \boldsymbol{\nu}_0)\}$$

This transformation just excludes from $\mathcal{M}(\mathcal{R}, k)$ repeated equations for the variables which are provably equal, and therefore is exact.

3.3.3 *Reduction of the detailed model*

The community effect model's structure resembles a star, just as Figure 10 on page 53 does. It is easy to see that the community effect model exhibits the symmetries required by Theorem 3.3.1, which allows to reduce its moment equations for any number of cells to a system of constant size, similar to the example in subsection 3.3.1.

We have applied the symmetric reduction to the normal closure of the detailed community effect model shown in Figure 16. The reduced model contains 146 equations for any N. The deterministic approximation, which is equivalent to the first order moment closure, can also be reduced using the same method. This kind of reduction, among others, has been done in [Saka et al., 2011], where the deterministic approximation consisted of only 8 ODEs for any N. Our Maple implementation of the MC method and the reduction for this model are available online[3].

3.3.4 *Comparison of approximations*

Figure 20 plots the Bp_{out} dynamics, computed by three different approximations. First is a *mean of many stochastic simulations*. As the number of simulations increases, this converges to the true mean - however it is noisy and the simulations take very long time. The simulations were done using COPASI software [Hoops et al., 2006]. Second

3 http://www.lifl.fr/~batmanov/cmsb2012-files/

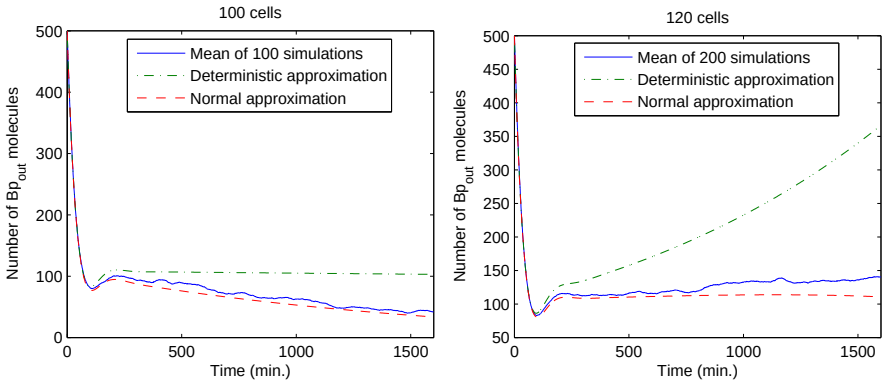

(a) $N < N_c$ (b) $N > N_c$

Figure 20: Traces of Bp_{out} over time for systems of sizes below and above N_c, computed using stochastic simulations, deterministic approximation and the reduced second order moment closure using normal approximation.

is a (usual) *deterministic approximation* of the system, with one ODE per species, which is the fastest in terms of computation. However, it tends to diverge from the stochastic estimates. This indicates the presence of significant stochastic effects in the model. Third is a *reduced moment closure of order two*, using the normal approximation for truncation. The normal approximation is not the best choice for chemical reaction systems generally, but it is simple to implement and it gives good results in this case.

Due to the complexity of the resulting system of ODEs in the moment closure, we couldn't derive an analytical solution for N_c. By examining the numerical solutions for different values of N, we found that the moment closure gives $N_c = 117$, the same as derived from statistical analysis of stochastic simulations.

The deterministic approximation, on the other hand, predicts $N_c = 97$, and therefore miscalculates the qualitative behaviour of the system for a range of N. In addition, the deterministic estimate of Bp_{out} strongly diverges from the stochastic one, especially when the cell number N is close to N_c.

4

SPATIAL MODELS OF COMMUNITY EFFECTS

In this chapter, several spatial models of community effects will be presented, which appeared first in [Batmanov et al., 2012b].

In Section 4.1 a formal language is introduced which we will use to define the models. Section 4.2 presents the *minimal model* of a community effect, whose GRN is illustrated in Figure 21a. It is a simple model with a single species u which promotes its own production. In Section 4.3, this model is refined to represent the community effect in *Xenopus* in more detail, following Saka et al. [2011], but now with space.

The analysis of these models shows that community effects spread through space without restriction. Two other models are proposed in the following sections, which include different mechanisms to control the area of community effects.

The Turing pattern model, which is based on the reaction-diffusion theory, is presented in Section 4.4. It adds a second diffusible factor v with an inhibitory effect to the minimal model's self-sustaining species u, as illustrated in Figure 21b.

The dynamic morphogen gradient model of Section 4.5 is sketched in Figure 2c. It introduces a diffusible factor s, which activates two mutually inhibitory species v and u. The latter participates in a self-activating feedback loop with w, another diffusible species. Figure 2c highlights the u-w community effect loop in red. Without the community effect loop and diffusion of the morphogen s in continuous space, this GRN was previously considered in [Saka and Smith, 2007].

What has emerged from the analyses described in this chapter is that diffusible factors for intercellular communication could provide many benefits to embryonic patterning, when interlinked with developmental GRNs.

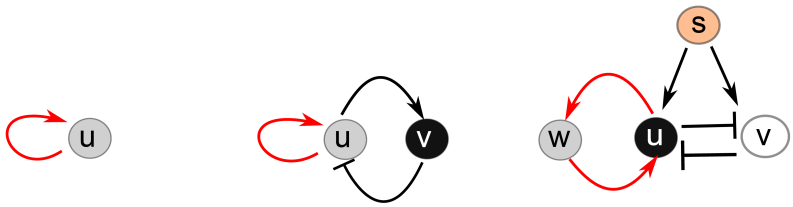

(a) minimal model (b) Turing pattern model (c) dynamic morphogen gradient model

Figure 21: GRNs of three models analysed in this chapter. The feedback loop responsible for community effects is highlighted in red.

Later in this chapter, spatial models of community effects will be presented. The models consist of two parts: a description of chemical reaction network, given as a list of chemical reactions; and a description of space in which these reactions take place.

The analysis is then performed using two different methods as appropriate. The simple choice is to treat the model as a reaction-diffusion system, with continuous concentrations and space. When we are interested in effects of the stochastic noise in the system, we use the RDME approach.

For the RDME, a natural discretization of space is chosen, where one subvolume represents a single cell. Therefore we assume that diffusion of molecules inside cells is fast, while diffusion through cell membranes and in the extracellular space is slower.

Since we consider a one-dimensional row of cells, each subvolume inside the population will have two neighbours, and two subvolumes on the borders will have one neighbor each. The subvolumes can be assigned a one-dimensional integer coordinate x, and the diffusion will take place between subvolumes x and $x+1$. Moreover, since the surface area of common boundaries of neighbour subvolumes is the same for all cells, the rates of diffusion reactions added by the RDME will be all the same. This allows reformulating the RDME as a simpler rule-based model with chemical species indexed by coordinates of the subvolumes where they reside, so species A in subvolume x is written as $A(x)$. The coordinate $x+1$ indicates the neighbour subvolume to the right of x. Diffusion reactions then convert species of one subvolume into species of another subvolume, for example $A(x) \xrightarrow{D} A(x+1)$. All reactions except diffusion must only involve species with the same coordinate, because the reactions can only take place between species in the same subvolume in the basic RDME model.

To unambiguously define rate laws of reactions, we will write its full expression above the arrow. In these expressions, the count of molecule X will be written as $\sharp X$. For example, the system $A + B \xrightarrow{\lambda} C$ with the mass action law will be written as $A + B \xrightarrow{\lambda \sharp A \sharp B} C$.

4.2 MINIMAL MODEL OF A COMMUNITY EFFECT

4.2.1 *Minimal model of a community effect in one dimension*

In this section, we present a *minimal model* of a community effect in one dimensional space. Its GRN is minimal, in the sense that the positive feedback loop for a community effect loop is the smallest possible, with the single species u – illustrated in Figure 21a. Previous work considered a well-mixed system of cells, in which a factor could diffuse from one cell to any other with equal probability [Saka et al., 2011],

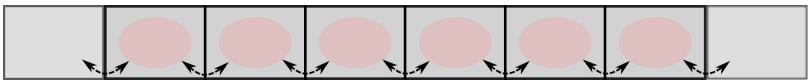

Figure 22: Diffusion model scheme: row of N_a active cells, flanked by $2 \times N_p$ passive cells. Here $N_a = 6, N_p = 1$.

or didn't include multiple cells explicitly at all [Bolouri and Davidson, 2010]. The following model renders molecular diffusion in a more realistic way, considering a one-dimensional row of cells, in which we distinguish *active cells* (implementing the community effect GRN) flanked by *passive cells* (that merely support diffusion). With the restriction that molecules travel over longer distances by a random walk between immediate neighbours, we can see how a community effect behaves in space.

Space specification

Our model of space is illustrated in Figure 22. Cells are arranged in a *row* of finite length. The row contains a domain of *active cells* in the middle, which is flanked by *passive cells*. Only active cells can respond to the inducing signal and produce the diffusible factors for a community effect. Passive cells do not respond to inducing signals and merely occupy the space on both sides of the active cells. N_p and N_a henceforth refer to the numbers of passive and active cells, respectively.

In the RDME treatment, which we will consider first, molecular *diffusion*, i.e. the exchange of a diffusible factor, occurs stepwise between adjacent positions. Molecules can move throughout the entire row by random walk.

In the continuous, deterministic PDE treatment the diffusion works according to Fick's second law.

In our model, passive cells are required to obtain certain aspects of community effects. Without passive cells, those effects do not occur, regardless of initial conditions. We prove this later in subsection 4.2.4 after formally defining the model.

The common structure of GRNs for community effects [Davidson, 2010] is a self-sustaining feedback loop with diffusible factors. The GRN of our active cells illustrated in Figure 21a implements such a feedback loop in a minimal fashion: the diffusible factor u directly enhances its own production. Cells in the system are induced by a transient signal, applied either locally or globally. In our model, the inducing signal is represented by a number of diffusible factor molecules, which are deposited at some cells at time zero.

Rule-based formalization of the minimal model

Chemical reactions which happen in active cells of the minimal model are defined in Figure 23.

$$\text{self-activation:} \quad u \xrightarrow{\alpha_u \frac{\sharp u}{k_u + \sharp u}} 2u \tag{27}$$

$$\text{degradation:} \quad u \xrightarrow{\mu_u \sharp u} 0 \tag{28}$$

Figure 23: Reactions of the minimal model.

$$\text{self-activation:} \quad \forall x \in \mathsf{ActiveCells}, \quad u(x) \xrightarrow{\alpha_u \frac{\sharp u(x)}{k_u + \sharp u(x)}} 2u(x) \tag{29}$$

$$\text{degradation:} \quad \forall x \in \mathsf{AllCells}, \quad u(x) \xrightarrow{\mu_u \sharp u(x)} \tag{30}$$

$$\text{diffusion:} \quad \forall x \in \mathsf{AllCells} - \{\mathsf{LastCell}\}, \quad u(x) \underset{D_u \sharp u(x+1)}{\overset{D_u \sharp u(x)}{\rightleftharpoons}} u(x+1) \tag{31}$$

where $\mathsf{ActiveCells} = \{1 + N_p, \ldots, N_p + N_a\}$, $\mathsf{AllCells} = \{1, \ldots, \mathsf{LastCell}\}$, and $\mathsf{LastCell} = 2N_p + N_a$.

Figure 24: Rules of minimal model's RDME.

Reaction (27) describes u's self-activation, which is the GRN of this model. It creates two u molecules from a single one. The rate law is described by the expression $\alpha_u \frac{\sharp u}{k_u + \sharp u}$ which defines a Michaelis-Menten kinetic law. α_u and k_u are the rate parameter and the Michaelis constant. Michaelis-Menten law is a standard way to model saturating reactions in biochemistry. We need the self-activation to be saturating, otherwise $\sharp u$ may grow indefinitely.

Reaction (28) describes degradation of u, with mass action kinetics.

The RDME corresponding to the minimal model is presented in Figure 24, using the rule-based language defined in Section 4.1. Here, rules (29) and (30) describe u's self-activation and degradation. The self-activation rule applies to u at positions from the set of active cells, which is denoted $\mathsf{ActiveCells}$. The degradation rule applies throughout the entire row.

The last rule (31) defines diffusion with diffusion rate D_u. D_u is constant throughout the space because it is assumed that all cells have the same volume and geometry, and that the distance between all neighbours is the same. The diffusion rate D_u can be related to Fick's diffusion coefficient, which is invariant to geometry and discretization of space. The relationship can be derived by applying the finite volume method [Eymard et al., 2000] to Fick's second law, which describes diffusion in continuous space. The derivation can be found in [Bernstein, 2005].

Parameter	Description	Value
α_u	u self-activation maximum rate	33.25
k_u	u self-activation Michaelis constant	450
α_v	activation of v by u maximum rate	60
k_v	activation of v by u Michaelis constant	450
α_i	inhibition of u by v maximum rate	0.04
k_i	inhibition of u by v Michaelis constant	0.1
μ_u	degradation of u	0.035
μ_v	degradation of v	0.1
D_u	diffusion of u	0.4
D_v	diffusion of v	15

Table 2: Parameter values for stochastic simulations in Sections 4.2.2 and 4.4.2.

The parameter values for the minimal model are listed in Table 2 on page 75 (where applicable), with the exception of D_u, which is set to 1.6 for this case. The parameters choice is such that the model can be simulated in a reasonable time, and shows the required properties.

All the models used in this chapter are available in SBML at `http://www.lifl.fr/~batmanov/fi2012-models/`.

4.2.2 *Stochastic simulations show a community effect with unlimited spread*

We performed stochastic simulations of rule-based models using a variant of the Gibson and Bruck method [Gibson and Bruck, 2000], an optimization of Gillespie's algorithm [Gillespie, 1976]. It was implemented in the Scala language[1]. The source code of Gillespie simulators, as well as a Mathematica notebook showing PDE solutions used later in this chapter, is available at
`http://www.lifl.fr/~batmanov/thesis/simulationCode.zip`.

We show typical single simulation runs in Figures 25a and 25b. The plots show the dynamics of u across the cell row over time with different numbers of active cells, below ($N_a = 9$, a) and above ($N_a = 11$, b) the community effect's activation threshold ($N_a = 10$). Both simulations start from an initial induction with $\sharp u(x) = 10$ molecules per active cell at time zero. The system can reach either a state with $\sharp u(x) = 0$ in all cells, the zero state, or enter the self-sustained activation state, where $\sharp u(x)$ stabilizes above zero. Since u can degrade at any moment, there is a non-zero probability for the system to collapse to the zero state at all time points. However, this probability becomes negligibly

1 `http://www.scala-lang.org/`

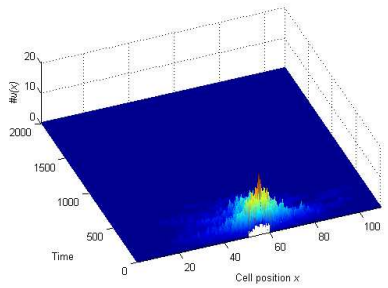

(a) $N_a = 9$, $N_p = 50$.

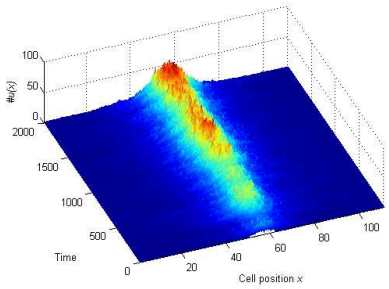

(b) $N_a = 11$, $N_p = 50$.

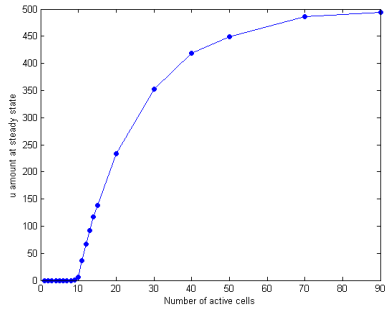

(c) Number of u molecules in the middle cell at $t = 2000$, averaged across 100 runs.

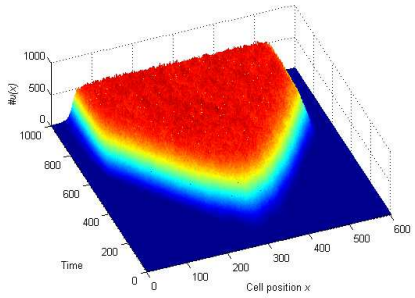

(d) $N_a = 500$, $N_p = 50$. Initial induction localized at $x = 300$.

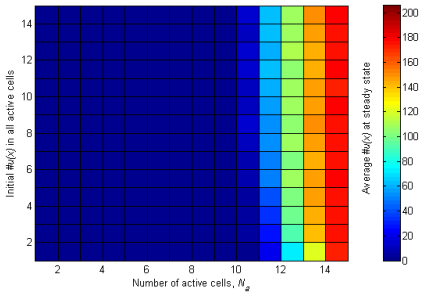

(e) Effect of the initial u amount on the threshold. $N_p = 50$.

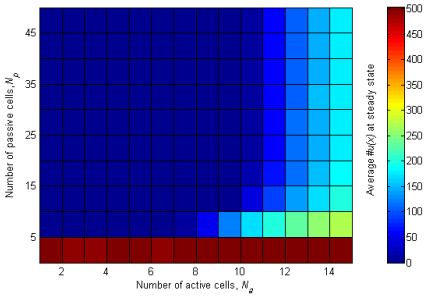

(f) Effect of N_p on the threshold. Initial $\sharp u(x) = 10$.

Figure 25: Stochastic simulations of the minimal model of a community effect. (a, b, d): single simulation runs. (c, e, f): summary of many simulations.

low for the cases studied here once the system reaches self-sustaining activation; therefore we call this outcome a steady state.

- **Figure 25a**. $N_a = 9$: the system is unable to sustain activation. The u molecules for induction at $t = 0$ are visible as a peak in all active cells. However, they quickly dissipate. This is a typical simulation outcome. Only 1 out of 100 simulations showed any residual activity at $t = 2000$.

- **Figure 25b**. $N_a = 11$: the system enters sustained activation in all 100 simulation runs.

To check if the system has reached self-sustaining activation, we simulate until $t > 2000$. This is long enough for the initial induction to degrade. Any residual activity in the system can be ascribed to self-sustaining activation. We used this criterion to systematically investigate the activation threshold number of active cells:

- **Figure 25c** summarizes simulation results (2100 runs in total). Each point in this plot is the mean u amount at $t = 2000$ in the cell in the middle of the community, for 100 simulations with the given N_a. The threshold value of $N_a = 10$ clearly appears. The system enters sustained activation only when N_a is above this value. As N_a increases, the steady state amount of u approaches 500, its theoretical maximum when the feedback loop saturates.

Next, we examined the dynamics of the system in space and made an interesting observation.

- **Figure 25d**. With $N_a = 500$ well above the threshold, the system enters sustained activation with high probability even when inducing only *one* active cell at the centre of the row, with $\sharp u(x) = 10$ at time zero. Note that, in Figure 25a and Figure 25b, the same amount was injected into *all* active cells. Significantly, *activation spreads over the entire row of active cells* from the location of the initial induction in the middle of the row.

The probability of sustained activation varies with the total amount of the initial induction when it is low. We found that initial activation by $\sharp u(x) = 10$ molecules per cell is sufficient to exclude this variation:

- **Figure 25e**. The effect of initial u amount on activation threshold N_a. Each square in the grid displays the colour-coded $\sharp u(x)$ in the middle of the community at steady state ($t = 1000$), averaged over 25 simulations, with a given combination of N_a and initial $\sharp u(x)$ per active cell. For low initial u amounts, the threshold N_a for self-sustaining activation increases. Beyond $\sharp u(x) = 10$, the threshold stabilizes. Note that $N_p = 50$ for all simulations.

- **Figure 25f**. The impact of the number of passive cells N_p on the threshold of active cell number N_a. The lower N_p, the higher the chance for u to re-enter the active area after being reflected back at the system's boundary. When $N_p = 0$, this boundary effect increases and effectively eliminates the N_a threshold, down to zero (see also subsection 4.2.4). With increasing N_p, the boundary effect becomes negligible, and the critical N_a threshold becomes independent of N_p.

Simulations indicate that the steady-state number of u, if the system ever reaches a non-zero steady state, is independent of the location, size (width), and the amplitude of the initial induction. Similar behaviour was observed in the spaceless model of the community effect in [Saka et al., 2011]. We generally observed that, for a self-sustaining activation, the number of active cells must exceed a critical threshold, which is one of the hallmarks of a community effect. We observed that the community effect spreads in an unlimited manner in the minimal model described in this section.

4.2.3 *Biological relevance of the minimal model*

The minimal model introduced in this section is abstract, but nonetheless useful because it is simple and it reproduces the essential features of community effects. We also modelled the community effect in *Xenopus* in greater detail, using the RDME as well as PDE treatments. See Section 4.3 for the description of those detailed models and discussions.

The saturating self-activation reaction abstracts a process by which a diffusible factor enhances its own production. In real cells this involves binding of a diffusible factor to the cell surface, activation of the signalling pathway and the induction of the corresponding gene. In addition, the gene that produces the diffusible factors may be induced indirectly, by a cascade of inductions of intermediate genes, as happens in the community effect of *Xenopus* muscle precursor cells [Saka et al., 2011].

The diffusion scheme with the row of active cells between two layers of passive cells reflects the *sandwich*-like experimental setup of Gurdon *et al.* [Gurdon et al., 1996, 1993], in which an inducer-soaked bead is placed between two slices of ectoderm tissue. To be more precise, our model's row corresponds to a vertical cut through the sandwich of cells. The inner layer of the ectoderm tissue corresponds to active cells and outer-most layer to passive cells.

4.2.4 *Passive cells are required for the cell number-dependent community effect*

We conclude the analysis of the minimal model by proving that the closed system without passive cells cannot have the threshold of N_a where its steady state changes. To formally analyse the steady states of the minimal model, we treat it deterministically using the continuous reaction-diffusion theory (see subsection 2.5.1). The PDE of the minimal model is:

$$\frac{\partial u}{\partial t} = \frac{\alpha_u u}{k_u + u} - \mu_u u + \lambda_u \Delta u \tag{32}$$

where $u(x,t)$ is the average $\sharp u$ at space coordinate x and time t, which remain always implicit in PDEs. λ_u is a diffusion coefficient, which can be derived from D_u and the spatial configuration. The precise expression for it is not important for the following analysis. There are no passive cells in this PDE model because the activation term is applicable everywhere. All the parameters are assumed to be positive. This model is using the Laplacian Δu to describe the diffusion of u, and therefore is applicable to n-dimensional case. $\lambda_u \Delta u(x,t)$ defines the rate of u diffusing to point x at time t. Let $\Omega \subset \mathbb{R}^n$ be the spatial domain of the system, a compact, connected set, and $\overline{\Omega}$ its boundary. We consider a closed system with no passive cells, so one of the boundary conditions is

$$\nabla u(x,t) \cdot n(x) = 0, \forall x \in \overline{\Omega}, \forall t \geqslant 0 \tag{33}$$

where $n(x)$ is an outward unit normal of the boundary $\overline{\Omega}$ and ∇ is the gradient operator. This states that the flux of u across the boundary is zero at all points. Another boundary condition is the initial induction

$$u(x,0) = f(x) \geqslant 0, \forall x \in \Omega \tag{34}$$

Let $g(u) = \frac{\alpha_u u}{k_u + u} - \mu_u u$ and $u_c = \frac{\alpha_u - \mu_u k_u}{\mu_u}$. Note that $g(u)$ has two zero points: $g(0) = 0$ and $g(u_c) = 0$, and $g(u) > 0, \forall u : 0 < u < u_c$.

First, note that $\forall t \geqslant 0, \forall x \in \Omega, u(x,t) \geqslant 0$. It follows from the initial condition being nonnegative and $g(0) = 0$.

Second, note that if $f(x) = 0$ for some x, but $\int_\Omega f(x) d\Omega > 0$ and $u_c > 0$, then $\forall t > 0, u(x,t) > 0$, because diffusion distributes concentration across space instantly. To show this, we consider initial induction to be a δ function and consider the heat equation $\frac{\partial u}{\partial t} = \lambda_u \Delta u$. It has an analytical fundamental solution which is positive for $t > 0$, but the solution of (32) is always greater or equal to the solution of the heat equation, because $g(u) \geqslant 0$.

Also $u(x,t)$ is continuous $\forall t > 0, \forall x \in \Omega$. So, without loss of generality, we consider the initial induction $f(x)$ to be continuous, and if $u_c > 0$ then also $f(x) > 0$.

We will introduce simple lower and upper bounds on the solutions, which can be easily analysed.

Lemma 4.2.1 (Lower bound). *If* $u_c > 0$, *then* $\forall x \in \Omega, \forall t \geqslant 0, u(x,t) \geqslant \underline{u}(x,t)$, *where* $\underline{u}$ *is the solution of* (32)-(33) *with initial condition* $\underline{u}(x,0) = \min_{\Omega} f(x)/2$.

First, note that $\underline{u}$ is homogeneous in space at all times. The initial condition is homogeneous, so there is no diffusion inside the system; also by (33) there is no diffusion through the borders. So we can write $\underline{u}(x,t) = \underline{u}(t)$, which is the solution of the ODE

$$\begin{aligned} \frac{d\underline{u}}{dt} &= g(\underline{u}) \\ \underline{u}(0) &= \min_{\Omega} f(x)/2 \end{aligned} \tag{35}$$

The initial condition of $\underline{u}$ is chosen in this way to guarantee $0 < \underline{u}(0) < u(x,0), \forall x \in \Omega$.

The idea of the proof can be summarized as follows. We consider a point x_* where u crosses $\underline{u}$ the first time. Then it must be the minimum of u, and thus u will grow there at least as fast as $\underline{u}$, because u cannot diffuse out of the minimum point. Then it cannot go below $\underline{u}$ at this point.

Proof. Suppose that $u(x,t) < \underline{u}(t)$ somewhere. Note that $u(x,0) > \underline{u}(0), \forall x \in \Omega$. Let $t_* = \inf\{t \geqslant 0 : \exists x \in \Omega : u(x,t) < \underline{u}(t)\}$. Note that

$$u(x,t_*) \geqslant \underline{u}(t_*), \forall x \in \Omega, \tag{36}$$

because the solutions are continuous. It follows that

$$\exists x_* : u(x_*,t_*) = \underline{u}(t_*), \tag{37}$$

and for any sufficiently small $\epsilon > 0 : u(x_*, t_* + \epsilon) < \underline{u}(t_* + \epsilon)$. Subtracting $u(x_*,t_*)$ from the left side and $\underline{u}(t_*)$ from the right side of the last inequality, dividing by ϵ, and taking $\lim_{\epsilon \to 0}$, we get

$$\frac{\partial u}{\partial t}(x_*,t_*) < \frac{d\underline{u}}{dt}(t_*) \tag{38}$$

From (36) and (37), $u(x_*,t_*) \leqslant u(x,t_*), \forall x \in \Omega$, i.e. $u(x_*,t_*)$ is a local minimum in space. Then $\Delta u(x_*,t_*) \geqslant 0$, and we have

$$\frac{\partial u}{\partial t}(x_*,t_*) = g(u(x_*,t_*)) + \Delta u(x_*,t_*) \geqslant g(u(x_*,t_*)) = g(\underline{u}(t_*)) = \frac{d\underline{u}}{dt}(t_*),$$

but this contradicts (38). □

Lemma 4.2.2 (Upper bound). $\forall x \in \Omega, \forall t \geqslant 0, u(x,t) \leqslant \overline{u}(x,t)$, *where* $\overline{u}$ *is the solution of* (32)-(33) *with initial condition* $\overline{u}(x,0) = \max_{\Omega} f(x) \cdot 2$.

The proof is analogous to lemma 4.2.1, exchanging max and min and reversing inequalities as appropriate.

Theorem 4.2.3. *If* $u_c > 0$, *then* $\lim_{t\to\infty} u(x,t) = u_c, \forall x \in \Omega$.

Proof. From the lemmas we have $\underline{u}(t) \leqslant u(x,t) \leqslant \overline{u}(t), \forall t \geqslant 0, \forall x \in \Omega$. Since $u_c > 0$, the ODEs for $\underline{u}$ and $\overline{u}$ have an attractor at u_c, to which they will converge asymptotically starting from any point greater than zero. Therefore, $\lim_{t\to\infty} \underline{u}(t) = \lim_{t\to\infty} \overline{u}(t) = u_c$, from which follows the statement. □

Theorem 4.2.4. *If* $u_c \leqslant 0$, *then* $\lim_{t\to\infty} u(x,t) = 0, \forall x \in \Omega$.

Proof. From the lemmas we have $0 \leqslant u(x,t) \leqslant \overline{u}(t), \forall t \geqslant 0, \forall x \in \Omega$. Since $u_c \leqslant 0$, $g(u) \leqslant 0$ in the ODE for $\overline{u}$, and it has an attractor at $u = 0$, to which it will converge asymptotically starting from any point greater than zero. Therefore, $\lim_{t\to\infty} \overline{u}(t) = 0$, from which follows the statement. □

From the theorems it follows that for the closed system, where all cells are active, the outcome does not depend on the geometry of space and the initial conditions; it depends solely on the parameters of the GRN. Therefore we cannot observe the property that there exists a threshold on the number of cells below which there is no sustained activation. Number of cells in this model corresponds to the volume of Ω. We see that for any spatial configuration, the system will either always enter the sustained activation, or, if $u_c \leqslant 0$, the activity will always fall to zero. For the parameters we used in the simulations, $u_c = 500$.

If we introduce the passive cells, in terms of the PDE the areas where $g(u) = -\mu_u u$, the lemmas still seem to hold, but the PDEs for $\underline{u}$ and $\overline{u}$ can no longer be reduced to ODEs, since the solutions will not be homogeneous anymore. We do not investigate the system with passive cells further, because its PDE contains discontinuous functions and thus its formal analysis is difficult. Rather, the behaviour of the system in this case was investigated above in the stochastic regime, using the RDME simulations.

4.3 SPATIAL MODEL OF A COMMUNITY EFFECT IN *xenopus*

In this section we present a model of the community effect in *Xenopus*. It can be seen as an expansion of our minimal model in Section 4.2 on two levels. First, the community effect loop here involves two genes and their protein products, instead of one, in intercellular communication (Figure 26). Second, instead of collapsing a gene expression into one

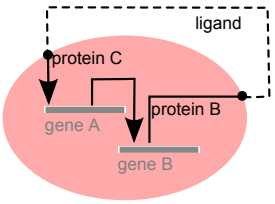

Figure 26: The GRN for the community effect in an active cell with genes A and B. Gene A activates gene B, protein B is expelled from the cell, transformed into a diffusible factor, here called *ligand*, that diffuses to adjacent cells. This signal's reception activates protein C, which in turns activates gene A.

reaction, we consider separately transcription of genes into messenger RNA, and its translation into proteins. This detailed reaction network was previously investigated in [Saka et al., 2011]. The new contribution of this section is to consider the same detailed network of a community effect *in space*. Based on a RDME analysis (subsection 4.3.3), we observe an unlimited spread of a community effect in stochastic simulation. This confirms our observations based on the minimal model in Section 4.2. To confirm our results observed in *discrete space*, we investigate a deterministic PDE model with explicit diffusion in *continuous* one-dimensional space in subsection 4.3.4. The findings confirm our previous conclusions in [Saka et al., 2011] and strengthen the results we have presented in Section 4.2.

4.3.1 *Informal description of the GRN with one-dimensional diffusion*

Due to the greater level of details, we resort to a different graphical notation for the *GRN of active cells* in Figure 26. Each cell contains two genes A and B, where A *activates* B. In turn, B *activates* A over a feedback loop mediated by inter-cellular communication: Gene B expresses a protein, which is then exported out of the cell and turned into a diffusible factor, named `ligand`. This `ligand` either degrades, or *diffuses* to a directly neighbouring cell. Reception of a ligand by an active cell results in an intra-cellular signal, which creates a protein C. This protein C then activates gene A.

4.3.2 *Chemical reactions of the detailed model*

The detailed reaction network including the intermediate steps of transcription and translation is listed in Figure 27. Note that terms such as $Gene(\mathsf{A})$ include the species variables $\in \{\mathsf{A}, \mathsf{B}, \mathsf{C}\}$ as the parameter. As with position variables, this means that for each value of the variable there is a separate chemical species, as well as an instance of the reaction where this species appear. All listed reactions are present in the active cells, while in passive cells only degradation of proteins occurs (reactions (43), (44), and (47)).

Reaction (39) denotes the activation of the gene A in an active cell, represented by the term $Gene(\mathsf{A})$, by the protein $Prot(\mathsf{C})$. It results

$$Gene(\mathsf{A}) + Prot(\mathsf{C}) \underset{\alpha_2}{\overset{\alpha_1}{\rightleftharpoons}} InducedGene(\mathsf{A}) \tag{39}$$

$$Gene(\mathsf{B}) + Prot(\mathsf{A}) \underset{\alpha_2}{\overset{\alpha_2}{\rightleftharpoons}} InducedGene(\mathsf{B}) \tag{40}$$

$$InducedGene(\mathsf{s}) \xrightarrow{\beta} InducedGene(\mathsf{s}) + mRNA(\mathsf{s}) \tag{41}$$

$$mRNA(\mathsf{s}) \xrightarrow{\gamma} mRNA(\mathsf{s}) + Prot(\mathsf{s}) \tag{42}$$

$$mRNA(\mathsf{s}) \xrightarrow{\delta_m} \tag{43}$$

$$Prot(\mathsf{s}') \xrightarrow{\delta_p} \tag{44}$$

$$InducedGene(\mathsf{s}) \xrightarrow{\delta_p} Gene(\mathsf{s}) \tag{45}$$

$$Prot(\mathsf{B}) \xrightarrow{\kappa} Ligand \tag{46}$$

$$Ligand \xrightarrow{\delta_\ell} \tag{47}$$

$$Ligand \xrightarrow{\epsilon} Prot(\mathsf{C}) \tag{48}$$

where $\mathsf{s} \in \{\mathsf{A}, \mathsf{B}\}, \mathsf{s}' \in \{\mathsf{A}, \mathsf{B}, \mathsf{C}\}$.

Figure 27: Chemical reactions of the community effect in *Xenopus*.

in an induced gene, represented by $InducedGene(\mathsf{A})$. This is indeed a complex between the protein C and the gene A's promoter. α_1 and α_2 are the rate parameters for the forward and reverse reactions, respectively. These parameters define the mass action rate of this event. In this model, we only write the rate parameters, since all the rate expressions are defined by the mass action rule. Likewise, the reaction (40) describes the activation of gene B by protein A.

Transcription and translation of a gene are defined by reaction (41) and (42). Transcription requires an induced gene. Both mRNA and protein degrade according to the rules (43) and (44). Proteins may also degrade while they are bound to a gene, as stated in rule (45). The rate of this degradation is the same as the degradation rate of the unbound protein, δ_p.

4.3.3 *RDME analysis of the detailed model*

First, we analysed the detailed model in the RDME framework. The spatial configuration is the same as for the minimal model of Section 4.2, therefore its RDME can be formulated in the rule-based language with one-dimensional coordinate variable as before. This model is given in Figure 28. Now every species has an additional parameter which is the coordinate of the cell, so there are $2N_p + N_a$ copies of every species in the model.

$$\forall x \in \mathit{ActiveCells},$$
$$\mathit{Gene}(A,x) + \mathit{Prot}(C,x) \underset{\alpha_2}{\overset{\alpha_1}{\rightleftharpoons}} \mathit{InducedGene}(A,x) \tag{49}$$

$$\forall x \in \mathit{ActiveCells},$$
$$\mathit{Gene}(B,x) + \mathit{Prot}(A,x) \underset{\alpha_2}{\overset{\alpha_2}{\rightleftharpoons}} \mathit{InducedGene}(B,x) \tag{50}$$

$$\forall x \in \mathit{ActiveCells}, \quad \mathit{InducedGene}(s,x) \xrightarrow{\beta} \mathit{InducedGene}(s,x) + \mathit{mRNA}(s,x) \tag{51}$$

$$\forall x \in \mathit{ActiveCells}, \quad \mathit{mRNA}(s,x) \xrightarrow{\gamma} \mathit{mRNA}(s,x) + \mathit{Prot}(s,x) \tag{52}$$

$$\forall x \in \mathit{ActiveCells}, \quad \mathit{mRNA}(s,x) \xrightarrow{\delta_m} \tag{53}$$

$$\forall x \in \mathit{ActiveCells}, \quad \mathit{Prot}(s',x) \xrightarrow{\delta_p} \tag{54}$$

$$\forall x \in \mathit{ActiveCells}, \quad \mathit{InducedGene}(s,x) \xrightarrow{\delta_p} \mathit{Gene}(s,x) \tag{55}$$

$$\forall x \in \mathit{ActiveCells}, \quad \mathit{Prot}(B,x) \xrightarrow{\kappa} \mathit{Ligand}(x) \tag{56}$$

$$\forall x \in \mathit{AllCells} - \mathsf{LastCell}, \quad \mathit{Ligand}(x) \underset{D}{\overset{D}{\rightleftharpoons}} \mathit{Ligand}(x+1) \tag{57}$$

$$\forall x \in \mathit{AllCells}, \quad \mathit{Ligand}(x) \xrightarrow{\delta_\ell} \tag{58}$$

$$\forall x \in \mathit{ActiveCells}, \quad \mathit{Ligand}(x) \xrightarrow{\epsilon} \mathit{Prot}(C,x) \tag{59}$$

where $s \in \{A,B\}, s' \in \{A,B,C\}$, $\mathit{ActiveCells} = \{1+N_p,\ldots,N_p+N_a\}$, $\mathit{AllCells} = \{1,\ldots,2N_p+N_a\}$, and $\mathsf{LastCell} = \{2N_p+N_a\}$.

Figure 28: Detailed rule-based model of a community effect with diffusion in one-dimensional space.

Parameter	Description	Value
α_1	binding of a transcription factor to a gene	1.93×10^{-4}
α_2	dissociation of a transcription factor from a gene	3.47×10^{-2}
β	transcription of a gene to mRNA	1.16×10^{-2}
γ	translation of mRNA, creating a protein	2.31×10^{-2}
δ_m	degradation of mRNAs	1.16×10^{-3}
δ_p	degradation of proteins	3.47×10^{-4}
δ_l	degradation of Ligand	1.4×10^{-2}
κ	export of Prot(B) outside of a cell, creating a Ligand	3.85×10^{-4}
ϵ	binding of Ligand to an active cell, creating a Prot(C)	5.78×10^{-5}
D	diffusion of Ligand between two adjacent cells	5.205×10^{-2}

Table 3: Parameter values for stochastic simulations are the same as in [Saka et al., 2011], except those concerning Ligand.

Diffusion is implemented in a more fine-grained manner than the one described previously. Rule (56) defines the export of a B protein from the x^{th} cell into the extracellular space and its conversion into a ligand. The position of a ligand is specified by an integer $x \in \mathit{AllCells}$, the same coordinate system as the cell. Note the distinction between active cells (pink ovals) and its neighbourhood (grey box without ovals) in Figure 22 on page 73. A secreted ligand hops from one position to the next by random walk, which approximates its diffusion in the entire extracellular space via (57). Note that Ligand is the only diffusing species in this model. In any position, the ligand can degrade (see rule (58)). Finally, the binding of a ligand to a cellular receptor of an active cell and subsequent production of protein C is governed by rule (59).

Stochastic simulations

We simulated the dynamics of the one-dimensional cell row over time by stochastic simulations similar to those used previously. Again, we first consider typical single simulation runs in Figure 29. Panels (a, c, e) show the dynamics of the Ligand number across the cell row over time. Panels (b, d, f) are snapshots of Prot(A) taken at the end of those simulations. All simulations are initiated by the initial induction with 100 Ligand molecules in the leftmost active cell at time zero. We tested three different combinations of (N_a, N_p) for simulations. See Table 3 for the parameter values used in simulations.

We observe essentially the same behaviour as in the minimal model in Section 4.2:

- $N_a = 25$, $N_p = 100$: below the threshold number of active cells, the system is unable to sustain activation (Figure 29a, Figure 29b).

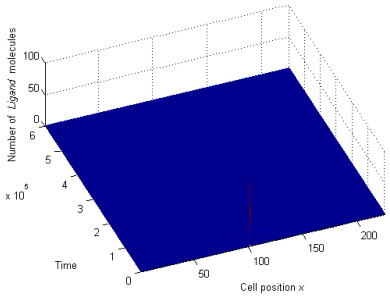

(a) Ligand: $N_a = 25$, $N_p = 100$.

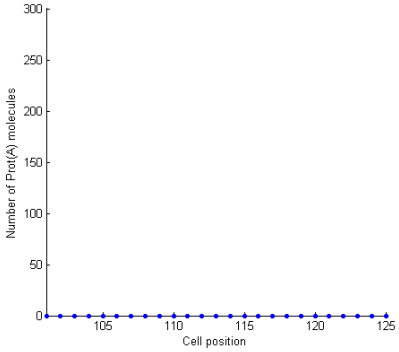

(b) Prot(A): $N_a = 25$, $N_p = 100$, $t = 6 \times 10^5$.

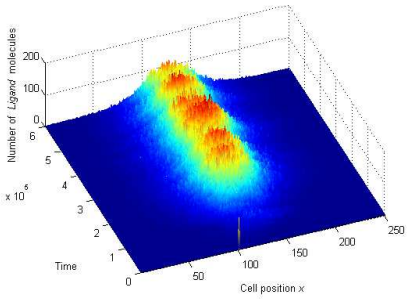

(c) Ligand: $N_a = 50$, $N_p = 100$.

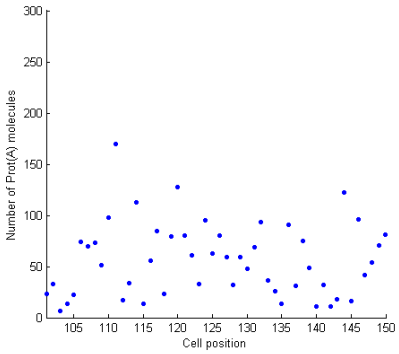

(d) Prot(A): $N_a = 50$, $N_p = 100$, $t = 6 \times 10^5$.

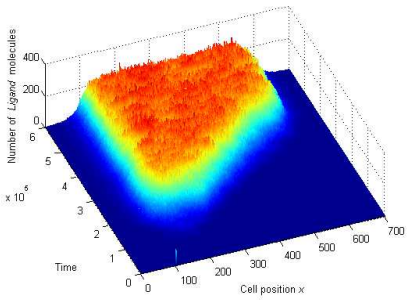

(e) Ligand: $N_a = 500$, $N_p = 100$.

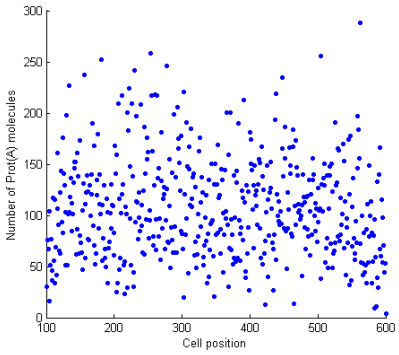

(f) Prot(A): $N_a = 500$, $N_p = 100$, $t = 6 \times 10^5$.

Figure 29: Single runs of stochastic simulation of the detailed model of a community effect. Left column: time course of Ligand over the entire cell row. Right column: at the end of the simulation to the left, level of protein A in active cells.

Only 16 of 100 simulations showed any residual activity at $t = 6 \times 10^5$.

- $N_a = 50$, $N_p = 100$: the system enters sustained activation in all of 100 simulation runs, as shown for a typical run in Figure 29c. Thus the activation threshold lies in the range between 25 and 50 active cells. At the end of the simulation, $\mathsf{Prot}(A)$ is present in all active cells (Figure 29d), indicating a coordinated gene expression in the community.

- $N_a = 500$, $N_p = 100$: With N_a well above the threshold, all simulations showed sustained activation, as in the run in Figures 29e and 29f, where all active cells reached a self-sustaining gene expression at a significant level. We observe that, as in the minimal model, a community effect spreads all over the active cells, similar to Figure 25d on page 76.

To better understand our observation in stochastic simulations and the relationship between N_p, N_a and the community effect, we constructed a deterministic model, which we describe below.

4.3.4 *PDE analysis of the detailed model*

The PDE model is made using the reaction-diffusion framework from the reactions defined in Figure 27 and the spatial configuration of the system. In this deterministic model molecular diffusion happens in *continuous* one-dimensional space. To avoid any confusion, we use different nomenclatures for terms in the rule-based model (representing *numbers* of molecules) and variables in this deterministic model (which stand for *concentrations*), as summarized in Table 4.

There are several additional complications. First, the model is slightly reduced using conservation laws. Second, we introduce the concept of *cell density*, which was implicit in RDME thanks to simple space subdivision, with one cell being represented with one subvolume. Third, the spatial inhomogeneities, namely the presence of active-passive cell border and non-uniform initial induction, requires special treatment. The detailed explanation is as follows:

Because the number of gene copies per cell ($= 1$ in our model) is conserved, in the region occupied by active cells,

$$\begin{aligned} Ag + Agi &= \rho \\ Bg + Bgi &= \rho, \end{aligned} \tag{60}$$

where ρ is the cell density. The dynamics of the variables are described by a set of PDEs:

Molecules	**PDE variables**	**Rule-based terms**
Gene A	Ag	$Gene(A, x)$
Gene B	Bg	$Gene(B, x)$
Induced gene A	Agi	$InducedGene(A, x)$
Induced gene B	Bgi	$InducedGene(B, x)$
Transcripts (mRNA) of gene A	Ar	$mRNA(A, x)$
Transcripts (mRNA) of gene B	Br	$mRNA(B, x)$
Protein product of gene A	Ap	$Prot(A, x)$
Protein product of gene B	Bp	$Prot(B, x)$
Protein C	Cp	$Prot(C, x)$
The diffusible factor	Lp	$Ligand(x)$

Table 4: Terms of the stochastic model and corresponding variables of the deterministic model. Variables in the PDE model, briefly referred to as e.g. Ap, are indeed functions of (continuous) space x and time t, e.g. $Ap(x, t)$.

$$\frac{\partial Agi}{\partial t} = \alpha_1 \, Ag \, Cp - (\alpha_2 + \delta_p) \, Agi, \tag{61}$$

$$\frac{\partial Bgi}{\partial t} = \alpha_1 \, Bg \, Ap - (\alpha_2 + \delta_p) \, Bgi, \tag{62}$$

$$\frac{\partial Ar}{\partial t} = \beta \, Agi - \delta_m \, Ar, \tag{63}$$

$$\frac{\partial Br}{\partial t} = \beta \, Bgi - \delta_m \, Br, \tag{64}$$

$$\frac{\partial Ap}{\partial t} = \gamma \, Ar + \alpha_2 \, Bgi - \alpha_1 \, Bg \, Ap - \delta_p \, Ap, \tag{65}$$

$$\frac{\partial Bp}{\partial t} = \gamma \, Br - (\kappa + \delta_p) \, Bp, \tag{66}$$

$$\frac{\partial \, Cp}{\partial t} = \epsilon \, Lp + \alpha_2 \, Agi - \alpha_1 \, Ag \, Cp - \delta_p \, Cp, \tag{67}$$

$$\frac{\partial Lp}{\partial t} = \lambda \, \Delta Lp - \delta_\ell \, Lp + J + I, \tag{68}$$

where the functions J and I in (68) are defined as

$$J(x, t) = \kappa \, Bp(x, t) - \epsilon \, Lp(x, t), \tag{69}$$

$$I(t) = \eta \, \theta(\tau - t). \tag{70}$$

Here, θ is the unit step function:

$$\theta(x) = \begin{cases} 0, & x < 0 \\ 1, & x > 0 \end{cases}$$

and J is the net flow of Lp in and out of the cell. The function I is the initial induction of amplitude η and duration τ. The term $\lambda \, \Delta Lp$

Parameter	Description	Value	Range
α_1	binding of Cp to Ag	1.93×10^{-4}	fixed value
α_2	dissociation of Cp from Ag	3.47×10^{-2}	fixed value
β	transcription	1.16×10^{-2}	fixed value
γ	translation w	2.31×10^{-2}	fixed value
δ_m	degradation of mRNAs	1.16×10^{-3}	fixed value
δ_p	degradation of proteins	5.78×10^{-4}	fixed value
δ_ℓ	degradation of Lp	5×10^{-4}	fixed value
ϵ	import and conversion of Lp into Cp	10^{-5}	n.a.
κ	export and conversion of Bp into Lp	3.85×10^{-4}	fixed value
λ	diffusion rate of Lp	20	fixed value
ρ	cell density	see Fig.30	$0 \leqslant \rho \leqslant 20$
η	amplitude of induction	2	fixed value
τ	duration of induction	200	fixed value
r_a	domain size of active cells (community size)	see Fig.30	$0 \leqslant r_a \leqslant 400$
r_p	domain size of passive cells	see Fig.30	see Fig.30

Table 5: Parameter values for numerical simulations of a community effect in subsection 4.3.4. Used for simulations, unless defined explicitly in the main text. Parameter ranges in the last column are used for phase diagrams.

describes diffusion of Lp, where λ is the diffusion coefficient. The boundary condition is

$$Ag(x,0) = Bg(x,0) = \rho,$$

and all other variables are 0 at $t = 0$. We consider the system in $0 \leqslant x \leqslant d$ with closed boundaries, therefore

$$\frac{\partial Lp}{\partial x} = 0,\ x = \begin{cases} 0 \\ d \end{cases}. \tag{71}$$

As in the rule-based model, the active cells occupy the middle domain of width r_a, and are flanked by a passive cell region of size r_p on each side. Therefore,

$$d = r_a + 2r_p.$$

Community effects are size- and density-dependent in the one-dimensional model

The simulation results of the PDE model are qualitatively similar to what we observed in stochastic simulations (Figure 30). The most no-

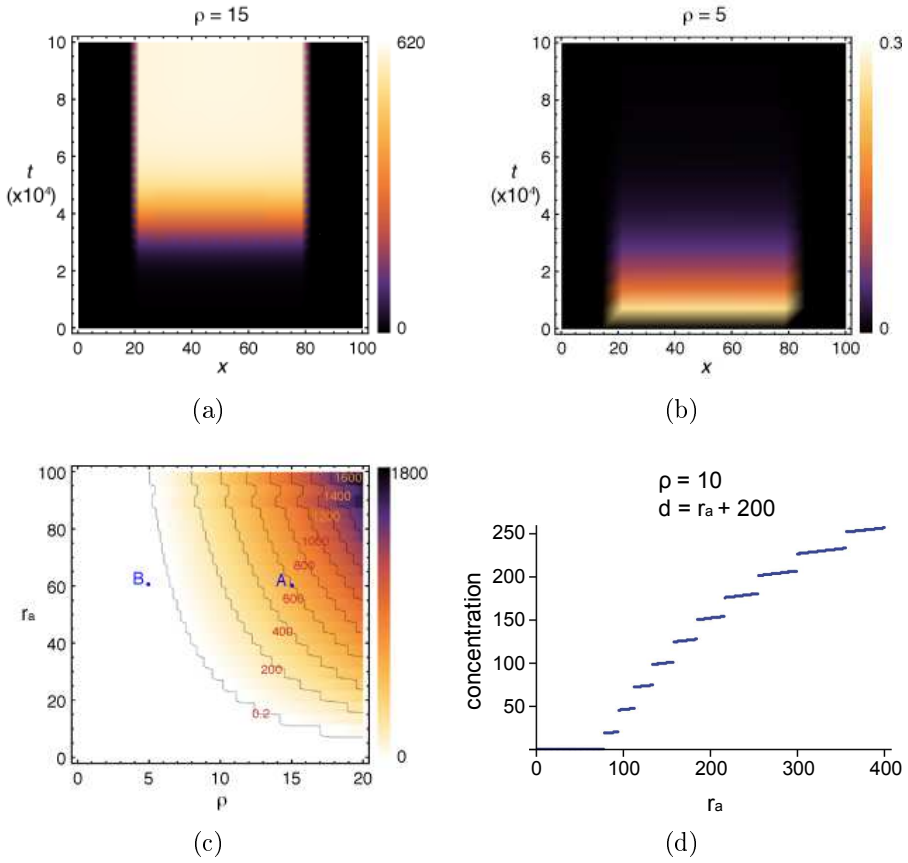

Figure 30: Simulations of the deterministic model of a community effect. **(a, b)** The dynamics of Ap in 1D space over time, for two different densities. The concentration is colour-coded as indicated. **(a)** At high density ($\rho = 15$) the community effect spreads rapidly once initiated. **(b)** With low density ($\rho = 5$), gene expression is transient. Note the different scale of colour-coding for gene expression level. Parameter values for induction are $\eta = 2, \tau = 200$ and the width of induction is 1. **(c)** Phase diagram in the parameter plane (ρ, r_a). Initial induction is applied uniformly across the community. Ap concentration at quasi-steady state ($t = 4 \times 10^5$) is colour-coded as indicated. Contours are also shown. Gene expression depends on the cell density ρ and the size of the community r_2. The blue dots correspond to the parameter sets in panels (a) and (b). **(d)** Ap concentration plotted as a function of the community size r_a. Simulations are performed with the constant $r_p = 100$ and $\rho = 10$. Initial induction is applied uniformly across the community. The plot shows many discontinuous jumps in concentration, which is most likely an artefact of the numerical integration.

table observation is that self-sustained gene expression depends on the cell density and the size of the community relative to that of the whole system. This indicates that community effects are influenced by the spatial arrangement of cells. Let us now explain the simulation results of the PDE model.

Figure 30a and Figure 30b show the typical dynamics of Ap concentration in one dimensional space with different cell densities. In these simulations, $d = 100$ and $r_a = 60$ ($r_p = 20$). Although only the narrow middle region of width one is induced for a brief period, the entire domain of active cells starts expressing Ag after a time lag. This seemingly dormant period before the surge of gene expression was previously observed with a spaceless model of a community effect [Saka et al., 2011]. Such expression surge happens almost simultaneous across the community in the simulations. The speed of the expansion of a community effect obviously depends on the diffusion rate of the ligand δ_ℓ. With lower diffusion rates, it becomes slower and is qualitatively similar to the spread of a community effect shown in Figure 25d and Figure 29e. In the simulation in Figure 30a, the ligand concentration becomes almost uniform across the whole system at steady state (data not shown).

The system reproduces a community effect: once the size and density of the community exceeds certain thresholds the group can maintain gene expression after a transient induction. We next asked what is the *relationship between the size of the community and the density of the cell group*. Figure 30c is a phase diagram plotted for the parameter pair (ρ, r_a), with a constant system size $d = 100$. The diagram indicates that the condition for a self-sustained gene expression is strongly correlated with the cell density and the community size. The critical *contour* for $Ap = 0.2$ (an arbitrary number close to 0) shown in the panel does not fit to $r_a\rho$ (number of cells) $= \mathtt{constant}$, indicating that the observed community effects are not a simple *cell number*-dependent phenomena, but are influenced by the cell density and the community's size.

We also performed simulations with a constant cell density, constant passive region $r_p = 100$ and varying r_a, that is, $d = r_a + 200$: this scenario resembles that of the stochastic rule-based model of subsection 4.3.3. The results are consistent with the stochastic simulation results, showing the clear minimal critical r_a that is required for a community effect (Figure 30d). The observed behaviour is qualitatively similar to the minimal model of the community effect, see Figure 25c.

4.4 Regulation of a community effect by a Turing pattern mechanism

The community effect spreads in an unlimited manner over the entire range of active cells in Section 4.2's minimal model, contradicting experimental observations [Bolouri and Davidson, 2010, Duboc et al., 2008, Gurdon et al., 1993]. We address the issue of unlimited spread by two different models in the remainder of this chapter. In this section, we consider a system with *two interacting diffusible factors*: the self-enhancing species for a community effect, and a second species which negatively regulates it. We review this combination, which was introduced in Turing's reaction-diffusion theory [Turing, 1952], in subsection 4.4.1. In

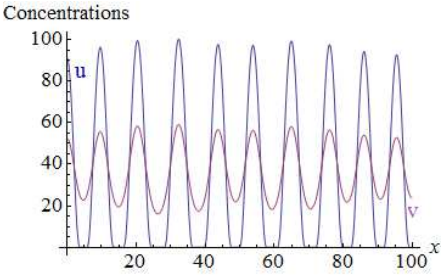

(a) A typical Turing pattern in one dimensional space.

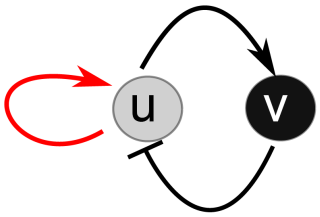

(b) GRN of the Turing pattern model.

Figure 31: A Turing pattern and the corresponding GRN.

subsection 4.4.2, we show that it allows limiting community effects in space. Establishing this connection between the community effect and Turing's reaction-diffusion theory constitutes one of the core contributions of this chapter.

4.4.1 *Turing's reaction-diffusion theory*

Turing investigated reaction-diffusion systems (see subsection 2.5.1) with two interacting and diffusing species in general, regardless of the type of their interaction. The following set of PDEs describing the dynamics of two interacting and diffusing species u and v, is the simplest deterministic model of such a system [Kondo and Asai, 1995]:

$$\frac{\partial u}{\partial t} = c_1\, u + c_2\, v + c_3 + \lambda_u\, \Delta u - \mu_u\, u,$$
$$\frac{\partial v}{\partial t} = c_4\, u + c_5\, v + c_6 + \lambda_v\, \Delta v - \mu_v\, v,$$

where $u(x,t)$ and $v(x,t)$ are concentrations of the two species at space point x and time t. The continuous space is of arbitrary dimension, i.e. $x \in \mathbb{R}^n$, similar to the model used in subsection 4.2.4. The interactions between u and v are specified by the parameters $c_1, \ldots, c_6$. By taking positive or negative values, these can represent activation or inhibition, exerted by either species on itself (c_1, c_5), on the other (c_2, c_4), or basal production (c_3, c_6). Diffusion coefficients λ_u and λ_v define diffusion speeds of u and v, following Fick's second law, as usually done in the reaction-diffusion models. Finally, μ_u and μ_v are degradation rates.

Turing showed that, starting from homogeneous initial distributions of the two species in space, with small random perturbations, this system eventually converges to a steady state. It can reach six different states, depending on the values of the parameters [Turing, 1952].

Turing patterns are the most interesting among the six possible stable states of such reaction-diffusion systems. In two dimensional space,

they can generate a nearly endless variety of spatial patterns. For the simpler case of one-dimensional space that we consider in this work, Turing patterns correspond to *stable periodic waves*. Figure 31a shows a typical example. u and v concentrations are plotted against the space coordinate x, they oscillate in space. Note that the pattern is stable in time, i.e. it is a steady state of the system. Generally, the following *conditions* must hold on the two species of a reaction-diffusion system, in order for Turing patterns to appear [Meinhardt and Gierer, 1974]:

- One of the species, called *activator*, must have a positive effect on both itself and the other. The second species, called *inhibitor*, must have a negative effect on the activator. Figure 31b illustrates this GRN, with activator u and inhibitor v. We refer to this GRN as the *Turing pattern model*.
- The inhibitor must diffuse faster than the activator.

For real biological systems, it is hard to prove experimentally that these conditions are fulfilled. However, reaction-diffusion systems explain many observed patterns. One well-studied case is the formation of the oral ectoderm in sea urchin embryos. There is significant evidence [Duboc et al., 2008] that its area is established by a reaction-diffusion system with Nodal (activator) and Lefty (inhibitor). In this system, a community effect is suggested to occur with Nodal as diffusible factor for cell-to-cell communication Bolouri and Davidson [2010]. Thus, it may not seem too speculative to expect some connection between the reaction-diffusion system and the community effect.

One of our important insights is that *Turing patterns can explain the spatial restriction of the community effect* in our one-dimensional model. We will show that while in the minimal model for a community effect, u's activity spreads over the entire available space, embedding the minimal model into the Turing pattern model confines u's activity to a single wave of limited width.

4.4.2 *Turing pattern model*

In Figure 32, we present chemical reactions of a new model of a community effect, called *Turing pattern model*. It has two diffusible species, u and v. The first two reactions, (72) and (73), are equal to those of the minimal model of a community effect with the diffusible factor u (Figure 23 on page 74). The behaviour of the second diffusible factor v is described by three additional reactions. Reactions (74) and (75) represent activation of the inhibitor and inhibition of the activator required for Turing patterns, with Michaelis-Menten kinetic laws. Reaction (76) defines degradation of v, similar to that of u.

These reactions occur in space defined similarly to that of the minimal model: a single row of cells with active cells being flanked by passive cells, the latter only supporting diffusion and degradation reactions.

$$\text{self-activation of } u\text{:}\quad u \xrightarrow{\alpha_u \frac{\sharp u}{k_u+\sharp u}} 2u \tag{72}$$

$$\text{degradation of } u\text{:}\quad u \xrightarrow{\mu_u \sharp u} \tag{73}$$

$$\text{activation of } v\text{:}\quad u \xrightarrow{\alpha_v \frac{\sharp u}{k_v+\sharp u}} u+v \tag{74}$$

$$\text{inhibition of } u\text{:}\quad u+v \xrightarrow{\alpha_i \sharp v \frac{\sharp u}{k_i+\sharp u}} v \tag{75}$$

$$\text{degradation of } v\text{:}\quad v \xrightarrow{\mu_v \sharp v} \tag{76}$$

Figure 32: Reactions of the Turing pattern model.

$$\text{self-activation of } u\text{:}\quad \forall x \in \mathit{ActiveCells},\quad u(x) \xrightarrow{\alpha_u \frac{\sharp u(x)}{k_u+\sharp u(x)}} 2u(x)$$

$$\text{degradation of } u\text{:}\quad \forall x \in \mathit{AllCells},\quad u(x) \xrightarrow{\mu_u \sharp u(x)}$$

$$\text{diffusion of } u\text{:}\quad \forall x \in \mathit{AllCells}-\{\mathit{LastCell}\},\quad u(x) \underset{D_u \sharp u(x+1)}{\overset{D_u \sharp u(x)}{\rightleftharpoons}} u(x+1)$$

$$\text{activation of } v\text{:}\quad \forall x \in \mathit{ActiveCells},\quad u(x) \xrightarrow{\alpha_v \frac{\sharp u(x)}{k_v+\sharp u(x)}} u(x)+v(x)$$

$$\text{inhibition of } u\text{:}\quad \forall x \in \mathit{ActiveCells},\quad u(x)+v(x) \xrightarrow{\alpha_i \sharp v(x) \frac{\sharp u(x)}{k_i+\sharp u(x)}} v(x)$$

$$\text{degradation of } v\text{:}\quad \forall x \in \mathit{AllCells},\quad v(x) \xrightarrow{\mu_v \sharp v(x)}$$

$$\text{diffusion of } v\text{:}\quad \forall x \in \mathit{AllCells}-\{\mathit{LastCell}\},\quad v(x) \underset{D_v \sharp v(x+1)}{\overset{D_v \sharp v(x)}{\rightleftharpoons}} v(x+1)$$

where $\mathit{ActiveCells} = \{1 + N_p, \ldots, N_p + N_a\}$, $\mathit{AllCells} = \{1, \ldots, \mathit{LastCell}\}$, $\mathit{LastCell} = 2N_p + N_a$.

Figure 33: Rules of Turing pattern model.

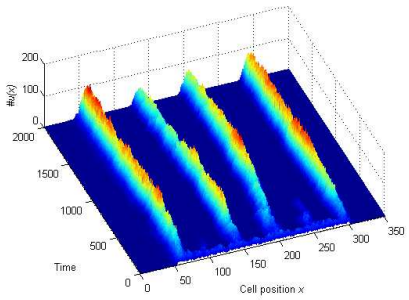

(a) Initial distribution of u is uniform across all active cells.

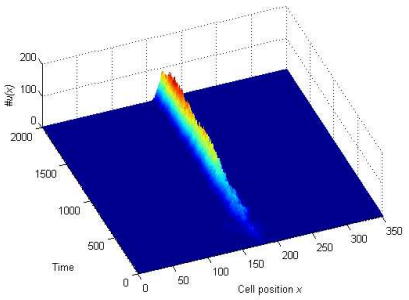

(b) Initial distribution of u is localized at cell 175.

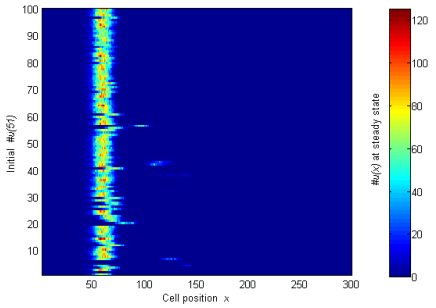

(c) Varying initial u amount is localized at cell 51.

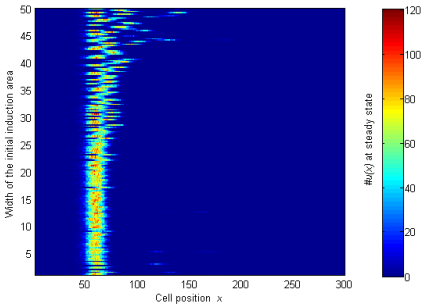

(d) Fixed initial amount of $u = 10$ is spread over an area of varying width starting at cell 51.

Figure 34: Stochastic simulations of Turing pattern model, $N_a = 200$, $N_p = 50$. **(a, b)**: single runs, number of u molecules against time and space coordinates. **(c, d)**: Impact of initial conditions at $t = 1000$.

The RDME formulation of the spatial model is given in the rule-based language in Figure 33. As before, the diffusible activator at the x^{th} position is $u(x)$, and the diffusible inhibitor is $v(x)$.

Figure 34a and Figure 34b show typical stochastic simulation results of the system, using the same visualization as in Figure 25. The parameter values for these simulations are given in Table 2 on page 75. The system is very sensitive to the choice of the parameters, and they were tuned in a way that allows demonstration of the patterns while keeping simulation time reasonable. Only u is shown, as the amount of v is strongly correlated with it, see Figure 31a. As with the minimal model, the system is initialized with ten u molecules in some cells at time zero, which represent the transient signal that starts the differentiation in biological systems. The main difference between the two cases we show originates from *how many active cells* are initialized with u at time zero: either all of them (a), or just one (b). *The community effect is present in either case*: with $N_a = 5$, 13 out of 100 simulations show activity at $t = 1000$, while with $N_a = 10$ all 100 simulations enter sustained activation. Thus the critical number for the used parameter set is between 5 and 10.

With homogeneous initial conditions in all active cells (Figure 34a), the system exhibits a one-dimensional Turing pattern, i.e., stable periodic waves of high u levels over time. This occurs because the stochastic noise in $\sharp u$ and $\sharp v$ introduces an initial random asymmetry, which is later amplified by the system to larger scales. Note that this is impossible in the deterministic model, where starting from a homogeneous initial condition will always give a homogeneous solution.

The following observation is essential: if the initial signal is localized to a narrower area than the width of one wave of the pattern (e.g., a single cell as in Figure 34b), the sustained activation also remains localized. It appears as an isolated wave that is stable over time. The reader might want to refer back to Figure 25d: when no negative feedback is present, a community effect spreads over the entire range of active cells from an initial localized stimulation. In this model, the activated area is centred on the initial signal's location and it is about 20 cells wide.

Figure 34c and Figure 34d show the outcomes of the pattern formation under different initial conditions. Each row is a snapshot of one simulation of a system at $t = 1000$, with $N_a = 200$ and $N_p = 50$ for all cases.

Figure 34c shows the effect of varying the initial u amount, while localizing it at the leftmost active cell. Localization at the edge of the active area is biologically plausible, since the induction signal usually comes from another tissue; also the resulting pattern is better aligned in this case. Generally, a stronger initial signal yields a more stable pattern. If present, the width of the pattern is mostly the same. In rarer cases, secondary patterns can be seen - in real embryos those could be suppressed by other, less precise mechanisms.

Figure 34d shows the effect of variable initial induction area on the pattern. The initial induction signal is 10 u molecules in every cell in the induction area, which is again located on the left of the active cells row. The width of the generated pattern does not depend on the width of the initial signal, provided that the initial signal is smaller than the pattern itself.

Therefore, the system is organized into a robust stable pattern, which is not fully specified by the initial signal. Rather, it is defined by the properties of the gene regulatory network. In summary, *the self-regulation imposed by this RD system constrains the community effect within an area with well-defined boundaries.*

4.5 PATTERN FORMATION BY A DYNAMIC MORPHOGEN GRADIENT AND A COMMUNITY EFFECT

We now introduce a second model that prevents the spread of a community effect in one-dimensional space. It is based on a gene regulatory network controlling pattern formation in response to a morphogen gradient in *Xenopus* embryos [Saka and Smith, 2007]. Figure 35a shows

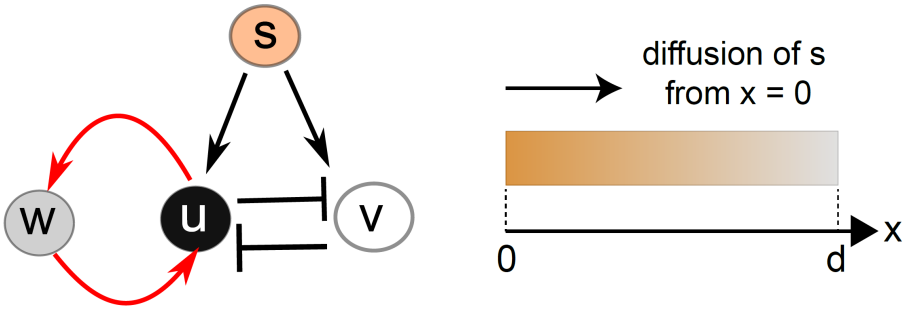

(a) (b)

Figure 35: A model of embryonic induction by dynamic morphogen gradient and a community effect. (a) GRN. (b) Illustration of the morphogen gradient along one dimensional space of length $\mathtt{d}$, with cells implementing the GRN.

this GRN we refer to as the *dynamic morphogen gradient model*. First, it contains a community effect loop between two mutually activating genes $\mathtt{u}$ and w. The latter is a diffusible factor for cell-to-cell communication, which controls the community effect. Second, it has a genetic toggle switch [Gardner et al., 2000] – a well-known GRN motif – formed by the mutual repression between $\mathtt{u}$ and $\mathtt{v}$. Third, both $\mathtt{u}$ and $\mathtt{v}$ are positively controlled by $\mathtt{s}$. Fourth, and importantly, $\mathtt{s}$ is a morphogen - forming a gradient by diffusion from a source in space, as illustrated in Figure 35b.

As before in this chapter, we formulate the model in terms of chemical reactions. The space is defined the same way as for the minimal model. We provide a deterministic analysis of the model first, using the reaction-diffusion framework. We also provide a stochastic analysis of the morphogen gradient model using its RDME formulation in the rule-based language defined earlier.

The insights of this section are the following:

- We show that a pattern of gene expression emerges with a sharp boundary in space, and that the community effect orients this spatial pattern.
- We examine the system's behaviour as the morphogen saturates the entire space. Surprisingly, the established pattern is maintained in the community with uniform morphogen concentration. *This shows that positional information is not provided by morphogen concentration alone, but is encoded in the morphogen dynamics.*
- A community effect is dispensable for pattern formation. However, it is essential for the refinement of gene expression boundary and confers *robustness* to patterning processes.

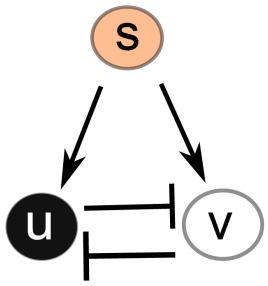

Figure 36: GRN without positive feedback and a community effect, analysed in Figure 42.

$$\text{activation of } u \text{ by } s: \quad s \xrightarrow{k_1 \frac{\sharp s}{(\delta \sharp v)^n + 1}} s + u \tag{77}$$

$$\text{activation of } v \text{ by } s: \quad s \xrightarrow{k_3 \frac{\sharp s}{(\delta \sharp u)^n + 1}} s + v \tag{78}$$

$$\text{activation of } u \text{ by } w: \quad w \xrightarrow{k_2 \frac{(\delta \sharp w)^n}{\delta((\delta \sharp v)^n + 1)((\delta \sharp w)^n + 1)}} w + u \tag{79}$$

$$\text{activation of } w \text{ by } u: \quad u \xrightarrow{k_4 \frac{(\delta \sharp u)^n}{\delta((\delta \sharp u)^n + 1)}} u + w \tag{80}$$

$$\text{degradation of } u: \quad u \xrightarrow{\mu_1 \sharp u} \tag{81}$$

$$\text{degradation of } v: \quad v \xrightarrow{\mu_2 \sharp v} \tag{82}$$

$$\text{degradation of } w: \quad w \xrightarrow{\mu_3 \sharp w} \tag{83}$$

$$\text{degradation of } s: \quad s \xrightarrow{\mu_4 \sharp s} \tag{84}$$

Figure 37: Reactions of dynamic morphogen gradient model.

4.5.1 *Dynamic morphogen gradient model*

It was previously shown [Saka and Smith, 2007] that the network in Figure 36, without the positive feedback mediated by w, can convert a graded morphogen signal into a binary output (u ON v OFF, or vice versa). We now explicitly take account of molecular diffusion of s and w. We consider a gradient of the morphogen s, that arises by diffusion from the origin at position $x = 0$ into one-dimensional space. At the start of a simulation ($t = 0$), the levels of the other species u, v and w are set to zero. This corresponds to an undifferentiated state, before the morphogen s starts to induce the system.

The chemical reactions of the model are given in Figure 37. Reaction (77) defines the activation of u by s, inhibited by v. Reaction (78) defines the activation of v by s, inhibited by u. Reaction (79) defines u's

activation by w with saturation, which is also inhibited by v. Reaction (80) defines w's saturating activation by u. Reactions (81)-(84) define the degradation of all species.

$\delta = \Omega^{-1}$, the inverse of the system volume, is the scaling coefficient which relates concentrations in the deterministic model to number of molecules in the stochastic models. It is introduced to facilitate transition between deterministic and stochastic rate laws with complicated higher-order expressions, which are used in this model. δ is set to $1/100$, corresponding to 100 molecules per one unit of concentration. k_1 to k_4 are synthesis rates and μ_1 to μ_4 are degradation rates. The synthesis terms for u (laws of reactions (77), (79)) are inversely proportional to $(\delta\sharp v)^n + 1$ to model repression of u by v. Repression of v by u is implemented in a similar way. The Hill coefficient n represents cooperativity, which introduces non-linearity to the network [Saka and Smith, 2007].

4.5.2 *PDE treatment*

First, we analysed the model in the reaction-diffusion framework, with continuous space and concentration variables. The PDEs of the model are as follows:

$$\begin{aligned}
\frac{\partial u}{\partial t} &= \frac{k_1 s + k_2 (\frac{w^n}{w^n+1})}{v^n + 1} - \mu_1 u \\
\frac{\partial v}{\partial t} &= \frac{k_3 s}{u^n + 1} - \mu_2 v \\
\frac{\partial w}{\partial t} &= D_1 \Delta w + k_4 (\frac{u^n}{u^n + 1}) - \mu_3 w \\
\frac{\partial s}{\partial t} &= D_2 \Delta s - \mu_4 s,
\end{aligned} \tag{85}$$

where D_1 and D_2 are diffusion coefficients. Note that the δ coefficients are cancelled out. The boundary conditions are:

$$s = 1 - e^{-\tau t}, \quad x = 0 \tag{86}$$

$$\frac{\partial s}{\partial x} = 0, \qquad x = d \tag{87}$$

$$\frac{\partial w}{\partial x} = 0, \qquad x = \begin{cases} 0 \\ d. \end{cases} \tag{88}$$

We assume that the morphogen s is produced outside of our one-dimensional space, left of the origin ($x < 0$), and that its concentration at $x = 0$ is defined by (86). The speed of injection of the morphogen s into the one dimensional space varies according to the control parameter τ. For this deterministic model, the system is closed, meaning that except for the supply of s from the boundary $x = 0$, no diffusion of any molecule into or out of the system occurs. This boundary condition corresponds to equations (87) and (88).

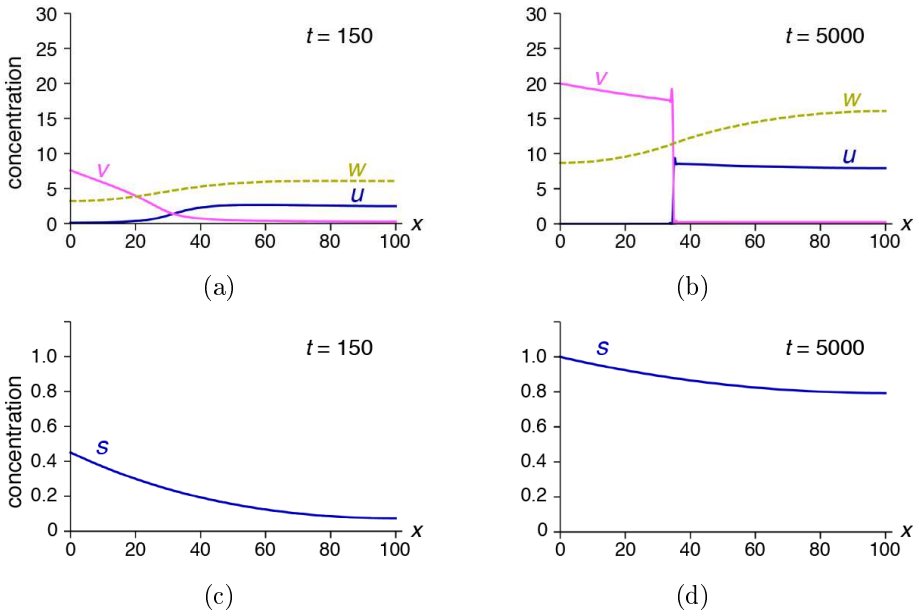

Figure 38: Pattern formation by a dynamic morphogen gradient and a community effect.

Numerical simulations of the PDE model

We performed numerical simulations to analyse the system's dynamics, fixing the length of one-dimensional space to $d = 100$ for all simulations. Exploring the parameter space of the system, we found three categories of *patterns of gene expression at steady state* along the one dimensional space (beyond the trivial case of $u = v = w = 0$):

- uniform expression of u, denoted as $[u]$,
- uniform expression of v, denoted as $[v]$,
- $[v, u]$, denoting: v on and u off close to the origin $x = 0$, and further away, v off and u on.

Figure 38a and Figure 38b show concentration profiles of u, v and the diffusible molecule w over the entire range of cells, at time points $t = 150$ (a) and $t = 5000$ (b), obtained by simulation of the PDE model, with the parameter values in Table 6 on page 101. Concentration profiles of the morphogen s at the same time points are shown in Figure 38c and Figure 38d.

At the stable state ($t = 1500$), simulation yields a sharp boundary of gene expression for the pattern $[v, u]$. This gene expression pattern is self-organising and is refined spatially in response to the dynamic gradient of the morphogen s. Small bumps at the $[v, u]$ boundary in Figure 38b are artefacts of numerical integrations. Interestingly, once established, the $[v, u]$ boundary is maintained even when the morphogen concentration along space becomes uniform at steady state, i.e., even when the gradient is transient (Figure 39). This observation indicates

Parameter	Description	Value	Range
D_1	diffusion of w	20	$0 \leqslant D_1 \leqslant 100$
D_2	diffusion of s	20	$0 \leqslant D_2 \leqslant 100$
k_1	activation of u by s	0.6	$0 \leqslant k_1 \leqslant 1$
k_2	activation of u by w	0.2	n.a.
k_3	activation of v by s	0.8	$0 \leqslant k_3 \leqslant 1$
k_4	activation of w by u	0.2	n.a.
μ_1	degradation of u	0.08	n.a.
μ_2	degradation of v	0.04	n.a.
μ_3	degradation of w	0.01	n.a.
μ_4	degradation of s	0.001	n.a.
τ	control parameter for $s(0,t)$	0.004	$10^{-3} \leqslant \tau \leqslant 10^{-1}$
d	responding tissue size	100	n.a.

Table 6: Parameter values for numerical simulations in Section 4.5. Used for simulations, unless defined explicitly in the main text. Parameter ranges in the last column are used for phase diagrams. n.a., not applicable.

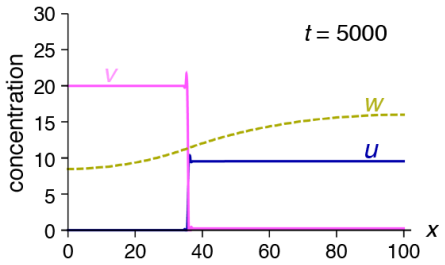

(a)

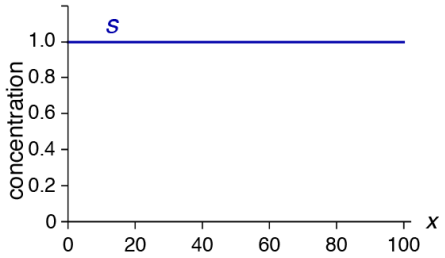

(b)

Figure 39: Pattern formation in a uniform concentration of morphogen along one dimensional space at steady state. Uniform distribution of the morphogen at steady state is established with $\mu_4 = 0$. The simulation result at a quasi-steady state ($t = 5000$) is shown. Parameter values used for the simulation are listed in Table 6 except $\mu_4 = 0$.

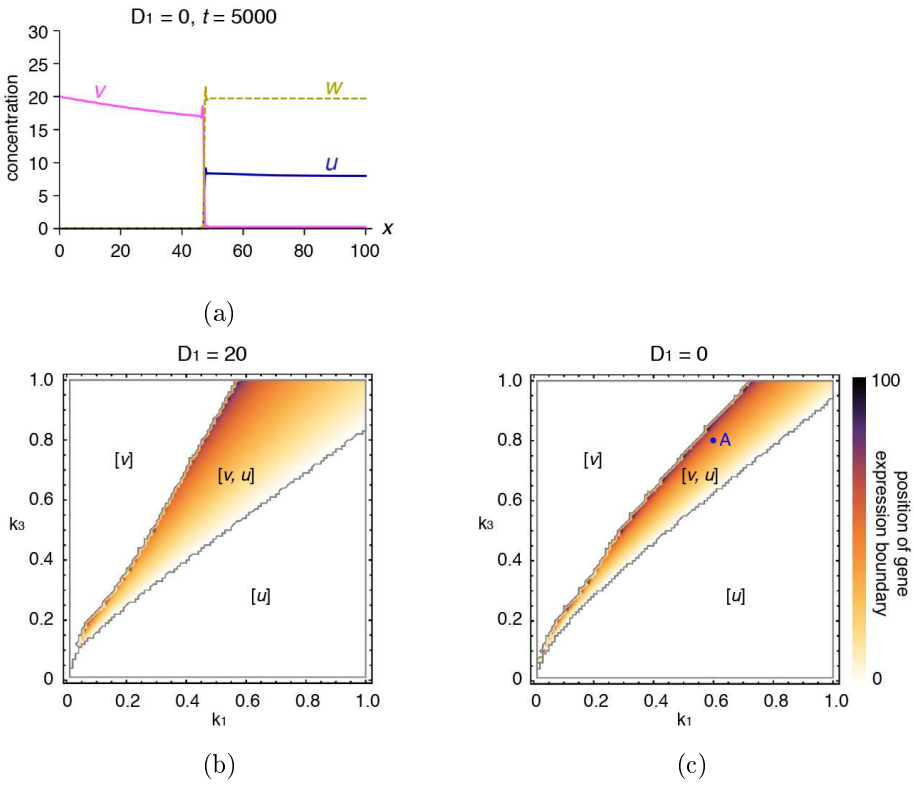

Figure 40: Simulations of the PDE model show that cell-to-cell communication by the diffusible factor w is dispensable for pattern formation, but is essential for community effects. **(a)** Steady state profile. **(b, c)** Phase diagrams in the parameter plane (k_1, k_3) with $D_1 = 20$ (b) and $D_1 = 0$ (c). The position of the expression boundary for $[v, u]$ pattern is colour-coded as indicated. Borders between the patterns $[u]$, $[v]$ and $[v, u]$ are indicated by grey lines. Simulation parameters for (b,c) are listed in Table 6, except k_1, k_3 and D_1as indicated in the panels.

that *a transient morphogen gradient is sufficient*, and that maintenance of the morphogen gradient at steady state is not a prerequisite for pattern formation in our model.

We found that the steady-state pattern is either $[u]$, $[v]$ or $[v, u]$, over a wide range of parameter values, as shown by phase diagrams of the parameter plane in Figure 40. We will later show that the pattern $[u, v]$ only appears in the absence of the community effect and positive feedback loop. Therefore it seems that the *positive feedback of community effect introduces an asymmetry to the system, and orients the spatial pattern of gene expression.* We next examined how the gene expression pattern is affected by the dynamics of the diffusible factors s (morphogen) and w (community effect factor).

DISABLING THE CELL-TO-CELL COMMUNICATION MEDIATED BY w. First, we tested the system's behaviour without cell-to-cell

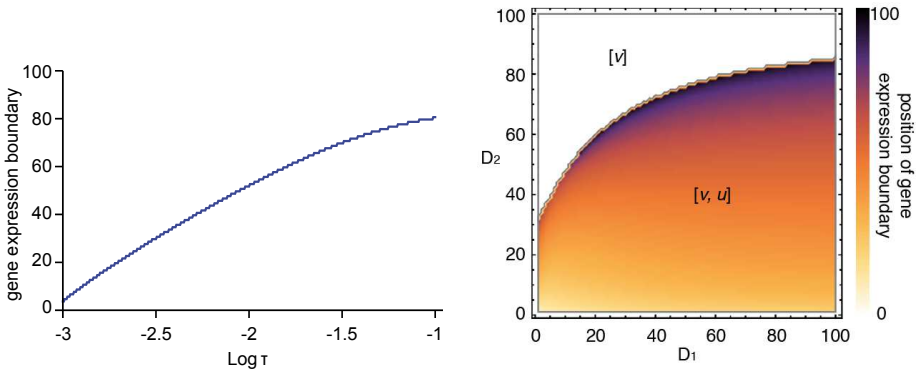

(a) (b)

Figure 41: The position of the gene expression boundary depends on the dynamics of the morphogen s. The figures are derived from simulations of the *PDE model*. **(a)** Position of gene expression boundary is plotted as a function of τ (in log scale). τ defines the speed of morphogen supply (the larger τ is, the faster the supply and s gradient reaches a steady state). The parameter values used are the same as Figure 38, except τ. **(b)** Phase diagram in the parameter plane (D_1, D_2). The parameter values used can be found in Table 6, except D_1 and D_2. The expression boundary is relatively insensitive to the fluctuation of D_1, the diffusion rate of w. By contrast, the boundary position is sensitive to the dynamics of the morphogen s and shifts by changes in τ or D_2 value.

communication mediated by w (by setting $D_1 = 0$) – while preserving the mutual activation between w and u within the same cell ($k_2, k_4 > 0$). Numerical simulation of the PDE model shows that the $[v, u]$ pattern of gene expression can be established without cell-to-cell communication (Figure 40a). Figure 40b and Figure 40c show phase diagrams in the parameter plane (k_1, k_3) obtained from the PDE model with cell-to-cell communication (b), versus without (c). They were obtained by leaving w's diffusion rate on ($D_1 = 20$) and switching it off ($D_1 = 0$). We recall that k_1 is the rate for u's activation by the morphogen s, and k_3 is the rate of v's activation by the morphogen. The parameter pair (k_1, k_3) for the simulation in Figure 40a is marked by a blue dot in Figure 40c. As the phase diagrams show, the parameter range for a $[v, u]$ pattern widens in the presence of cell-to-cell communication.

PATTERN FORMATION IS SENSITIVE TO THE DYNAMICS OF MORPHOGEN GRADIENT. We next examined how the gene expression pattern is affected by the dynamics of the morphogen s and the community effect factor w. Figure 41a shows a plot of the position of the boundary between v and u as a function of τ ($\log \tau$), the parameter controlling the supply of s to the system. The plot demonstrates that the boundary shifts as τ changes: the faster the supply of s to the system, the broader the expression domain of v is at steady state.

Figure 41b is a phase diagram in the parameter plane (D_1, D_2). The diagram indicates that faster diffusion of the morphogen, i.e., larger diffusion coefficient D_2 shifts the expression boundary away from the origin. This is consistent with the above results shown in Figure 41a. In contrast, as shown in the same diagram, the boundary of $[v, u]$ is insensitive to the change of D_1, the diffusion rate of w, especially when D_2 value is low. This is also evident in the stochastic simulations, following in subsection 4.5.3.

PATTERN FORMATION WITHOUT BOTH POSITIVE FEEDBACK AND COMMUNITY EFFECT. Finally we consider the system without both positive feedback and a community effect (Figure 36). This gene regulatory network without w is effectively identical to the one described in [Saka and Smith, 2007], with the addition of the diffusion term of s. In contrast to the network with w, this system still forms the $[v, u]$ pattern at steady state, but also the previously unseen pattern $[u, v]$, in which u is on in a domain closer to the origin, while v is on further away. The pattern depends on the parameter values (Figure 42). However, a phase diagram in the parameter plane (k_1, k_3) shows that the $[u, v]$ and $[v, u]$ *patterns only appear for narrow parameter ranges* (Figure 42a, Figure 42c). In fact, stochastic simulations confirm that the system mostly ends up with no clear pattern, and a heterogeneous population of u-ON and v-ON cells at steady state (data not shown). These results highlight an important role of the community effect that *confers robustness to this patterning system.*

4.5.3 *RDME treatment*

In order to study robustness of pattern formation in the presence of noise, we analysed the same model in the RDME framework. In Figure 43 the spatial model is written in the 1D rule-based language which we used earlier.

Several points need clarification. Rules (97), (98) define the diffusion for w and s, following the diffusion scheme of Section 4.2. $\tilde{D_1}$ and $\tilde{D_2}$ are diffusion rates of w and s between neighbour cells. These generally depend on D_1 and D_2, as well as on further details about cell geometries which we did not specify; therefore they are chosen in a way that makes simulation results close to the curves obtained using the PDE model. Rule (99) describes the creation of s at the leftmost active cell, approximating the boundary condition of the PDEs (86) on page 99. Since we did not perform simulations with varying τ, τ is not present in the reaction rate. In the presence of only rule (99), the mean number of $\sharp s(N_p + 1)$ at time t would be $(1 - e^{-t})\delta^{-1}$, which corresponds to the boundary condition with $\tau = 1$. Because $\sharp s(N_p + 1)$ is also affected by rules (96) and (98), its actual number will be lower in general. Its maximum, for example, is about 55 instead of 100. This is the main source

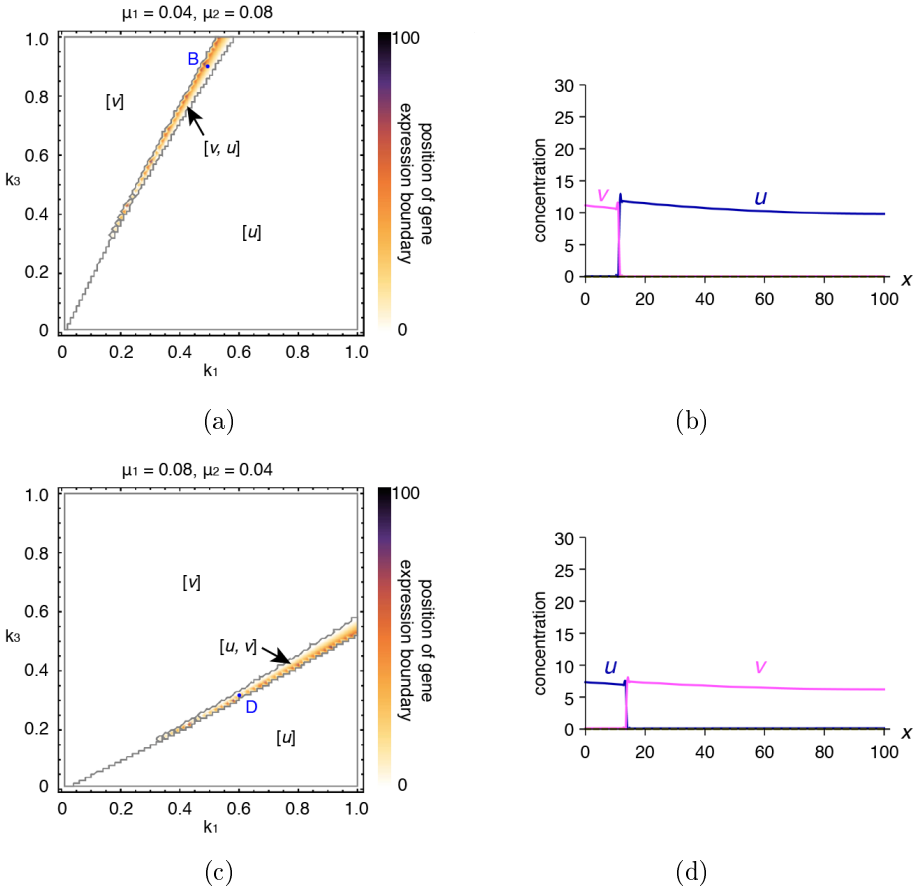

Figure 42: Pattern formation without positive feedback and a community effect ($k_2 = k_4 = 0, D_1 = 0$) in the deterministic model. **(a)** Phase diagram in parameter plane (k_1, k_3) for $(\mu_1, \mu_2) = (0.04, 0.08)$. **(b)** Steady-state profile ($t = 5000$) for the parameter values indicated as a blue dot in (a). **(c)** Phase diagram for $(\mu_1, \mu_2) = (0.08, 0.04)$. **(d)** Steady-state profile ($t = 5000$) for the parameter values indicated as a blue dot in (c). The parameter space for $[v, u]$ (a) or $[u, v]$ pattern (b) (i.e., without w) is much smaller than in the system with positive feedback and a community effect. Without w, both $[v, u]$ and $[u, v]$ patterns are possible. Except for those indicated in the figure, the parameter values for simulations are listed in Table 6.

activation of u by s: $\forall x \in \mathit{ActiveCells}, \quad s(x) \xrightarrow{k_1 \frac{\sharp s(x)}{(\delta \sharp v(x))^n + 1}} s(x) + u(x)$ (89)

activation of v by s: $\forall x \in \mathit{ActiveCells}, \quad s(x) \xrightarrow{k_3 \frac{\sharp s(x)}{(\delta \sharp u(x))^n + 1}} s(x) + v(x)$ (90)

activation of u by w: $\forall x \in \mathit{ActiveCells}$,

$$w(x) \xrightarrow{k_2 \frac{(\delta \sharp w(x))^n}{\delta((\delta \sharp v(x))^n + 1)((\delta \sharp w(x))^n + 1)}} w(x) + u(x) \quad (91)$$

activation of w by u: $\forall x \in \mathit{ActiveCells}$,

$$u(x) \xrightarrow{k_4 \frac{(\delta \sharp u(x))^n}{\delta((\delta \sharp u(x))^n + 1)}} u(x) + w(x) \quad (92)$$

degradation of u: $\forall x \in \mathit{ActiveCells}, \quad u(x) \xrightarrow{\mu_1 \sharp u(x)}$ (93)

degradation of v: $\forall x \in \mathit{ActiveCells}, \quad v(x) \xrightarrow{\mu_2 \sharp v(x)}$ (94)

degradation of w: $\forall x \in \mathit{AllCells}, \quad w(x) \xrightarrow{\mu_3 \sharp w(x)}$ (95)

degradation of s: $\forall x \in \mathit{AllCells}, \quad s(x) \xrightarrow{\mu_4 \sharp s(x)}$ (96)

diffusion of w: $\forall x \in \mathit{AllCells} - \{\mathit{LastCell}\}$,

$$w(x) \underset{\vec{D}_1 \sharp w(x+1)}{\overset{\vec{D}_1 \sharp w(x)}{\rightleftharpoons}} w(x+1) \quad (97)$$

diffusion of s: $\forall x \in \mathit{AllCells} - \{\mathit{LastCell}\}$,

$$s(x) \underset{\vec{D}_2 \sharp s(x+1)}{\overset{\vec{D}_2 \sharp s(x)}{\rightleftharpoons}} s(x+1) \quad (98)$$

external inflow of s: $\xrightarrow{max(\delta^{-1} - \sharp s(N_p+1), 0)} s(N_p + 1)$ (99)

where $\mathit{ActiveCells} = \{1 + N_p, \ldots, N_p + N_a\}$, $\mathit{AllCells} = \{1, \ldots, \mathit{LastCell}\}$, and $\mathit{LastCell} = 2N_p + N_a$.

Figure 43: Rules of dynamic morphogen gradient model.

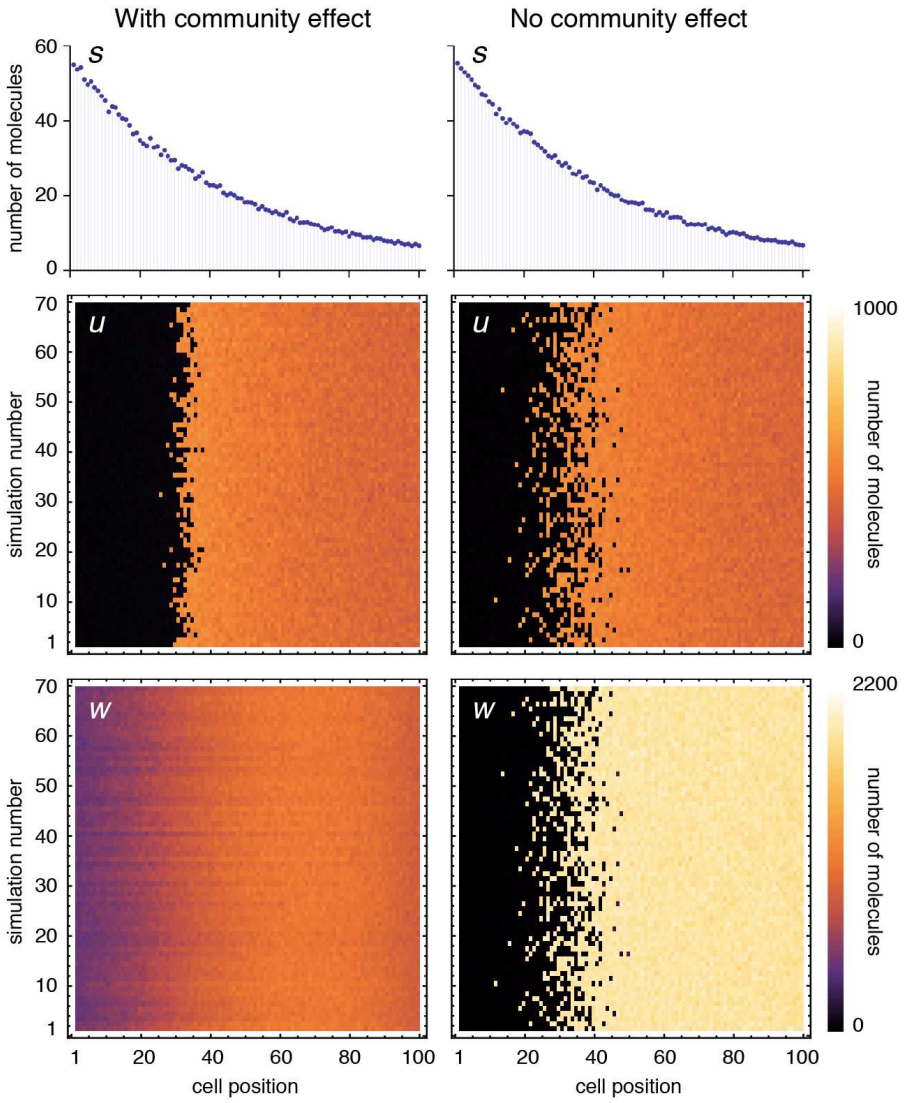

Figure 44: Stochastic simulations of the morphogen gradient model, enabling a community effect (left column) or disabling it (right column).

of numerical differences between the stochastic and the deterministic models.

Stochastic simulations

We carried out stochastic simulations of this system, results of which are shown in Figure 44. We paid particular attention to the roles of the community effect, and observed the impact of enabling or disabling it. Disabling the community effect can be achieved in two technical ways in the rule based model, either by setting w's diffusion rate to zero, following the PDE model, or equivalently by withdrawing (97) from our rule based model in Figure 43.

Figure 44 shows snapshots at $t = 990$ (quasi-steady state) for 70 simulations with community effect (left column) and without community effect (right column). The panels in the first row show the active cells' level of s, averaged over all simulations. The second and third row in Figure 44 show the number of u and w molecules, respectively, in active cells at $t = 990$. Each plot contains 70 lines, each corresponding to the outcome of one stochastic simulation. We do not show the distribution of v molecules across active cells; it is opposite to that of u (middle panels). Simulation parameters are the same as those of the PDE model (Table 6 on page 101), except $k_2 = 0.3$ that represents u's activation by w.

The community effect being turned on (left column), the result of the stochastic simulations are similar to those of the deterministic model, except stochastic noise. In stochastic simulations, although a boundary is formed around $x = 30$, minor populations of *rogue* cells with opposite gene expression pattern are evident in both u-ON and v-ON domains around the boundary in approximately 80% of simulations.

Interestingly, simulations revealed that stochasticity near the expression boundary is more pronounced in the absence of a community effect with more *rogue* cells (Figure 44, right column). This result demonstrates that *a community effect sharpens the gene expression boundary in our model*, although rogue cells are not completely eliminated. Without the community effect the boundary is blurred. It has revealed an interesting role of the community effect for refining gene expression boundaries during patterning, in addition to its known role for a coordinated gene expression in a group of cells.

In conclusion, stochastic simulations showed that the dynamic morphogen gradient model has more robust pattern formation when including a community effect. Although a community effect is dispensable for patterning process *per se* (see Figure 41), it plays a crucial role for refining the gene expression boundary.

5 DISCUSSION

5.1 MODELLING METHODS

5.1.1 *Stochastic modelling*

Stochastic analysis derived from CME, as used in the previous chapters, rests upon the assumptions of well-mixed compartments and elementary reactions. It is unclear to which extent these assumptions apply to intracellular reactions.

A review of methods which model intracellular diffusion in detail is given in [Klann and Koeppl, 2012]. These include methods reviewed in Chapter 2, as well as more complicated simulators which model repulsive forces between molecules in crowded environments (referred to as Brownian dynamics simulators) and flexible chains of connected molecules.

Derivations of stochastic behaviour from CME assumes that the CME describes the system completely. This can never be the case: there are always missing details about the chemical interactions in all but very simple systems. For example, models given before all include gene expression in some form, which is usually modelled as one or two reactions. In the reality this is a complicated multi-step process which takes considerable time and involves thousands of intermediate interactions with other molecules. To model all this as an elementary reaction is a huge simplification. Random fluctuations of molecule counts will have different distributions than what is predicted by the elementary reaction model. Considering this, stochastic models may not predict well statistics of the variables beyond first order (which is typically fit to the observations), such as variances.

Perhaps a cleaner approach to take stochastic noise into account would be to consider it explicitly as another parameter (or parameters), e.g. using SDEs. In this work, since we are more interested in qualitative behaviour than exact quantitative predictions, we use the CME for simplicity.

5.1.2 *Moment closures*

The main difficulty in applying moment closures is the lack of understanding of conditions under which they give good results. It is made worse by the lack of control of the approximation error. In theory, the higher order closure should be more precise, but in practice we can only apply second order closures, because third order ones are already too

large for most systems. In addition, tests of simple systems indicate that raising the order doesn't help to reduce the error in some cases.

This leaves us the only practical method to control the approximation precision: changing the type of the closure by trial and error. The normal approximation is usually the first choice, but it can behave badly even for very simple systems, e.g. $2A \rightarrow$, as demonstrated in [Vidal et al., 2010]. Generally is has troubles when count of some species approaches zero: under normal approximation the count will happily cross zero (recall that the normal approximation allows negative values), which has devastating effect on subsequent calculations. In this respect, the lognormal closure may be more appropriate [Singh and Hespanha, 2006b].

For now, the only reasonable method to check if a moment closure is working correctly is to compare it to many stochastic simulations. Of course, doing so for every run of moment closure would defeat its purpose, so it has to be done selectively, presumably in places where its result looks abnormal. This makes its use inconvenient, unlike 'single click' solutions offered by other approximations.

Hopefully this can be improved in the future by developing more robust closures, or checking the conditions for closures at run time (e.g., species count approaching zero) and adjusting the solution accordingly.

5.1.3 *Symmetric reduction*

Despite its shortcomings, the moment closure method is a flexible tool for approximate stochastic analysis. It allows manipulations of moment equations similar to those that can be done with deterministic ODEs, but including, approximately, the stochastic effects.

Model reduction is one kind of such manipulations. It aims to eliminate redundant variables from the system of ODEs, making it easier to solve. For moment closure, which tend to generate a large number of ODEs, reductions are especially important. We have described a model reduction method based on symmetries, which in case of moment closure is more complicated than what is used with deterministic approximation.

Currently, the only way to exploit such symmetries while performing stochastic analysis of a system is through moment closure: reduced models are not amenable to Gillespie simulation. If the corresponding species in the cells are "lumped" together, in the same way as in the deterministic approximation, the results diverge quickly from the non-reduced system. Also note that, as the order of the closure grows, the symmetric reduction can eliminate a smaller fraction of moments, suggesting that for the limit case of the exact solution the gain from the reduction will be negligible. We believe that, for the community effect model, the approach presented here provides the only tractable analysis.

Symmetry-based reduction is potentially applicable to many highly regular systems. For example, in [Camporesi and Feret, 2011] a model reduction method for deterministic approximation is applied to a system that contains a protein with symmetric activation sites. That system is also symmetric in the sense described here, w.r.t. exchanging activation states for different sites. Thus, its moment closure could be reduced with our method as well. Another example is a discrete ring of identical cells, considered in [Turing, 1952], which is symmetric under rotation of all cells. Many higher order moments could be eliminated with our method using this property.

5.2 COMMUNITY EFFECT

5.2.1 *Stochastic phenomena*

During development of a multicellular organism, the cell populations expands quickly while differentiating into different types. This poses a threat of error amplification, whereby a random switch to an incorrect cell fate in the wrong place or at the wrong time could have detrimental consequences for the developing embryo [Balázsi et al., 2011]. Collective decision making was previously found to be essential for noise reduction during development [Gregor et al., 2007]. Therefore it is an interesting question how community effects behave in the presence of noise.

Our analysis showed that community effects do not change significantly if the noise is considered, compared to the noise-free deterministic case. The minimum number of cells required to make a decision is higher in the presence of noise (Figure 19a), which is not surprising: the noise interferes with the cellular decision mechanism and, in this case, biases it towards the inactive state, which is absorbing.

Another interesting observation in this respect is that with more cells in the population, the convergence of the expression to its quasi steady state seems to happen faster, visible on Figure 18. This may be connected to the results of Gregor et al. [2007], who found the dependency between the number of cells participating in a cell fate decision in the presence of noise, and the shortest possible time to take this decision.

A noise-suppressing feature of the community effect in *Xenopus* is demonstrated in Figure 44, where it helps to sharpen the gene expression boundary. Such an effect is clearly useful during development, making the patterning mechanisms more robust.

5.2.2 *Self-organized patterning*

Spatial analysis of the three GRNs in Chapter 4 led to several insights about the self-organisation related to community effects.

AN INCONVENIENT TRUTH OF THE COMMUNITY EFFECT. We have shown that a community effect spreads across the system, without any interlocked negative feedback. Although this is indeed an inconvenient property for patterning of the embryo, it has turned into a control mechanism for coordinated gene expression in nature. Our two different models demonstrated that it can play another role as a control sub-circuit for pattern formation.

We have also shown that, when the spatial dimension is taken into account, the community effect must be treated as not a simple cell-number dependent phenomenon, but also as tissue size and cell-density dependent (Section 4.3).

COMMUNITY EFFECTS AND PATTERN FORMATION BY TURING MECHANISM. Turing patterns emerge from a uniform signal with noise as shown in Figure 34a. Embryonic induction, by contrast, is initiated by diffusion of signalling molecules from a localised source. Our simulation results suggested that the Turing pattern mechanism can be exploited as a mechanism to restrict the effective range of a community effect, in response to a localised inducing signal (Figure 34b). Such an isolated area is maintained as a stable wave. A community effect may also coordinate the gene expression within the area.

The Turing pattern theory was initially met with scepticism, but recently many experimental results pointed to possibility of such mechanisms in many organisms. This includes works of Kondo and Miura [2010] and Müller et al. [2012], who found that interaction between Lefty and Nodal proteins, which diffuse with different speeds, leads to formation of a reaction-diffusion system in zebrafish. Similar findings are reported by Duboc et al. [2008] for Lefty and Nodal interaction which are shown to specify the area of oral ectoderm in sea urchin. In [Su et al., 2009] a GRN of sea urchin oral ectoderm specification circuit is given. Together with the fact that Nodal is involved in a community effect found in the same system [Bolouri and Davidson, 2010], they provide evidence to support the Turing pattern model studied in Section 4.4.

In other organisms, Turing patterns, or, more generally, reaction-diffusion systems, have been found: Shiratori and Hamada [2006], Nakamura et al. [2006] show that Lefty-Nodal interaction establishes left-right asymmetry in mouse, a complex phenomenon also studied by Turing [1952]; Sheth et al. [2012] show that Hox genes regulate a Turing pattern mechanism which is responsible for patterning of digits in mice. A review of experimental evidence for Turing patterns in development is given by Marcon and Sharpe [2012].

The paper of Hsia et al. [2012], using deterministic and stochastic spatial modelling, shows how an oscillatory circuit combined with a Turing pattern GRN can form many types of patterns, focusing on ease of implementation of such a circuit artificially.

ROLES OF COMMUNITY EFFECT IN DYNAMIC MORPHOGEN GRADIENT INTERPRETATION. Dynamic assessment of a morphogen gradient has been suggested previously based on experimental evidence [Dessaud et al., 2010, Gurdon et al., 1995, Harvey and Smith, 2009, Jaeger et al., 2004a]. Surprisingly, our simulations indicate that a morphogen gradient at steady state is not a prerequisite for pattern formation. It turned out that a transient gradient is sufficient for patterning and the steady-state morphogen distribution can be uniform (Figure 39).

In our dynamic morphogen gradient model, therefore, positional information is encoded in the dynamics of diffusing morphogens, rather than by the concentration in a stable gradient. In other words, the system confers memory of morphogen dynamics. The dynamic morphogen gradient model thus provides an alternative to the so-called French flag model and the concept of positional information for embryonic patterning [Wolpert, 1969]. Pattern formation mechanisms based on dynamic interactions between genes have also been modelled previously for *Drosophila* by Lembong et al. [2009].

The network of a mutually-repressive pair of genes has been implicated in interpretation of positional information in the gradients of maternal proteins, which work as morphogens [Jaeger et al., 2004a] in the segmentation of *Drosophila* embryos. However, because it involves a complex GRN, its exact mechanism remains unresolved. We found that, when being combined with a community effect, this cross repression sub-circuit (genetic toggle switch) turned into a robust patterning GRN with coordinated gene expression. The community effect plays a role in refining patterns by sharpening gene expression boundaries.

Our simulation results have also shown that a community effect helps orient gene expression patterns in space (Figure 38). This is one of the roles of a community effect not recognised previously. In the context of animal development, the community effect and the GRN depicted in Figure 35a is a robust system to establish an asymmetric pattern in embryonic tissues. These results indicate that diffusible factors for cell-to-cell communication, either with positive or negative influence from one cell to the other, may provide myriad mechanisms for embryonic patterning when interlinked with a sub-circuitry of developmental GRNs.

6

CONCLUSIONS AND FUTURE WORK

The goal of this work was to model community effects in more detail than was considered in previous studies, in particular including spatial and stochastic aspects. In the context of development, spatial phenomena are obviously important, since formation of spatial organisation of tissues is an essential task of embryogenesis. It is also important to consider stochasticity, because developmental processes have to be robust with respect to fluctuations inherent in chemical systems.

In the following, we list the specific research questions and the obtained results, together with some directions for the future work.

WHAT IS THE INFLUENCE OF STOCHASTIC NOISE ON A COMMUNITY EFFECT? We have analysed a detailed model of a community effect in *Xenopus* and concluded that the only influence that the stochastic noise has in that model is the increase of the critical number by about 20%.

As a part of this work, a model reduction method was developed in [Batmanov et al., 2012a], which can greatly reduce a symmetric model, facilitating advanced stochastic analysis.

Symmetric reduction presented here can be extended in a number of ways. Checking and finding the required symmetric properties of a reaction set can be automated rather easily. The symmetries considered here are just the automorphisms of the reaction graph with the additional constraints that the initial conditions of the corresponding species must be equal and the rates of the corresponding reactions must be equal. The problem of finding all automorphisms belongs to the NP class of complexity, however for real systems the requirement of having the same rates and initial conditions restricts the number of possible symmetries. Verification of a specified symmetry can be done in polynomial time.

One direction for future developments here is to directly derive a reduced moment closure from a rule-based representation, without expanding it to the full system. This becomes interesting if the expanded system's size is huge, and the system is highly symmetric, so that it can be described by a manageable set of moment equations. In this case, the expansion of the rule-based model to chemical reactions becomes the computational bottleneck, which can possibly be avoided. It resembles what is done in [Camporesi and Feret, 2011].

However, the current method is not applicable to spatial systems with borders. By borders, we mean the outermost cells in a one dimensional row of cells, or in a two-dimensional grid, those cells that frame the grid. In such system, a distinct distance from the border(s) uniquely identifies

each cell. For example, one-dimensional spatial models of the community effect from Chapter 4 can be reduced in half by central symmetry. But, for a second order moment closure, the quadratic dependency of number of equations on the system size remains. Because of this, we resorted to lengthy stochastic simulations for the spatial models.

Moment closures for spatial models have been previously derived in ecology [Gandhi et al., 2000] and statistical physics [Levermore, 1996]. In the future, we plan to develop methods to infer spatial moment closures automatically for chemical reaction systems as well.

HOW COMMUNITY EFFECTS BEHAVE IN SPACE? To answer this question, we have constructed a minimal model and analysed its behaviour in one-dimensional space. One finding was that for a community effect which depends only on the number of cells, i.e. if we consider size of the cells and distances between them fixed, it is necessary to have a loss of the diffusible factor. This was implemented in a biologically plausible way with active and inactive cells, and this setup was used in the rest of the work.

Our minimal model of community effect illuminated another property of community effects, that is, its uniform unrestricted expansion throughout the cell population. This property is obviously inconvenient for pattern formation during embryogenesis. This raised the next question:

HOW CAN THE SPREAD OF A COMMUNITY EFFECT BE LIMITED? To resolve this issue, we have proposed two different models that limit the spread of a community effect within a cell population: the Turing pattern model and the dynamic morphogen gradient model. These not only presented mechanisms of regulating community effects, but also revealed several interesting insights into embryonic patterning. Our findings are summarised as follows:

1. A community effect spreads out without any negative feedback (Figure 25d).

2. With negative feedback, a community effect does not spread unrestrictedly. We show that localised induction leads to localised gene expression in our Turing pattern model (Figure 34b).

3. Community's cell density and size become critical for self-sustaining gene expression by a community effect (subsection 4.3.4). This is relevant to embryonic patterning, because embryos undergo dynamic morphogenetic movement. It raises a question: *How does tissue geometry affect patterning?* We plan to address this issue in the future.

4. A modified form of genetic toggle switch combined with a community effect loop converts a dynamic morphogen gradient into

a spatially-asymmetric pattern of gene expression (Figure 38). The community effect loop introduces an asymmetry to the GRN, which biases pattern formation towards $[v, u]$ pattern. However, the fundamental, non-trivial question remains unanswered: how does the topological asymmetry of the GRN bring about the bias in pattern formation? This is a subject of our future work.

5. A transient and dynamic morphogen gradient is sufficient for patterning. Moreover, a uniform morphogen distribution across the induced tissue can maintain the established pattern with a well-demarcated boundary (Figure 39).

In this work, we have only analysed one-dimensional spatial models. They represent an idealized, spherically-symmetric case. This configuration was chosen for computational efficiency. In order to study patterning in more complicated geometries, however, two- or three-dimensional space representations will be needed, which is significantly harder in terms of required computations. Building such models is another subject of our future work.

6.1 On authorship of contributions

This thesis is a result of collaborative work. In order to keep the presentation coherent, I have included all the material from co-authored publications. While in general it is difficult to attribute ideas to a single person, I will list several clear cases below.

The dynamic morphogen gradient model from Section 4.5 was created by Yasushi Saka. All PDE-based analysis of it, as well as that of the detailed spatial model in subsection 4.3.4 was also done by him. He made the Mathematica notebook provided in the supporting on-line code (`http://www.lifl.fr/~batmanov/thesis/simulationCode.zip`).

While the idea of the symmetric reduction first occurred to me, the formalization of the proof presented in subsection 3.3.2 is done by Cédric Lhoussaine.

The Maple code to derive moment closures was largely inspired by a similar package written by Michel Petitot.

BIBLIOGRAPHY

Gary K. Ackers, Alexander D. Johnson, and Madeline A. Shea. Quantitative model for gene regulation by λ phage repressor. *Proceedings of the National Academy of Sciences USA*, 79(4):1129–1133, February 1982. (Cited on page 16.)

Noam Agmon. Diffusion with back reaction. *The Journal of Chemical Physics*, 81(6):2811, 1984. ISSN 00219606. doi: 10.1063/1.447954. URL http://link.aip.org/link/JCPSA6/v81/i6/p2811/s1&Agg=doi. (Cited on page 27.)

Uri Alon. Network motifs: theory and experimental approaches. *Nature reviews Genetics*, 8(6):450–61, June 2007. doi: 10.1038/nrg2102. URL http://www.ncbi.nlm.nih.gov/pubmed/17510665. (Cited on page 20.)

Steven S Andrews and Dennis Bray. Stochastic simulation of chemical reactions with spatial resolution and single molecule detail. *Physical biology*, 1(3-4):137–51, December 2004. ISSN 1478-3967. doi: 10.1088/1478-3967/1/3/001. URL http://www.ncbi.nlm.nih.gov/pubmed/16204833. (Cited on pages 27 and 31.)

Steven S Andrews, Nathan J Addy, Roger Brent, and Adam P Arkin. Detailed simulations of cell biology with Smoldyn 2.1. *PLoS computational biology*, 6(3):e1000705, January 2010. ISSN 1553-7358. doi: 10.1371/journal.pcbi.1000705. URL http://www.pubmedcentral.nih.gov/articlerender.fcgi?artid=2837389&tool=pmcentrez&rendertype=abstract. (Cited on page 51.)

Alfonso Martinez Arias and Penelope Hayward. Filtering transcriptional noise during development: concepts and mechanisms. *Nature reviews. Genetics*, 7(1):34–44, January 2006. ISSN 1471-0056. doi: 10.1038/nrg1750. URL http://www.ncbi.nlm.nih.gov/pubmed/16369570. (Cited on page 14.)

Gábor Balázsi, Alexander van Oudenaarden, and James J Collins. Cellular decision making and biological noise: from microbes to mammals. *Cell*, 144(6):910–25, March 2011. ISSN 1097-4172. doi: 10.1016/j.cell.2011.01.030. URL http://www.pubmedcentral.nih.gov/articlerender.fcgi?artid=3068611&tool=pmcentrez&rendertype=abstract. (Cited on pages 13 and 111.)

F Baras and M Malek Mansour. Reaction-diffusion master equation: A comparison with microscopic simulations. *Physical Review E*, 54(6): 6139–6148, 1996. (Cited on page 48.)

David J Barnes and Dominique Chu. *Introduction to modeling for biosciences*. Springer, 2010. (Cited on page 13.)

K. Batmanov, C. Kuttler, F. Lemaire, C. Lhoussaine, C. Versari, et al. Symmetry-based model reduction for approximate stochastic analysis. *Computational Methods in Systems Biology 2012 (CMSB 2012)*, 2012a. (Cited on pages 14, 17, 65, and 115.)

K Batmanov, C Kuttler, C Lhoussaine, and Y Saka. Self-organized patterning by diffusible factors: roles of a community effect. *Fundamenta Informaticae*, 2012b. URL http://hal.inria.fr/hal-00633921. (Cited on pages 14, 17, and 71.)

H. C. Berg. *Random Walks in Biology*. (Princeton University Press, Princeton, 1993). (Cited on page 25.)

Yu. a. Berlin, P. Cordier, and J. a. Delaire. Modified Smoluchowski equation and a unified theory of the diffusion-controlled recombination. *The Journal of Chemical Physics*, 73(9):4619, 1980. ISSN 00219606. doi: 10.1063/1.440701. URL http://link.aip.org/link/JCPSA6/v73/i9/p4619/s1&Agg=doi. (Cited on page 27.)

David Bernstein. Simulating mesoscopic reaction-diffusion systems using the Gillespie algorithm. *Physical review. E, Statistical, nonlinear, and soft matter physics*, 71(4 Pt 1):041103, April 2005. URL http://www.ncbi.nlm.nih.gov/pubmed/15903653. (Cited on pages 48 and 74.)

H. Bolouri and E. H. Davidson. The gene regulatory network basis of the "community effect," and analysis of a sea urchin embryo example. *Developmental Biology*, 340(2):170–8, 2010. (Cited on pages 12, 16, 53, 54, 73, 91, 93, and 112.)

Hamid Bolouri and Eric H Davidson. Transcriptional regulatory cascades in development: initial rates, not steady state, determine network kinetics. *Proceedings of the National Academy of Sciences of the United States of America*, 100(16):9371–6, August 2003. ISSN 0027-8424. doi: 10.1073/pnas.1533293100. URL http://www.pubmedcentral.nih.gov/articlerender.fcgi?artid=170925&tool=pmcentrez&rendertype=abstract. (Cited on page 55.)

J. M. Bower and H. Bolouri, editors. *Computational Modeling of Genetic and Biochemical Networks*. MIT Press, 2001. (Cited on page 20.)

F Camporesi and J Feret. Formal reduction of rule-based models. In *Math Foundations Programming Semantics*, volume 276C of *ENTCS*, pages 31–61, 2011. (Cited on pages 111 and 115.)

Nathalie Chabrier-Rivier, François Fages, and Sylvain Soliman. The Biochemical Abstract Machine BIOCHAM. In *Computational Methods in Systems Biology*, pages 172–191, 2004. (Cited on page 51.)

Canhe Chen and Michael M Shen. Two Modes by which Lefty Proteins Inhibit Nodal Signaling. *Current*, 14:618–624, 2004. doi: 10.1016/j. (Cited on page 55.)

WW Chen, Mario Niepel, and PK Sorger. Classic and contemporary approaches to modeling biochemical reactions. *Genes & development*, pages 1861–1875, 2010. doi: 10.1101/gad.1945410.Freely. URL http://genesdev.cshlp.org/content/24/17/1861.short. (Cited on page 22.)

J L Cherry and F R Adler. How to make a biological switch. *Journal of Theoretical Biology*, 203(2):117–33, March 2000. doi: 10.1006/jtbi.2000.1068. URL http://www.ncbi.nlm.nih.gov/pubmed/10704297. (Cited on page 16.)

Kenneth Antonio Connors. *Chemical kinetics: the study of reaction rates in solution*. John Wiley & Sons, 1990. (Cited on page 21.)

G Cossu, R Kelly, S Di Donna, E Vivarelli, and M Buckingham. Myoblast differentiation during mammalian somitogenesis is dependent upon a community effect. *Proceedings of the National Academy of Sciences of the United States of America*, 92(6):2254–8, March 1995. ISSN 0027-8424. URL http://www.pubmedcentral.nih.gov/articlerender.fcgi?artid=42462&tool=pmcentrez&rendertype=abstract. (Cited on page 12.)

Vincent Danos and Cosimo Laneve. Formal molecular biology. *TCS*, 325(1):69–110, 2004. (Cited on page 51.)

Eric H. Davidson. *The Regulatory Genome: Gene Regulatory Networks In Development And Evolution*. Academic Press, 2006. (Cited on page 12.)

Eric H. Davidson. Emerging properties of animal gene regulatory networks. *Nature*, 468(7326):911–920, December 2010. doi: 10.1038/nature09645. URL http://www.nature.com/doifinder/10.1038/nature09645. (Cited on pages 20 and 73.)

Hidde de Jong. Modeling and simulation of genetic regulatory networks: A literature review. *Journal of Computational Biology*, 9:69–105, 2002. (Cited on page 19.)

Eric Dessaud, Vanessa Ribes, Nikolaos Balaskas, Lin Lin Yang, Alessandra Pierani, Anna Kicheva, Bennett G Novitch, James Briscoe, and Noriaki Sasai. Dynamic assignment and maintenance of positional identity in the ventral neural tube by the morphogen sonic hedgehog. *PLoS Biology*, 8(6):e1000382, January 2010. doi: 10.1371/journal.pbio.1000382. (Cited on page 113.)

Barbara Di Ventura, Caroline Lemerle, Konstantinos Michalodimitrakis, and Luis Serrano. From in vivo to in silico biology and back. *Nature*, 443(7111):527–33, October 2006. ISSN 1476-4687. doi: 10.1038/nature05127. URL http://www.ncbi.nlm.nih.gov/pubmed/17024084. (Cited on page 23.)

M Doi. Stochastic theory of diffusion-controlled reaction. *Journal of Physics A: Mathematical and General*, 1479, 1976. URL http://iopscience.iop.org/0305-4470/9/9/009. (Cited on page 27.)

Brian Drawert, Stefan Engblom, and Andreas Hellander. URDME: a modular framework for stochastic simulation of reaction-transport processes in complex geometries. *BMC Systems Biology*, pages 1–17, 2012. URL http://www.biomedcentral.com/1752-0509/6/76/. (Cited on page 51.)

Véronique Duboc, François Lapraz, Lydia Besnardeau, and Thierry Lepage. Lefty acts as an essential modulator of nodal activity during sea urchin oral–aboral axis formation. *Developmental biology*, 320(1):49–59, 2008. (Cited on pages 16, 55, 91, 93, and 112.)

Leah Edelstein-Keshet. *Mathematical models in biology*, volume 46. Society for Industrial and Applied Mathematics, 2005. (Cited on page 47.)

Avigdor Eldar and Michael B Elowitz. Functional roles for noise in genetic circuits. *Nature*, 467(7312):167–73, September 2010. ISSN 1476-4687. doi: 10.1038/nature09326. URL http://www.ncbi.nlm.nih.gov/pubmed/20829787. (Cited on page 13.)

Johan Elf and Mans Ehrenberg. Spontaneous Separation of Bi-Stable Biochemical Systems into Spatial Domains of Opposite Phases. *Systems Biology, IEE Proceedings*, 1(2):230–236, 2004. doi: http://dx.doi.org/10.1049/sb:20045021. URL http://dx.doi.org/10.1049/sb:20045021. (Cited on page 48.)

Johan Elf, Andreas Doncic, and Mans Ehrenberg. Mesoscopic reaction-diffusion in intracellular signaling. In *SPIE's First International Symposium on Fluctuations and Noise*, pages 114–124. International Society for Optics and Photonics, 2003. (Cited on page 48.)

P. Erdi and J. Toth. *Mathematical Models of Chemical Reactions - Theory & Applications of Deterministic & Stochastic Models*. Nonlinear Science: Theory and Applications. John Wiley & Sons, 1992.

ISBN 9780471935155. URL http://books.google.fr/books?id=jxnsPQAACAAJ. (Cited on pages 22 and 39.)

Robert Eymard, Thierry Gallouet, and Raphaele Herbin. *Finite volume methods*, volume 7 of *Handbook of Numerical Analysis*. Elsevier, 2000. doi: DOI:10.1016/S1570-8659(00)07005-8. URL http://www.sciencedirect.com/science/article/pii/S1570865900070058. (Cited on pages 47 and 74.)

David Fange and Johan Elf. Noise-induced min phenotypes in e. coli. *PLoS Comput Biol*, 2(6):e80, 06 2006. doi: 10.1371/journal.pcbi.0020080. URL http://dx.plos.org/10.1371%2Fjournal.pcbi.0020080. (Cited on page 48.)

David Fange, Otto G Berg, Paul Sjöberg, and Johan Elf. Stochastic reaction-diffusion kinetics in the microscopic limit. *Proceedings of the National Academy of Sciences of the United States of America*, 107(46):19820–5, December 2010. ISSN 1091-6490. doi: 10.1073/pnas.1006565107. URL http://www.pubmedcentral.nih.gov/articlerender.fcgi?artid=2993376&tool=pmcentrez&rendertype=abstract. (Cited on page 24.)

Chetan Gadgil, Chang Hyeong Lee, and Hans G Othmer. A stochastic analysis of first-order reaction networks. *Bulletin of mathematical biology*, 67(5):901–46, September 2005. ISSN 0092-8240. doi: 10.1016/j.bulm.2004.09.009. URL http://www.ncbi.nlm.nih.gov/pubmed/15998488. (Cited on page 34.)

A Gandhi, S Levin, and S Orszag. Moment expansions in spatial ecological models and moment closure through gaussian approximation. *Bull Math Biol*, 62:595–632, 2000. ISSN 0092-8240. URL http://dx.doi.org/10.1006/bulm.1999.0119. 10.1006/bulm.1999.0119. (Cited on page 116.)

C. W. Gardiner, K. J. McNeil, D. F. Walls, and I. S. Matheson. Correlations in stochastic theories of chemical reactions. *Journal of Statistical Physics*, 14(4):307–331, April 1976. ISSN 0022-4715. doi: 10.1007/BF01030197. URL http://link.springer.com/10.1007/BF01030197. (Cited on page 47.)

T S Gardner, C R Cantor, and J J Collins. Construction of a genetic toggle switch in Escherichia coli. *Nature*, 403(6767):339–42, January 2000. doi: 10.1038/35002131. URL http://www.ncbi.nlm.nih.gov/pubmed/10659857. (Cited on page 97.)

Michael A. Gibson and Joshua Bruck. Efficient exact stochastic simulation of chemical systems with many species and many channels. *J. Phys. Chem.*, 104:1876–1889, 2000. (Cited on pages 43 and 75.)

Alfred Gierer and Hans Meinhardt. A theory of biological pattern formation. *Kybernetik*, 12(1):30–39, 1972. (Cited on page 13.)

CS Gillespie. Moment-closure approximations for mass-action models. *IET Sys Biol*, 3(1):52, 2009a. (Cited on pages 38, 40, and 51.)

Daniel T. Gillespie. A General Method for Numerically Simulating the Stochastic Time Evolution of Coupled Chemical Reactions. *Journal of Computational Physics*, 22(4):403–434, December 1976. doi: 10.1016/0021-9991(76)90041-3. URL http://dx.doi.org/10.1016/0021-9991(76)90041-3. (Cited on pages 23 and 75.)

Daniel T. Gillespie. Exact stochastic simulation of coupled chemical reactions. *Journal of Physical Chemistry*, 81:2340–2361, 1977. (Cited on pages 34 and 42.)

Daniel T. Gillespie. A rigorous derivation of the chemical master equation. *Physica A: Statistical Mechanics and its Applications*, 188(1-3):404–425, September 1992. ISSN 03784371. doi: 10.1016/0378-4371(92)90283-V. URL http://linkinghub.elsevier.com/retrieve/pii/037843719290283V. (Cited on page 33.)

Daniel T. Gillespie. Approximate accelerated stochastic simulation of chemically reacting systems. *J. Chem. Phys*, 115:1716–1733, 2001. (Cited on page 43.)

Daniel T Gillespie. The Deterministic Limit of Stochastic Chemical Kinetics. *J. Phys. Chem. B*, 113(6):1640–1644, 2009b. doi: 10.1021/jp806431b. (Cited on pages 44 and 45.)

DT Gillespie. Chemical Langevin equation. *J Chem Physics*, 113:297–306, 2000. doi: 10.1063/1.481811. (Cited on page 36.)

Leo A. Goodman. Population growth of the sexes. *Biometrics*, 9(2):212–225, 1953. (Cited on page 38.)

Thomas Gregor, David W Tank, Eric F Wieschaus, and William Bialek. Probing the limits to positional information. *Cell*, 130(1):153–164, 2007. (Cited on page 111.)

B T Grenfell, K Wilson, V S Isham, H E Boyd, and K Dietz. Modelling patterns of parasite aggregation in natural populations. *Parasitology*, 111, January 1995. ISSN 0031-1820. URL http://www.ncbi.nlm.nih.gov/pubmed/8632919. (Cited on page 38.)

J. B. Gurdon. A community effect in animal development. *Nature*, 336(6201):772–4, 1988. (Cited on page 11.)

J. B. Gurdon, E. Tiller, J. Roberts, and K. Kato. A community effect in muscle development. *Current Biology*, 3(1):1–11, 1993. (Cited on pages 11, 12, 78, and 91.)

J. B. Gurdon, A. Mitchell, and D. Mahony. Direct and continuous assessment by cells of their position in a morphogen gradient. *Nature*, 376(6540):520–521, Aug 1995. doi: 10.1038/376520a0. URL http://dx.doi.org/10.1038/376520a0. (Cited on page 113.)

J B Gurdon, A Mitchell, and K Ryan. An experimental system for analyzing response to a morphogen gradient. *Proc Natl Acad Sci U S A*, 93(18):9334–8, Sep 1996. (Cited on page 78.)

Hiroshi Hamada, Chikara Meno, Daisuke Watanabe, and Yukio Saijoh. Establishment of vertebrate left-right asymmetry. *Nature reviews Genetics*, 3(2):103–13, February 2002. doi: 10.1038/nrg732. URL http://www.ncbi.nlm.nih.gov/pubmed/11836504. (Cited on page 15.)

Steven a Harvey and James C Smith. Visualisation and quantification of morphogen gradient formation in the zebrafish. *PLoS Biology*, 7 (5):e1000101, May 2009. doi: 10.1371/journal.pbio.1000101. (Cited on page 113.)

Johan Hattne, David Fange, and Johan Elf. Stochastic reaction-diffusion simulation with MesoRD. *Bioinformatics (Oxford, England)*, 21(12):2923–4, June 2005. ISSN 1367-4803. doi: 10.1093/bioinformatics/bti431. URL http://www.ncbi.nlm.nih.gov/pubmed/15817692. (Cited on page 51.)

M. Hegland. Approximating the solution of the chemical master equation by aggregation. In *14th Computational Techniques and Applications Conference*, volume 50 of *ANZIAM J.*, pages C371–C384, 2008. (Cited on page 36.)

Markus Hegland, Conrad Burden, Lucia Santoso, Shev MacNamara, and Hilary Booth. A solver for the stochastic master equation applied to gene regulatory networks. *Journal of Computational and Applied Mathematics*, 205(2):708–724, August 2007. ISSN 03770427. doi: 10.1016/j.cam.2006.02.053. URL http://linkinghub.elsevier.com/retrieve/pii/S0377042706003955. (Cited on page 36.)

S Hellander, A Hellander, and L Petzold. Reaction-diffusion master equation in the microscopic limit. *Physical Review E*, pages 1–9, 2012. URL http://pre.aps.org/abstract/PRE/v85/i4/e042901. (Cited on page 48.)

TA Henzinger, Maria Mateescu, and Verena Wolf. Sliding window abstraction for infinite Markov chains. *Computer Aided Verification*, 2009. URL http://link.springer.com/chapter/10.1007/978-3-642-02658-4_27. (Cited on page 35.)

Iain Hepburn, Weiliang Chen, Stefan Wils, and Erik De Schutter. STEPS: efficient simulation of stochastic reaction-diffusion

models in realistic morphologies. *BMC systems biology*, 6:36, January 2012. ISSN 1752-0509. doi: 10.1186/1752-0509-6-36. URL http://www.pubmedcentral.nih.gov/articlerender.fcgi?artid=3472240&tool=pmcentrez&rendertype=abstract. (Cited on pages 48 and 51.)

JP Hespanha and A Singh. Stochastic models for chemically reacting systems using polynomial stochastic hybrid systems. *J. Robust Control*, 15:669–689, 2005. (Cited on page 38.)

Desmond J Higham. An algorithmic introduction to numerical simulation of stochastic differential equations. *SIAM review*, 43(3):525–546, 2001. (Cited on page 37.)

Francis Begnaud Hildebrand. *Introduction to numerical analysis*. Courier Dover Publications, 1987. (Cited on page 13.)

Stefan Hoops, Sven Sahle, Ralph Gauges, Christine Lee, Jurgen Pahle, Natalia Simus, Mudita Singhal, Liang Xu, Pedro Mendes, and Ursula Kummer. Copasi – a complex pathway simulator. *Bioinformatics*, 22(24):3067–3074, 2006. doi: 10.1093/bioinformatics/btl485. URL http://bioinformatics.oxfordjournals.org/content/22/24/3067.abstract. (Cited on pages 51 and 68.)

Kazuki Horikawa, Kana Ishimatsu, Eiichi Yoshimoto, Shigeru Kondo, and Hiroyuki Takeda. Noise-resistant and synchronized oscillation of the segmentation clock. *Nature*, 441(7094):719–23, June 2006. ISSN 1476-4687. doi: 10.1038/nature04861. URL http://www.ncbi.nlm.nih.gov/pubmed/16760970. (Cited on page 14.)

Justin Hsia, William J. Holtz, Daniel C. Huang, Murat Arcak, and Michel M. Maharbiz. A feedback quenched oscillator produces turing patterning with one diffuser. *PLoS Comput Biol*, 8(1):e1002331, 2012. doi: 10.1371/journal.pcbi.1002331. URL http://dx.doi.org/10.1371%2Fjournal.pcbi.1002331. (Cited on page 112.)

M. Hucka, a. Finney, H. M. Sauro, H. Bolouri, J. C. Doyle, H. Kitano, a. P. Arkin, B. J. Bornstein, D. Bray, a. Cornish-Bowden, a. a. Cuellar, S. Dronov, E. D. Gilles, M. Ginkel, V. Gor, I. I. Goryanin, W. J. Hedley, T. C. Hodgman, J.-H. Hofmeyr, P. J. Hunter, N. S. Juty, J. L. Kasberger, a. Kremling, U. Kummer, N. Le Novere, L. M. Loew, D. Lucio, P. Mendes, E. Minch, E. D. Mjolsness, Y. Nakayama, M. R. Nelson, P. F. Nielsen, T. Sakurada, J. C. Schaff, B. E. Shapiro, T. S. Shimizu, H. D. Spence, J. Stelling, K. Takahashi, M. Tomita, J. Wagner, and J. Wang. The systems biology markup language (SBML): a medium for representation and exchange of biochemical network models. *Bioinformatics*, 19(4):524–531, March 2003. ISSN 1367-4803. doi: 10.1093/bioinformatics/

btg015. URL http://bioinformatics.oxfordjournals.org/cgi/doi/10.1093/bioinformatics/btg015. (Cited on page 50.)

S. A. Isaacson, D. M. McQueen, and Charles S. Peskin. The influence of volume exclusion by chromatin on the time required to find specific dna binding sites by diffusion. *Proceedings of the National Academy of Sciences*, 108(9):3815–3820, 2011. doi: 10.1073/pnas.1018821108. URL http://www.pnas.org/content/108/9/3815.abstract. (Cited on page 48.)

SA Isaacson. A Convergent Reaction-Diffusion Master Equation. *arXiv preprint arXiv:1211.6772*, pages 1–9, 2012. URL http://arxiv.org/abs/1211.6772. (Cited on pages 27, 28, and 48.)

Samuel a. Isaacson. Reaction-diffusion master equation, diffusion-limited reactions, and singular potentials. *Physical Review E*, 80(6): 066106, December 2009. ISSN 1539-3755. doi: 10.1103/PhysRevE.80.066106. URL http://link.aps.org/doi/10.1103/PhysRevE.80.066106. (Cited on page 48.)

L Isserlis. On a formula for the product-moment coefficient of any order of a normal frequency distribution in any number of variables. *Biometrika*, 12(1):134–139, 1918. URL http://biomet.oxfordjournals.org/content/12/1-2/134.short. (Cited on page 40.)

Johannes Jaeger, Maxim Blagov, David Kosman, Konstantin N Kozlov, Manu, Ekaterina Myasnikova, Svetlana Surkova, Carlos E Vanario-Alonso, Maria Samsonova, David H Sharp, and John Reinitz. Dynamical analysis of regulatory interactions in the gap gene system of Drosophila melanogaster. *Genetics*, 167 (4):1721–37, August 2004a. doi: 10.1534/genetics.104.027334. URL http://www.pubmedcentral.nih.gov/articlerender.fcgi?artid=1471003&tool=pmcentrez&rendertype=abstract. (Cited on pages 16 and 113.)

Johannes Jaeger, Svetlana Surkova, Maxim Blagov, Hilde Janssens, David Kosman, Konstantin N Kozlov, Manu, Ekaterina Myasnikova, Carlos E Vanario-Alonso, Maria Samsonova, David H Sharp, and John Reinitz. Dynamic control of positional information in the early Drosophila embryo. *Nature*, 430(6997):368–71, July 2004b. doi: 10.1038/nature02678. URL http://www.ncbi.nlm.nih.gov/pubmed/15254541. (Cited on page 16.)

Tobias Jahnke and Wilhelm Huisinga. Solving the chemical master equation for monomolecular reaction systems analytically. *Journal of mathematical biology*, 54(1):1–26, January 2007. ISSN 0303-6812. doi: 10.1007/s00285-006-0034-x. URL http://www.ncbi.nlm.nih.gov/pubmed/16953443. (Cited on page 34.)

M. John, C. Lhoussaine, J. Niehren, and C. Versari. Biochemical reaction rules with constraints. In Gilles Barthe, editor, *European Symposium On Programming (ESOP)*, volume 6602 of *Lecture Notes in Computer Science*, pages 338–357. Springer, 2011. (Cited on page 51.)

Henrik Jonsson, Marcus Heisler, G. Venugopala Reddy, Vikas Agrawal, Victoria Gor, Bruce E. Shapiro, Eric Mjolsness, and Elliot M. Meyerowitz. Modeling the organization of the wuschel expression domain in the shoot apical meristem. *Bioinformatics*, 21(suppl 1):i232–i240, 2005. doi: 10.1093/bioinformatics/bti1036. URL http://bioinformatics.oxfordjournals.org/content/21/suppl_1/i232.abstract. (Cited on page 16.)

Leo Kadanoff. *Statistical physics : statics, dynamics and renormalization*. World Scientific, Singapore River Edge, N.J, 2000. ISBN 9810237642. (Cited on page 28.)

Joel Keizer. Nonequilibrium statistical thermodynamics and the effect of diffusion on chemical reaction rates. *The Journal of Physical Chemistry*, 86(26):5052–5067, 1982. doi: 10.1021/j100223a004. URL http://pubs.acs.org/doi/abs/10.1021/j100223a004. (Cited on page 24.)

Hiroaki Kitano. Computational systems biology. *Nature*, 420(6912): 206–210, 2002. (Cited on page 13.)

Michael Klann and Heinz Koeppl. Spatial simulations in systems biology: from molecules to cells. *International journal of molecular sciences*, 13(6):7798–827, January 2012. ISSN 1422-0067. doi: 10.3390/ijms13067798. URL http://www.pubmedcentral.nih.gov/articlerender.fcgi?artid=3397560&tool=pmcentrez&rendertype=abstract. (Cited on page 109.)

S. Kondo and R. Asai. A reaction-diffusion wave on the skin of the marine angelfish Pomacanthus. *Nature*, 376(6543):765–768, 1995. URL http://www.tmd.ac.jp/med/phy2/Rindokupapers/Kondo_Nature_1995_Turing.pdf. (Cited on pages 47 and 92.)

S. Kondo and T. Miura. Reaction-Diffusion Model as a Framework for Understanding Biological Pattern Formation. *Science*, 329(5999):1616–1620, September 2010. doi: 10.1126/science.1179047. URL http://www.sciencemag.org/cgi/doi/10.1126/science.1179047. (Cited on pages 15 and 112.)

E Kotomin and V Kuzovkov. *Modern aspects of diffusion-controlled reactions: Cooperative phenomena in bimolecular processes*, volume 34. Elsevier Science, 1996. (Cited on page 27.)

Y Kuramoto. Effects of diffusion on the fluctuations in open chemical systems. *Prog Theor Phys*, 52:711–713, 1974. URL http://ptp.ipap.jp/link?PTP/52/711/. (Cited on page 47.)

Thomas G Kurtz. The relationship between stochastic and deterministic models for chemical reactions. *The Journal of Chemical Physics*, 57:2976, 1972. (Cited on pages 23 and 46.)

Jessica Lembong, Nir Yakoby, and Stanislav Y Shvartsman. Pattern formation by dynamically interacting network motifs. *Proceedings of the National Academy of Sciences of the United States of America*, 106(9): 3213–8, March 2009. ISSN 1091-6490. doi: 10.1073/pnas.0810728106. URL http://www.pubmedcentral.nih.gov/articlerender.fcgi?artid=2651296&tool=pmcentrez&rendertype=abstract. (Cited on page 113.)

C. Levermore. Moment closure hierarchies for kinetic theories. *Journal of Statistical Physics*, 83:1021–1065, 1996. ISSN 0022-4715. URL http://dx.doi.org/10.1007/BF02179552. 10.1007/BF02179552. (Cited on pages 38 and 116.)

Luciano Marcon and James Sharpe. Turing patterns in development: what about the horse part? *Current opinion in genetics & development*, 22(6):578–84, December 2012. ISSN 1879-0380. doi: 10.1016/j.gde.2012.11.013. URL http://www.ncbi.nlm.nih.gov/pubmed/23276682. (Cited on page 112.)

Alan D McNaught and Andrew Wilkinson. *Compendium of chemical terminology*, volume 1669. Blackwell Science Oxford, 1997. (Cited on page 21.)

Donald A McQuarrie. Stochastic approach to chemical kinetics. *Journal of Applied Probability*, 4(3):413–478, 1967. (Cited on page 34.)

H Meinhardt and a Gierer. Applications of a theory of biological pattern formation based on lateral inhibition. *Journal of Cell Science*, 15(2): 321–46, July 1974. URL http://www.ncbi.nlm.nih.gov/pubmed/4859215. (Cited on pages 47 and 93.)

Hans Meinhardt. *Models of biological pattern formation*, volume 6. Academic Press, 1982. URL http://www.eb.tuebingen.mpg.de/departments/former-departments/h-meinhardt/kurs/a_summary.pdf. (Cited on page 15.)

Hans Meinhardt. *The algorithmic beauty of sea shells*. The virtual laboratory. Springer, 1995. (Cited on page 15.)

Takashi Miura and Philip K Maini. Periodic pattern formation in reaction – diffusion systems : An introduction for numerical simulation Introduction : Periodic pattern formation. *Mathematica*, pages 112–123, 2004. (Cited on page 47.)

Patrick Müller, Katherine W Rogers, Ben M Jordan, Joon S Lee, Drew Robson, Sharad Ramanathan, and Alexander F Schier. Differential diffusivity of Nodal and Lefty underlies a reaction-diffusion patterning system. *Science (New York, N.Y.)*, 336(6082):721–4, May 2012. ISSN 1095-9203. doi: 10.1126/science.1221920. URL http://www.ncbi.nlm.nih.gov/pubmed/22499809. (Cited on page 112.)

B Munsky and M Khammash. The finite state projection algorithm for the solution of the chemical master equation. *Journal chemical physics*, 124(4):044104, 2006. ISSN 0021-9606. doi: 10.1063/1.2145882. URL http://www.ncbi.nlm.nih.gov/pubmed/16460146. (Cited on page 35.)

Brian Munsky and Mustafa Khammash. A multiple time interval finite state projection algorithm for the solution to the chemical master equation. *Journal of Computational Physics*, 226(1):818–835, September 2007. ISSN 00219991. doi: 10.1016/j.jcp.2007.05.016. URL http://linkinghub.elsevier.com/retrieve/pii/S0021999107002100. (Cited on page 35.)

Brian Munsky, Slaven Peles, and Mustafa Khammash. Stochastic analysis of gene regulatory networks using finite state projections and singular perturbation. *2007 American Control Conference*, pages 1323–1328, July 2007. ISSN 0743-1619. doi: 10.1109/ACC.2007.4283077. URL http://ieeexplore.ieee.org/lpdocs/epic03/wrapper.htm?arnumber=4283077. (Cited on page 35.)

Brian Munsky, Brooke Trinh, and Mustafa Khammash. Listening to the noise: random fluctuations reveal gene network parameters. *Molecular systems biology*, 5(318):318, January 2009. ISSN 1744-4292. doi: 10.1038/msb.2009.75. URL http://www.pubmedcentral.nih.gov/articlerender.fcgi?artid=2779089&tool=pmcentrez&rendertype=abstract. (Cited on page 30.)

Tetsuya Nakamura, Naoki Mine, Etsushi Nakaguchi, Atsushi Mochizuki, Masamichi Yamamoto, Kenta Yashiro, Chikara Meno, and Hiroshi Hamada. Generation of robust left-right asymmetry in the mouse embryo requires a self-enhancement and lateral-inhibition system. *Developmental cell*, 11(4):495–504, October 2006. doi: 10.1016/j.devcel.2006.08.002. URL http://www.ncbi.nlm.nih.gov/pubmed/17011489. (Cited on page 112.)

Jürgen Pahle. Biochemical simulations: stochastic, approximate stochastic and hybrid approaches. *Briefings in bioinformatics*, 10(1):53–64, January 2009. ISSN 1477-4054. doi: 10.1093/bib/bbn050. URL http://www.pubmedcentral.nih.gov/articlerender.fcgi?artid=2638628&tool=pmcentrez&rendertype=abstract. (Cited on page 43.)

Dmitri Papatsenko and Michael Levine. The drosophila gap gene network is composed of two parallel toggle switches. *PLoS ONE*, 6(7):e21145, 07 2011. doi: 10.1371/journal.pone.0021145. URL http://dx.doi.org/10.1371%2Fjournal.pone.0021145. (Cited on page 16.)

Slaven Peles, Brian Munsky, and Mustafa Khammash. Reduction and solution of the chemical master equation using time scale separation and finite state projection. *The Journal of chemical physics*, 125(20): 204104, November 2006. ISSN 0021-9606. doi: 10.1063/1.2397685. URL http://www.ncbi.nlm.nih.gov/pubmed/17144687. (Cited on page 35.)

Mark Ptashne. *A genetic switch: phage lambda revisited*. Cold Spring Harbor Laboratory Press, Cold Spring Harbor, N.Y., 3rd ed edition, 2004. URL http://www.loc.gov/catdir/toc/ecip0414/2004000803.html. (Cited on page 16.)

Arjun Raj and Alexander van Oudenaarden. Single-molecule approaches to stochastic gene expression. *Annual review of biophysics*, 38:255–70, January 2009. ISSN 1936-122X. doi: 10.1146/annurev.biophys.37.032807.125928. URL http://www.pubmedcentral.nih.gov/articlerender.fcgi?artid=3126657&tool=pmcentrez&rendertype=abstract. (Cited on page 13.)

Vanessa Ribes and James Briscoe. Establishing and interpreting graded sonic hedgehog signaling during vertebrate neural tube patterning: the role of negative feedback. *Cold Spring Harbor Perspectives in Biology*, 1(2):a002014, August 2009. doi: 10.1101/cshperspect.a002014. URL http://www.pubmedcentral.nih.gov/articlerender.fcgi?artid=2742090&tool=pmcentrez&rendertype=abstract. (Cited on page 16.)

Stephen A Rice. *Diffusion-limited reactions*, volume 25. Elsevier Science, 1985. (Cited on pages 25 and 28.)

Y. Saka and J. C. Smith. A mechanism for the sharp transition of morphogen gradient interpretation in xenopus. *BMC Developmental Biology*, 7:47, 2007. (Cited on pages 16, 71, 96, 98, 99, and 104.)

Yasushi Saka, Cédric Lhoussaine, Celine Kuttler, Ekkehard Ullner, and Marco Thiel. Theoretical basis of the community effect in development. *BMC Systems Biology*, 5:54, March 2011. (Cited on pages 14, 16, 53, 56, 63, 64, 68, 71, 72, 78, 82, 85, and 91.)

A.R. Sanderson, R.M. Kirby, C.R. Johnson, and L. Yang. Advanced reaction-diffusion models for texture synthesis. *Journal of Graphics Tools*, 11(3):47–71, 2006. URL http://www.sci.utah.

edu/publications/allen06/Sanderson_JGT_2006.pdf. (Cited on page 15.)

Yaki Setty. Multi-scale computational modeling of developmental biology. *Bioinformatics (Oxford, England)*, 28(15):2022–8, August 2012. ISSN 1367-4811. doi: 10.1093/bioinformatics/bts307. URL http://www.ncbi.nlm.nih.gov/pubmed/22628522. (Cited on page 19.)

Rushikesh Sheth, Luciano Marcon, M Félix Bastida, Marisa Junco, Laura Quintana, Randall Dahn, Marie Kmita, James Sharpe, and Maria a Ros. Hox genes regulate digit patterning by controlling the wavelength of a Turing-type mechanism. *Science (New York, N.Y.)*, 338(6113):1476–80, December 2012. ISSN 1095-9203. doi: 10.1126/science.1226804. URL http://www.ncbi.nlm.nih.gov/pubmed/23239739. (Cited on pages 47 and 112.)

Hidetaka Shiratori and Hiroshi Hamada. The left-right axis in the mouse: from origin to morphology. *Development (Cambridge, England)*, 133(11):2095–104, June 2006. ISSN 0950-1991. doi: 10.1242/dev.02384. URL http://www.ncbi.nlm.nih.gov/pubmed/16672339. (Cited on page 112.)

A Singh and J.P Hespanha. Lognormal Moment Closures for Biochemical Reactions. In *Decision and Control, 2006 45th IEEE Conference on*, pages 2063–2068, 2006a. (Cited on page 40.)

Abhyudai Singh and João Pedro Hespanha. Lognormal moment closures for biochemical reactions. In *Proc. of the 45th Conf. on Decision and Contr.*, Dec. 2006b. (Cited on page 110.)

Abhyudai Singh, Brandon S Razooky, Roy D Dar, and Leor S Weinberger. Dynamics of protein noise can distinguish between alternate sources of gene-expression variability. *Molecular systems biology*, 8 (607):607, January 2012. ISSN 1744-4292. doi: 10.1038/msb.2012.38. URL http://www.ncbi.nlm.nih.gov/pubmed/22929617. (Cited on page 30.)

Alexander Slepoy, Aidan P Thompson, and Steven J Plimpton. A constant-time kinetic Monte Carlo algorithm for simulation of large biochemical reaction networks. *The Journal of chemical physics*, 128 (20):205101, May 2008. ISSN 1089-7690. doi: 10.1063/1.2919546. URL http://www.ncbi.nlm.nih.gov/pubmed/18513044. (Cited on page 43.)

M von Smoluchowski. Versuch einer mathematischen theorie der koagulationskinetik kolloider lösungen. *Z. phys. Chem*, 92(129-168):9, 1917. (Cited on page 24.)

JR Stiles and TM Bartol Jr. Monte Carlo simulation of neurotransmitter release using MCell, a general simulator of cel-

lular physiological processes. *Computational ...*, pages 279–284, 1998. URL http://link.springer.com/chapter/10.1007/978-1-4615-4831-7_47. (Cited on page 51.)

Isabella Stüttem and José A Campos-Ortega. Cell commitment and cell interactions in the ectoderm of drosophila melanogaster. *Development*, 113(Supplement 2):39–46, 1991. (Cited on page 12.)

Yi-Hsien Su, Enhu Li, Gary K Geiss, William J R Longabaugh, Alexander Krämer, and Eric H Davidson. A perturbation model of the gene regulatory network for oral and aboral ectoderm specification in the sea urchin embryo. *Developmental biology*, 329(2):410–21, May 2009. ISSN 1095-564X. doi: 10.1016/j.ydbio.2009.02.029. URL http://www.pubmedcentral.nih.gov/articlerender.fcgi?artid=2677136&tool=pmcentrez&rendertype=abstract. (Cited on page 112.)

K. Takahashi, N. Ishikawa, Y. Sadamoto, H. Sasamoto, S. Ohta, a. Shiozawa, F. Miyoshi, Y. Naito, Y. Nakayama, and M. Tomita. E-Cell 2: Multi-platform E-Cell simulation system. *Bioinformatics*, 19(13):1727–1729, September 2003. ISSN 1367-4803. doi: 10.1093/bioinformatics/btg221. URL http://bioinformatics.oxfordjournals.org/cgi/doi/10.1093/bioinformatics/btg221. (Cited on page 51.)

Ei Teramoto and Nanako Shigesada. Theory of Bimolecular Reaction Processes in Liquids. *Progress of Theoretical Physics*, 37(1):29–51, January 1967. ISSN 0033-068X. doi: 10.1143/PTP.37.29. URL http://ptp.oxfordjournals.org/cgi/doi/10.1143/PTP.37.29. (Cited on page 27.)

A. M. Turing. The chemical basis of morphogenesis. *Philosophical Transactions of the Royal Society of London. Series B, Biological Sciences*, 237(641):37–72, 1952. (Cited on pages 11, 12, 13, 15, 47, 91, 92, 111, and 112.)

Jeroen van Zon and Pieter ten Wolde. Simulating Biochemical Networks at the Particle Level and in Time and Space: GreenâĂŹs Function Reaction Dynamics. *Physical Review Letters*, 94(12):128103, April 2005. ISSN 0031-9007. doi: 10.1103/PhysRevLett.94.128103. URL http://link.aps.org/doi/10.1103/PhysRevLett.94.128103. (Cited on page 30.)

S Vidal, Petitot, F Boulier, F Lemaire, and C Kuttler. Models of stochastic gene expression and Weyl algebra. *Algebraic Biology, LNCS*, June 2010. URL http://hal.inria.fr/hal-00492438. (Cited on pages 38, 40, 63, and 110.)

Eberhard O Voit. *Computational analysis of biochemical systems: a practical guide for biochemists and molecular biologists*. Cambridge University Press, 2000. (Cited on page 23.)

TR Waite. Theoretical treatment of the kinetics of diffusion-limited reactions. *Physical Review*, 935, 1957. URL http://prola.aps.org/abstract/PR/v107/i2/p463_1. (Cited on page 27.)

P. Whittle. On the use of the normal approximation in the treatment of stochastic processes. *Journal Royal Statistical Society. Series B*, 19(2):268–281, 1957. (Cited on page 38.)

L Wolpert. Positional information and the spatial pattern of cellular differentiation. *Journal of Theoretical Biology*, 25(1):1–47, October 1969. URL http://www.ncbi.nlm.nih.gov/pubmed/4390734. (Cited on pages 16 and 113.)

L Wolpert, R Beddington, J Brockes, T Jessell, P Lawrence, and E Meyerowitz. *Principles of development*. Current Biology Ltd London, 1998. (Cited on page 11.)